Computational systems biology of sucrose accumulation in sugarcane

Lafras Uys

Thesis presented in partial fulfilment
of the requirements for the degree
Master of Science
at the University of Stellenbosch

Supervisor: Prof. Johann M. Rohwer
April 2006

I, the undersigned, hereby declare that the work contained in this thesis is my own original work and that I have not previously in its entirety or in part submitted it at any university for a degree.

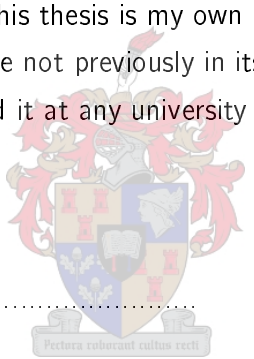

Signed:.....

Date:.....

Summary

This thesis is about the mathematical modelling of sucrose accumulation in the storage parenchyma of *Saccharum officinarum* (sugarcane). In 2001, Rohwer & Botha [76] published a kinetic model that described the defining feature of this process, i.e. the futile cycling of a fraction of the newly synthesised sucrose because of neutral invertase activity. A Metabolic Control Analysis was able to predict the control over this process, and on the basis thereof strategies were suggested to increase the flux of sucrose into the vacuole. The vacuole was not modelled as an explicit compartment, reactions catalysed by multiple isozymes were collapsed into single enzyme steps, carbon sequestration into insoluble fibre was not accounted for, and only internode 5 was modelled as a representative internode of medium-mature tissue.

The aim of the current work was to address these shortcomings and extend the model of Rohwer & Botha. The extensions involved modelling fructokinase and sucrose synthase in terms of their individual isozymes, including *UDP*-Glucose Dehydrogenase as a representative step of fibre formation, expanding the single glycolytic drain reaction into phosphofructokinase, pyrophosphate-dependant phospofructokinase and aldolase, and finally, creating a parameter set that makes the model relevant for immature (internode 3) to mature (internode 10) storage tissue. Open-source software tools such as Gnumeric (a spreadsheet), Python (a programming language) and PySCeS (cellular simulation software written in Python) were used to collect and organise data and perform the numerical analysis. The new reactions were added individually and the model analysed to gauge the difference between the old and new model. Once all the additions had been incorporated, the final model was solved for eight internodes and analysed in terms of the steady-state solution and control over futile cycling of sucrose. A review of the literature provided a test set of experimentally determined sucrose concentrations that could be used for comparison to steady-state sucrose concentrations as predicted by the new model.

The most important results of this work are that the model did not predict an increase in the steady-state cytoplasmic sucrose concentrations, as opposed to the increase seen in experimentally determined sucrose concentrations. We conclude that sucrose is probably stored in the vacuole and not in the cytoplasm. Futile cycling decreased on average by 6% per internode, while the shift in control over futile cycling did not change significantly with internode maturity.In future, this work

can be extended to incorporate the vacuole as an explicit storage organelle and link the model to current modelling endeavours on sucrose synthesis in source tissue. In summary, this work provides the foundation for a rational design approach in the selection of sugarcane hybrids and genetic engineering of sugarcane clones.

Opsomming

Hierdie tesis handel oor die wiskundige modellering van sukrose-berging in die swelgweefsel van *Saccharum officinarum* (suikerriet). Rohwer & Botha het in 2001 [76] 'n kinetiese model gepubliseer wat die kenmerkende eienskappe van díe proses beskryf, d.w.s. die afbraak van 'n gedeelte van die nuut gesintetiseerde sukrose vanweë die aktiwiteit van neutrale invertase. 'n Metaboliese kontrole-analise het die beheer oor die proses voorspel, en na aanleiding daarvan is strategieë voorgestel om die fluksie van sukrose na die vogselholte (vakuool) te verhoog. In hierdie model is die vakuool nie uitdruklik as 'n aparte kompartement gemodelleer nie, reaksies wat gekataliseer word deur meer as een isosiem is saam gebondel in 'n enkele ensiemreaksie, die vertakking van koolstof-vloei na onoplosbare veselsintese is nie ingereken nie, en slegs die vyfde stingellit (internode) is gemodelleer as 'n verteenwoordigende stingellit van medium-volwasse weefsel.

Die doel van die huidige studie was om hierdie tekortkominge aan te spreek en die model van Rohwer & Botha uit te brei. Dit het behels dat fruktokinase en sukrose-sintase gemodelleer word in terme van hul individuele isosieme, dat *UDP*-glukose dehidrogenase bygevoeg word as 'n verteenwoordigende reaksie van veselvorming, dat die enkele glikolitiese dreinreaksie uitgebrei word na fosfofruktokinase, pirovaat-afhanklike fosfofruktokinase en aldolase, en laastens dat 'n stel parameters versamel word wat die model toepas op onvolwasse (derde stingellit) tot volwasse (tiende stingellit) swelgweefsel. Oopbron-programmatuur soos Gnumeric ('n sigblad), Python ('n programmeringstaal) en PySCeS (sellulêre simuleringsprogrammatuur wat geskryf is in Python) is gebruik om die data te versamel, te organiseer, en numeries te analiseer. Die nuwe reaksies is stuksgewys bygevoeg en die model steeds geanaliseer om verskille tussen die ou en nuwe model te bepaal. Nadat al die veranderinge in die model ingebou is, is 'n oplossing verkry vir elk van agt stingelitte om die uiteindelike model te lewer. Die oplossings is gesamentlik geanaliseer in terme van elkeen se bestendige toestand en die graad van beheer wat elke individuele reaksie uitoefen op die sintese en afbraak van sukrose. 'n Oorsig van die literatuur het 'n toetsstel van eksperimenteel bepaalde sukrose-konsentrasies opgelewer. Die doel hiervan was om 'n datastel te genereer waarteen die voorspellings van die model geyk kan word.

Die belangrikste resultaat van hierdie werk is dat die model nie 'n noemenswaardige toename in sitoplasmiese sukrosekonsentrasies voorspel nie, in teenstelling met die eksperimenteel

bepaalde konsentrasies van die empiriese toets-datastel. Ons gevolgtrekking is dat die sukrose hoogs waarskynlik in die vakuool en nie in die sitoplasma gestoor word nie. Die afbraak van sukrose d.m.v. die futiele siklus het met gemiddeld 6% per stingellit verminder, terwyl die beheer oor sukrose-afbraak nie noemenswaardig verskuif het met die ouderdom van die stingellit nie. Die werk wat hier gerapporteer word, kan in toekoms verder uitgebrei word om die vakuool eksplisiet as 'n bergings-organel in te sluit en om die model te koppel aan huidige navorsingsaktiwiteite om sukrose-sintese in blaarweefsel te modelleer. Om op te som, stel hierdie werk 'n fondament daar vir 'n rasionele benadering tot die seleksie van suikerriet-kruisings en genetiese manipulering van suikerriet-klone.

Contents

List of Figures

List of Tables

List of Abbreviations

Metabolites

Glc	Glucose
Glc-1-P	Glucose-1-phosphate
Glc-6-P	Glucose-6-phosphate
Fru	Fructose
Fru-1-P	Fructose-1-phosphate
Fru-6-P	Fructose-6-phosphate
Fru-1,6-P_2	Fructose-1,6-bisphosphate
Fru-2,6-P_2	Fructose-2,6-bisphosphate
Suc	Sucrose
Suc-6-P	Sucrose-6-phosphate
HexP	Hexose phosphate
ATP	Adenosine Triphosphate
ADP	Adenosine Diphosphate
UDP	Uridine Diphosphate
UDPGlc	*UDP*-Glucose
UDPGA	*UDP*-Glucuronic acid

Enzymes

HK	Hexokinase (EC 2.7.1.1)
FRK	Fructokinase (EC 2.7.1.4)
UDPGDH	UDP-Glucose Dehydrogenase (EC 1.1.1.22)
PFK	Phosphofructokinase (EC 2.7.1.11)
PFP	Pyrophosphate-dependant PFK (EC 2.7.1.90)
NI	Neutral Invertase (EC 3.2.1.26)
SuSy or *SS*	Sucrose synthase (EC 2.4.1.13)

ALD	Aldolase (EC 4.1.2.13)
SPS	Sucrose Phosphate Synthetase (EC 2.4.1.14)
SP or *SPase*	Sucrose Phosphatase (EC 3.1.3.24)

Symbols

J_x	Flux through enzyme x
C_x^y	Control coefficient of x on y
ϵ_p^x	Elasticity coefficient of p on x
ν_x	Rate of enzyme x
V_x	Maximal velocity of enzyme x
K_{eq}	Equilibrium constant
K_m	Michaelis constant
$S_{0.5}$	Half-saturation constant for species, S
σ	Coefficient of modification
i	Internode
$\mathbf{M}$	Model of sucrose accumulation
$\mathbf{M}_\alpha$	Rohwer & Botha model
$\mathbf{M}_\beta$	Schäfer model
$\mathbf{M}_\gamma$	Bosch model
$\mathbf{M}_\delta^{(i)}$	Model in this dissertation

for emmerentia, susan, david and theo

Acknowledgments

- Many thanks to a very patient Professor Johann M. Rohwer
- Dr. Brett Olivier
- Arno Hanekom
- The National Bioinformatics Network provided funding in the form of a Master's bursary

Chapter 1

The kinetic modelling of sucrose accumulation

This thesis describes the extension of a kinetic, mathematical model of sucrose accumulation in sugarcane (*Saccharum* sp.) by adding new reactions to the model and modifying old ones. The result of this work is a model of sucrose accumulation that reflects more accurately what happens in the sugarcane plant.

The mathematical modelling of living systems is both an end in itself and a method of rationally deciding on future experimental work. In particular, applying computational methods to plant metabolism allows gaining a rapid overview of a process that is difficult, if not impossible, to observe directly in its entirety [14, 57, 97]. Modelling provides a means of integrating components studied in isolation into a snapshot of the progress made thus far in a particular field. It is also possible to make cautious inferences of what happens in a living system based on the properties of a model, such as the distribution and magnitude of systemic control on a particular pathway. A phase space of all possible solutions of a model provides a method of forecasting changes made to model parameters and initial conditions. Amongst others, this has implications for genetic engineering of plants, as well as understanding host-pathogen interactions.

The parts of metabolism involved in the accumulation of sucrose in sugarcane have been modelled mathematically by Rohwer & Botha [76]. The model was able to quantify the degree of sucrose futile cycling in sugarcane storage parenchyma and also predict the enzymes that exerted the most control over this futile cycle. The modelling process serves three goals in the present study:

1. Integrating results of kinetic studies on enzymes believed to be directly involved in the efficiency of sugarcane sucrose accumulation, into an existing model.

2. Calculating and analysing model properties with significant implications for sucrose accumulation in maturation of tissue.

3. Highlighting areas where experimental data are scarce or inconsistent.

A general introduction to kinetic modelling is given first (Section 1.1). This chapter will then also review the original model of Rohwer & Botha [76] and define the current standard model as proposed by Schäfer et al [80](Section 1.2). Sugarcane attributes, with the potential to be included in future modelling endeavours, are given a short review (Section 1.3). The extensions specific to this work (Section 1.4) and outline of this thesis (Section 1.5) conclude the chapter.

1.1 An overview of kinetic modelling

Computational systems biology can be considered the practice of mathematically describing living organisms. The advantages of this approach are many, amongst others, computational systems biology allows a formal, rigourous approach to be applied to biology. The logic, proofs and theorems of mathematics are a valuable addition to the arsenal of tools of a biologist. This section is adapted from the book by Heinrich & Schuster [30].

The following section will show how a small set of reactions is modelled in terms of a simple one to one stoichiometry, four rate equations and two ordinary differential equations. Consider the following reaction scheme:

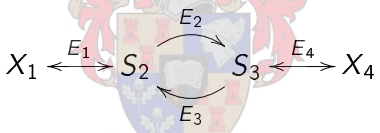

where X_1 and X_4 are external metabolites, the concentration of which is treated as constant. S_2 and S_3 are variable metabolites and E_1 to E_4 are enzymes catalysing a particular step. The rate at which an enzyme catalyses a reaction can be described by an appropriate rate equation for the specific enzyme,

$$\nu_j = \nu(\mathbf{S}, \mathbf{p}, t) \tag{1.1}$$

where ν_j is the rate of catalysis for an enzyme, $j \in \{1, 2, 3, 4\}$, t is time, $\nu(.)$ is some function, $\mathbf{S}$ and $\mathbf{p}$ are respectively a metabolite concentration- and parameter vector. In other words, the rate equation, in this case, is a function of metabolite concentrations, a set of parameters and time. Often the interest is only in the steady-state metabolite concentrations and rates. A steady-state can only be obtained if metabolite concentrations do not depend explicitly on time; we write the autonomous system of rate equations,

$$\nu_j = \nu(\mathbf{S}(t), \mathbf{p}) \tag{1.2}$$

In a reaction network, metabolites may be both a substrate of different enzymes and also the

product of different reactions. The topology of the above scheme can be captured in matrix form,

$$\mathbf{N} = \begin{array}{cccc|c} E_1 & E_2 & E_3 & E_4 & \\ \hline -1 & 0 & 0 & 0 & X_1 \\ 1 & -1 & 1 & 0 & S_2 \\ 0 & 1 & -1 & -1 & S_3 \\ 0 & 0 & 0 & 1 & X_4 \end{array} \tag{1.3}$$

Changes in metabolite concentrations are then given by,

$$\frac{\mathrm{d}\mathbf{S}}{\mathrm{d}t} = \mathbf{N}\boldsymbol{\nu} \tag{1.4}$$

where $\boldsymbol{\nu}$ is a vector of rate equations. The solution to the system,

$$\mathbf{N}\boldsymbol{\nu} = \mathbf{0} \tag{1.5}$$

describes the steady-state concentrations and fluxes. Steady-state rates are usually called fluxes. As an example, we let,

$$\boldsymbol{\nu} = \begin{pmatrix} \dfrac{V_f^{E_1} X_1/K_{X_1} - V_r^{E_1} S_2/K_{S_2}}{1 + X_1/K_{X_1} + S_2/K_{S_2}} \\ \dfrac{V_f^{E_2}}{1 + S_2/K_{S_2}} \\ \dfrac{V_f^{E_3}}{1 + S_3/K_{S_3}} \\ \dfrac{V_f^{E_4} S_3/K_{S_3} - V_r^{E_4} X_4/K_{X_4}}{1 + S_3/K_{S_3} + X_4/K_{X_4}} \end{pmatrix} \tag{1.6}$$

where $V_{f,r}^{j}$ are the respective forward- or reverse maximal velocities for each enzyme and a subscripted K is the Michaelis constant for a substrate or product of a reaction. In this example E_1 and E_4 are described by reversible Michaelis-Menten kinetics, while E_2 and E_3 are described by irreversible Michaelis-Menten kinetics.

We arbitrarily initialise X_1 at 10 and S_2, S_3 & X_4 at 1. All the Michaelis constants are set to 1, all $V_{f,r}^{1,4}$ are set to 1.5 and $V_f^{2,3}$ are set to 3.0. Units of concentration and rate in this fictitious example are arbitrary. The steady-state solution for metabolites is then 5.23 and 2.25 for S_2 and S_3 respectively. Steady-state fluxes are $J_{E_1} = 0.44$, $J_{E_2} = 2.52$, $J_{E_3} = 2.08$ and $J_{E_4} = 0.44$. Notice that $J_{E_1} = J_{E_4}$. This follows from the fact that flux into the system has to equal flux out of the system. If S_2 and S_3 are initialised at 10, the steady-state solution is identical to the previous solution. On the contrary, changing any of the parameter values does change the steady-state solution. This simply illustrates that this particular system is governed by **p** and not the initialisation values for the state variables. Another consequence of this observation is that metabolic behaviour of spatially removed yet identical reaction networks can be described by one model and the appropriate parameter set for a location.

This example was solved using the software suite PySCeS (pysces.sourceforge.net, [63]). Software programs written specifically for computational systems biology usually have a number of features in common. Like the example above, problems in systems biology are usually modelled as systems of ODEs. Most systems biology tools offer an easy interface to libraries that can solve ODEs, like PySCeS, and others such as Jarnac [79] and Gepasi [55]. Time course analysis of coupled sets of ODEs gives an idea of how a system behaves over a period of time. The steady-state solution of open systems is the limit of the ODE state variables as the time variable tends to infinity. The packages mentioned above are geared towards this type of analysis. ODEs can have more than one steady-state solution in some instances, in which case more specialised packages are required to solve a problem. Routines like PITCON [74] and packages like AUTO [18, 19] (to which xppaut is a front end, http://www.math.pitt.edu/~bard/xpp/xpp.html) are able to find multiple steady-state solutions.

Chapter 3 will show how kinetic modelling can be used to describe sugarcane stalk growth by using internode specific parameter sets. First, a description of the current sucrose model is given.

1.2 Synopsis of the core model of sucrose accumulation in sugarcane

The following list and Table 1.1 define some notation that will be encountered through the rest of the text.

- $\mathbf{M}$ is any model.
- $\mathbf{M}_\alpha$ refers to the Rohwer & Botha model [76].
- $\mathbf{M}_\beta$ is $\mathbf{M}_\alpha$ with corrections proposed by Schäfer et al [80]. It is also called the current standard model in the rest of this text.
- $\mathbf{M}_\gamma$ is $\mathbf{M}_\beta$ with the trehalose pathway added [8]. It is included here for chronological continuity, but has no immediate relevance on the current work.
- $\mathbf{M}_\delta^{(i)}$ will refer to $\mathbf{M}_\beta$ with extensions as proposed at the end of this chapter and refined in Chapter 3. $i \in \{3, 4, \ldots, 10\}$ refers to internodes 3 to 10.

The distinguishing feature of the sucrose accumulation pathway in sugarcane is the significant futile cycling of sucrose. This is in part due to three known invertase isoforms that are present in storage parenchyma [9, 28, 53, 67, 77, 106, 107, 108, 109, 117], as well as the easy reversibility of enzymes such as sucrose synthase [81]. Current opinion considers the latter to run predominantly in the sucrose breakdown direction. $\mathbf{M}_\alpha$ captured this property succinctly and predicted approximately 22% of synthesised sucrose to be broken down again.

Table 1.1: Notation for reaction and transport steps as used throughout the text.

Description	$\mathbf{M}_\beta$step	$\mathbf{M}_\delta^{(i)}$step	$\mathbf{M}_\delta^{(i)}$flux
Uptake of *Fru* & *Glc* by the cytosol	R1 & R2	Fru_{up}	J_{up}^{Fru}
		Glc_{up}	J_{up}^{Glc}
Hexokinase	R3 & R4	HK^{Glc}	J_{HK}^{Glc}
		HK^{Fru}	J_{HK}^{Fru}
Fructokinase	R5	*FRK A & B*	$J_{FRK}^{a,b}$
Sucrose phosphate synthetase	R6	*SPS*	J_{SPS}
Sucrose phosphatase	R7	*SPase*	J_{SP}
Sucrose synthase	R8	*SuSy A, B & C*	$J_{SS}^{a,b,c}$
Neutral invertase	R9	NI	J_{NI}
Glycolysis	R10	*PFP*, *PFK*& Aldolase (ALD)	J_{PFP}, J_{PFK}, J_{Ald} or J_{glyc}
Transport of *Suc* into the vacuole	R11	Suc_{store}	J_{vac}^{Suc}
UDPGlc conversion to *UDP*-Glucoronic acid (*UDPGA*)	-	-	*UDPGDH*

The assumption was made that, with increased flux into the vacuole, increased sucrose accumulation should follow. The study concluded that an increased efficiency in cytoplasmic glucose and fructose uptake, as well as vacuolar sucrose uptake, should benefit sucrose accumulation. A decrease in neutral invertase activity should do the same. Reducing glucose hexokinase activity, reduced futile cycling, but at the same time diminished sucrose flux into the vacuole.

$\mathbf{M}_\alpha$ was designed as a core model. The model assumptions allowed some simplifications, such as:

- the vacuole was not modelled as an explicit storage compartment,
- metabolic cofactors were clamped at experimentally determined concentrations,
- only internode 5 was considered as representative of developing internodes,
- hexoses were not utilised for fibre formation,

- enzyme catalysis was considered the weighted statistical average of any possible enzyme isoforms, and
- some maximal activities were estimated.

It is clear from this that the scope for model expansion exists. The next section deals with possible extensions. From these a subset will be chosen for inclusion in the model.

1.3 Possible extensions to the current standard model

1.3.1 Compartmentation

Terms in a rate equation are usually concentrations or a ratio of concentrations. Compartments at the physiological and cellular scale separate reactions from each other. A compartment is by definition a volume, and the effect this has on inter-compartmental movement of metabolites has obvious implications for concentration dependent terms. It is possible to assign physiological functions to a compartment based on the metabolic reactions that is enclosed within it. Describing a process, such as the fixation of carbon dioxide by plant leaves through to the storage of carbon in the form of sucrose, requires a clear conception of which compartments are important and what happens chemically inside them.

It should be mentioned that an anthropocentric bias is implied when talking of sucrose accumulation in sugarcane. The "purpose", if one can even call it that, of sugarcane is not to accumulate sucrose. This is a function imposed on sugarcane in its capacity as a agronomic crop. It is, however, a useful assumption to make when discussing the process of carbon fixation to sucrose storage.

Given the above framework to think in, the following list describes possible additions to the modelling of sucrose accumulation. Each of the points can be considered an individual model. Concatenating these models should provide us with a general model of sucrose accumulation.

Leaves Sucrose production requires carbon and energy. In the jargon of supply-demand analysis [33], these reactions would form a supply-block, providing a demand-block (storage parenchyma and roots) with photosynthate. Metabolism in the leaves is a natural starting point for the sucrose accumulation process.

Carbon fixation Sugarcane is a C4 plant [21, 66]. Rubisco does not directly capture carbonate, as in C3 plants, instead a shuttle mechanism between the bundle sheath cells and mesophyll transports carbonate to the photosynthetic apparatus. Dissolved carbonate in the bundle sheath cells of leaves is incorporated into phosphoenolpyruvate by a carboxylase. The resulting four carbon compound (hence the name, C4) is carried to the mesophyll where the carbonate is delivered to Rubisco. This process provides all the carbon in all metabolites.

Photosynthesis Energy derived from sunlight directly or indirectly drives all processes in a plant. Photosystem I captures incident radiation [17]. A series of electron transfer reactions are coupled to the reduction of $NADP^+$ to *NADPH* and phosphorylation of *ADP* to *ATP* [2]. Doubt exists as to the presence of photosystem II in C4 plants [116]. The reductive pentose phosphate cycle incorporates fixated carbon, powered by *ATP* and *NADPH*.

Carbohydrate synthesis Glucose and fructose are the immediate precursors to sucrose and are themselves derived from triose-phosphates. Sugarcane leaves are able to synthesise and store starch [13]. The role of foliar starch is uncertain. It has been proposed that competition for *UDPGlc* and *Glc-1-P* could negatively impact sucrose synthesis [2]. The synthesis of sucrose from starch at night could hypothetically perform a regulatory role further downstream in the plant.

Stem Carbohydrates are stored in the sugarcane stalk. In *S. officianarum* sucrose is the preferred soluble polysaccharide that is accumulated. Ancestral varieties of sugarcane tend to accumulate starch [2].

Phloem loading Exit of soluble sugars from source tissues is an energetically expensive process and, therefore, directly influences all other metabolic pathways. It is estimated that between 2.4 and 4.0 mol *ATP* /mol *Suc* is required to transport sucrose from the foliar apoplast to symplast [14]. The regulation of phloem loading has implications for downstream phloem unloading [102].

Transport Mass linkage between sucrose synthesising source tissue and sucrose accumulating sink tissue is facilitated by the phloem via a process that is not completely understood [72]. A possible model has been provided by Münch [49]. This model tries to explain phloem transport in terms of an osmotic pressure gradient between source- and sink tissue that drives solutes down the phloem tubes. A complete transport model should be able to describe the upflow of pure water in the xylem, downflow of sucrose solution in the phloem and the possible interaction between xylem and phloem. Chemically nothing interesting happens in the phloem. On the other hand, the physical process is not trivial. Factors such as the number and length of sieve tubes, sieve plate porosity, plasmodesmatal frequency, sap viscosity, phloem tube wall elasticity and many others, do not affect the chemistry of metabolites, but do affect the amount of and rate at which solutes are delivered to the stem tissue [49, 94, 103].

Phloem unloading Phloem unloading can possibly occur via symplastic or apoplastic routes [65]. Which route dominates in sugarcane is still a contentious issue. A symplastic route has been proposed by Komor [45]. Current opinion considers it to be a mix between the two routes

[72]. It is possible that modelling could provide an indication of the preferred pathway or partitioning between the pathways.

Storage This is $\mathbf{M}_{\beta}$. The current work elaborates on this model. Specific additions are listed in Section 1.4. The main points are the following:

Respiration A significant amount of carbohydrates are diverted into glycolysis, ranging from 31% (flux into glycolysis as a fraction of glucose uptake by the cell), in internode 3, to 13% in internode 10 [7]. The decrease is correlated to an increase in maturity of internodal tissue.

Fibre formation Carbohydrates are also stored in the form of insoluble fibre. A possible means of increasing sucrose accumulation would be to reduce the amount of fibre formed. The plant clearly needs fibre for structural support and stalk erectness is correlated to sucrose yield [4]. Modelling could in theory point the way to the optimal reduction in carbon partitioning to fibre.

Vacuolar and apoplastic storage Current opinion insists that sucrose is stored in the vacuole. If phloem unloading is primarily symplastic this leaves the apoplast as an extra possible compartment for storing sucrose. The relatively small volume of the apoplast compared to the vacuole would mean that the larger amount of sucrose would probably still be found in the vacuole. It is also argued that the only way sucrose can be mobilised again is via conversion to fructose and glucose by acid invertase [2]. Sucrose mobilisation would in all likelihood accompany sucker formation. Suckers are stalks growing from the sugarcane base and are morphologically distinct from the main stalk, as well as stalks formed during tillering. They usually appear late in the growing season and are characterised by high fibre- and low sucrose content. Sucker formation would lead to loss of sucrose in the main sugarcane stalk. Understanding of vacuolar storage mechanisms is important.

A more detailed description of each point under the storage heading is given in Chapter 3.

Roots Little is known about the biochemistry of the sugarcane root system, but its importance is undisputed. Recent studies have started to investigate the sugarcane root system [86].

Water Water content in plants is influenced by uptake in the roots and transpiration by the leaves. Photosynthetic rates decrease with applied water stress, this is probably due to stomatal closure to prevent water loss [20]. Similarly it has been shown that short-term flooding either increases photosynthetic rates or has no effect on photosynthesis [27]. Water content is also strongly correlated to internode maturity, with younger internodes having the higher water per gram dry mass values [52]. It is speculated that rapidly growing tissue requires more water.

The biochemistry behind water uptake, distribution and allocation to tissue would certainly affect metabolism in stems and leaves and, naturally, models of these organs as well.

Minerals Inorganic nutrients are also introduced into the plant via the roots. Nitrogen is required for amino acid synthesis, phosphorous is required for all nucleoside phosphates and sodium & potassium are important in osmotic control. These are just some of the requirements and possible functions associated with mineral uptake. High soil nitrogen content has also been linked to suckering and as mentioned sucker formation is best avoided to maximise sucrose yield [5].

1.3.2 Genetic control and signalling

It is possible for groups of reactions to affect the behaviour of other reaction networks without significant mass transfer occurring. Examples of this would be:

1. The effect on metabolism by the transcription and translation of metabolic enzymes. Enzyme number affects the maximal velocity of an enzyme, however enzyme number is not necessarily linearly correlated to the amount of mRNA transcripts. A theoretical framework in which to model this type of control has been suggested by [34].
2. Allosteric control by sugars, present in nano- to picomolar concentrations (e.g. $Fru\text{-}2,6\text{-}P_2$ on *PFP*) can change metabolic behaviour [88]. Modelling these effects would improve the resolution of enzyme behaviour.
3. Growth hormones, such as the gibberillins, indirectly affect compartmental volumes, which in turn affect every item under the compartmentation discussion above [26, 58].

1.4 Proposed extensions

A comprehensive model of sucrose accumulation would have to take into account some, if not all, the points discussed above. This study takes the standard current model one step closer to a complete kinetic description of this process by making the following extensions to $\mathbf{M}_\beta$:

1. Hexose phosphate intermediates will be converted to $Fru\text{-}1,6\text{-}P_2$ via *PFK* and *PFP*.
2. $Fru\text{-}1,6\text{-}P_2$ will be drained into glycolysis by *ALD*.
3. A fraction of the hexose phosphate pool will be diverted into fibre formation by addition of *UDPGDH* catalysed conversion of *UDPGlc* to *UDPGA*.
4. *SuSy* and *FRK* catalysis will be explicitly modelled in terms of the individual, respective enzyme isoforms.

A rationale for inclusion of each of the above enzymes in the model is given with their respective rate equations in Chapter 3.

The first two extensions will be collectively referred to as the glycolytic additions. Addition of *SuSy*- and *FRK*- isozymes to $\mathbf{M}_\beta$ will be called the isoform additions. *UDPGDH* is the fibre channel, where channeling does not refer to the phenomenon of "substrate channeling".

1.5 Aim and outline of this thesis

- Chapter 2 reviews reported sucrose concentrations in the literature and captures the available data into a test set with which to compare model predicted values.
- Chapter 3 describes extensions that are made to the original sucrose accumulation model of Rohwer and Botha. The model is then solved with activity parameter sets for internodes 3 to 10. An analysis of the model solution follows.
- Much of the programming used in building the model are custom written scripts. These scripts, data persistence, model checking with other software packages and automation of modelling is discussed in Chapter 4.
- Chapter 5 gives a detailed discussion of the work done. It then branches into a more general discussion, which includes future work that can be done and ends with a number of concluding statements.

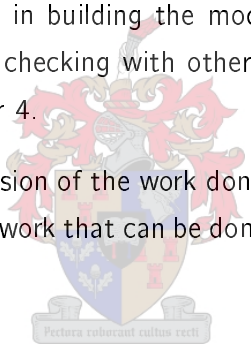

Chapter 2

A sugar test set

Given a particular parameter set, the steady-state solution of a kinetic model assigns unique values to state variables, provided that the steady-state is unique. In this study, sucrose, and to a lesser extent, fructose and glucose, are the metabolites of interest. The specific focus was on the metabolite concentrations in immature internodes. Model solutions are therefore interpreted as compartment specific concentrations measured in mmol l^{-1}. A collection of experimentally determined sugar concentrations provides a valuable data set with which to compare predicted sugar concentrations.

In general, experimentally determined sugar concentrations show two dominating trends with increasing internode maturity:

1. the sucrose concentration sample mean per internode increases as the glucose and fructose concentration sample means decrease,

2. the variance within an internode sample (and by implication the standard deviation) for sucrose concentrations increases up to internode 5 and then remains constant for the remaining internodes. The variance in the glucose and fructose concentrations decreases and then level out at internode 5.

A computational model of sucrose accumulation should ideally predict the changes in mean concentration while staying inside the boundaries set by the standard deviation. Both conditions need to be true, since it is conceivable that a downward trend in the means may be predicted while not straying out of the space of allowable sugar concentrations. The origin of the increasing variance is discussed in Section 2.2.

Understandably, a model designed to calculate a steady state may in effect never reach physiological sugar concentrations, purely because of limitations in the model. In such a case, mimicking the trend in sugar concentration changes would, in effect, be the model's main goal.

A vast amount of information on sugar concentrations exists in the literature and the purpose of this chapter is to discuss where values were obtained, what the original values were, how they

were converted to a common unit and consolidated into a cohesive test set against which model predicted values may be compared.

2.1 Harvesting numbers from the literature

Sucrose concentrations as originally reported Values for sucrose concentrations were collected from various literature sources (Table 2.1) and captured in a Gnumeric spreadsheet (www.gnumeric.org). Where values were read from a graph, the images were enlarged using software from The Gnu Image Manipulation Project ("The GIMP", www.gimp.org) and values were digitized using a pixel counting tool. All subsequent calculations were performed with Gnumeric or the R statistical package (www.r-project.org). 27 usable datasets were obtained from 8 different sugarcane varieties together with one dataset that had no variety specified. Data sets 1 to 8 represented hybrids between two of the varieties, *LA Purple* and *Mol*5829. Data sets 23 to 27 were measured in *Q*124 for 5 different harvest times, representing sample points from the summer growing season. 4 data sets each were found for fructose and glucose, see references in Table 2.6.

Units and supplementary data The disparity in units reported in the literature requires extra data to be obtained. The units of concentration can be divided into four classes;

a moles or mass sugar per unit sugarcane dry or fresh mass

b fraction (percentage) sugar on a dry or fresh mass basis

c moles sucrose per unit compartmental volume

d moles or mass per unit protein

The extra information needed to convert all concentration values to mmol l^{-1} is as follows;

1. for items **a**, **b** and **d** above, the cellular volume per unit fresh mass per internode is required,
2. the total amount of protein in an internode is needed for item **d**,
3. item **c** can be left as is,
4. items **a** and **b** may require a ratio of dry mass to fresh mass to eliminate the dry mass terms.
5. Compartmental volume ratios are needed to calculate distribution of sugars between compartments.

Table 2.1: Sucrose concentration ranges, their units, sugarcane variety and literature reference. abbreviations: DM - Dry mass, FM - Fresh mass.

Data Set	Range	Units	Varietal	Reference	Internodes
1	155 - 462	μmol/g FM	*LA Purple*	[117]	Ranges are for internodes 3 to 11, with even numbered internodes not measured
2	29 - 471		9043*		
3	12 - 291		9045*		
4	21 - 446		9052*		
5	10 - 279		9066*		
6	35 - 387		9068*		
7	10 - 273		9069*		
8	13 - 309		9076*		
9	9 - 406		9096*		
10	26 - 35		*Mol*5829		
11	11 – 55	% DM	*H*33/1937	[24]	5,7 and 10
12	1.5 – 8	% FM	*H*33/1937		5 to 10
13	100 - 542	mg/g DM	*N*19	[11]	3 to 10
14	28 -203	μmol/mg protein		[9]	3,6,9 and 12
15	29 - 186	μmol/mg protein		[77]	3,6 and 9
16	43 - 186	mmol l^{-1}		[7]	3,6 and 9
17	132 - 293	μmol/g FM	*US* 6656-15	[8]	3,6 and 11
18	113 - 283				
19	138 - 504	mg/g DM	*NCo*376	[12]	3 to 10
20	0.6 - 1.3	mmol/g DM		[113]	3 to 10
21	40 - 436	mmol l^{-1}	Not specified	[44]	3 to 10
22	10 - 46	% DM	*Q*117	[73]	3 to 10
23	5 - 118	mg/g FM	*Q*124	[110]	3 to 10
24	13 - 68				
25	17 - 141				
26	25 - 139				
27	26 - 128				

* Hybrid between *LA Purple* and *Mol*5829

Table 2.2: Total mass of protein per sugarcane internode (mg/internode). The average of 4 data sets was used in calculations.

Internode					Average	s.d.
3	4.5	4.0	4.1	5.8	4.6	0.8
4	6.2	12.9	8.6	10.8	9.6	2.9
5	7.3	10.0	10.1	9.7	9.3	1.3
6	8.8	9.6	9.7	12.9	10.3	1.8
7	11.2	11.3	11.5	14.9	12.2	1.8
8	12.4	11.4	11.5	13.4	12.2	0.9
9	14.3	12.6	12.7	13.9	13.4	0.9
10	15.6	15.1	15.1	14.1	15.0	0.6
References	[113]	[11]	[11]	[12]		

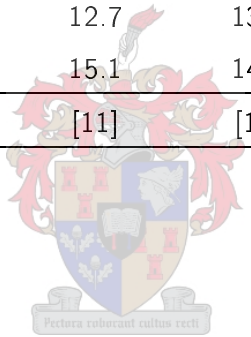

Table 2.3: The compartment volume per gram fresh mass per sugarcane internode (l /g FM)(S. Bosch, unpublished data).

Internode	Apoplast	Cell	Cytoplasm	Vacuole
3	8.56×10^{-5}	8.35×10^{-4}	1.09×10^{-4}	7.26×10^{-4}
4	8.84×10^{-5}	8.23×10^{-4}	1.05×10^{-4}	7.18×10^{-4}
5	9.06×10^{-5}	8.06×10^{-4}	1.01×10^{-4}	7.05×10^{-4}
6	9.20×10^{-5}	7.84×10^{-4}	9.61×10^{-5}	6.88×10^{-4}
7	9.29×10^{-5}	7.59×10^{-4}	9.12×10^{-5}	6.68×10^{-4}
8	9.44×10^{-5}	7.41×10^{-4}	8.72×10^{-5}	6.54×10^{-4}
9	9.68×10^{-5}	7.30×10^{-4}	8.41×10^{-5}	6.46×10^{-4}
10	9.97×10^{-5}	7.24×10^{-4}	8.16×10^{-5}	6.42×10^{-4}

Table 2.4: Compartmental volume ratios for internodes 3 to 10. (abbreviations: sym - symplast, apo - apoplast, vac - vacuole and cyt - cytoplasm)

Internode	$\frac{\text{apo}}{\text{cyt}}$	$\frac{\text{apo}}{\text{sym}}$	$\frac{\text{apo}}{\text{apo}+\text{sym}}$	$\frac{\text{cyt}}{\text{sym}+\text{apo}}$	$\frac{\text{sym}}{\text{sym}+\text{apo}}$	$\frac{\text{vac}}{\text{sym}}$
3	0.79	0.10	0.09	0.13	0.91	0.87
4	0.84	0.11	0.10	0.13	0.90	0.87
5	0.90	0.11	0.10	0.13	0.90	0.87
6	0.96	0.12	0.11	0.12	0.90	0.88
7	1.02	0.12	0.11	0.12	0.89	0.88
8	1.08	0.13	0.11	0.12	0.89	0.88
9	1.15	0.13	0.12	0.12	0.88	0.88
10	1.22	0.14	0.12	0.11	0.88	0.89

Conversion factors Since authors do not use consistent units of concentration, captured concentration values were coerced into consistent dimensions with the following data, as required by the criteria stipulated above. Factors calculated here are also used later to convert enzyme activities to a single comparable unit.

1. **Total protein mass per internode** Concentrations and enzyme activities are often reported as a function of the mass of total protein or some specific protein residing in a reference space. In this instance the total protein content of an internode is required to eliminate any protein mass terms in reported units. Four sets of data were used to calculate an average protein mass per internode. Data points for all relevant internodes were available (Table 2.2).

2. **Fresh mass to dry mass ratios** These values were obtained from the author of [10] as unpublished data. From these were calculated the metabolic volume per internode (Table 2.3).

3. **Volume ratios per internode** The ratio between apoplastic, cytoplasmic and vacuolar volume changes with internode maturity was calculated from two data sets. The first set was from [111] which calculated the apoplastic volume as a fraction of the total volume. The remaining symplastic volume is assumed here to be the total vacuolar plus cytoplasmic volume. The vacuolar to cellular volume ratio was found in [44], missing data values were inserted using a spline fit. See Table 2.4 for detail.

Estimating missing values Not all data sets obtained had values for the eight particular internodes (Table 2.1). Missing values were filled in by interpolation of the available data. Where possible, incomplete data sets had the available values converted to the appropriate units before a spline fit was performed. If values for internodes outside the range 3 to 10 were available then a smoothing spline interpolation could be performed directly. In cases where this could not produce a satisfactory fit, a better spline fit was obtained before unit conversion. Since the conversion factors themselves are nonlinear, a possible error propagation could occur. In all cases smoothing splines were selected that matched, or were very close to the predictor values. If data points outside the available data sets had to be estimated then anchoring predictors were borrowed from another data set with very similar concentration values. Only one value was introduced to such sets. Care was taken that the predicted values were close to the known predictor values thus ensuring that the point chosen only acted as an anchor for the spline. Data sets with three entries were completed by linear regression. This was only performed on data sets 11 and 12. The default values for the R functions (`smooth.spline` and `lm`) were used throughout. A typical spline fit procedure is shown in Example 2.1.

Assumptions and justification

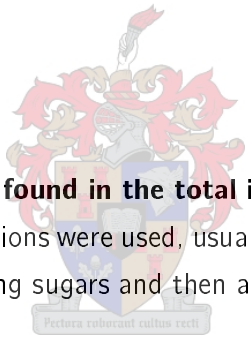

Concentrations represent sugars found in the total internode volume Where specified in the literature, whole stalk sugar extractions were used, usually along the lines of freezing a sample in liquid nitrogen, grinding it up, extracting sugars and then assaying for sugar quantity. For example see, materials and methods in [8, 117].

"Lateral" vs "vertical" distribution of sugars Sugar concentrations are treated separately for each internode, i.e. to each internode we assign a specific concentration. Furthermore sugars areassumed to be distributed evenly between vacuole and cytoplasm. There is some evidence to suggest that this is the case in sugarcane suspension cell cultures [70].

Sugars are homogeneously distributed within an internode Variations in metabolite concentration in an internode are sometimes reported, e.g. [77]. It is assumed that these are actually homogeneously distributed, so that concentrations are in effect an average concentration in an internode.

Compartment ratios remain constant through an internode Within an internode, vacuolar, apoplastic and cellular volumes are not consistent. We assume that a mean volume per compartment exists and that the fraction that each contributes to the total fresh internode volume remains constant.

Example 2.1 Example R-code of the smoothing spline routine used to fill in missing data points. All the points from data set 14 were used, i.e. reported concentrations from internodes 3,6,9,12 and 15. The $y output array shows the predicted concentrations.

```
> internodes <- seq(3,15,3)
> internodes
[1]  3  6  9 12 15
> concentrations <- c(28.7,138.3,190.5,203.5,291.6)
> concentrations
[1]  28.7 138.3 190.5 203.5 291.6
> spline_object <- smooth.spline(internodes,concentrations)
> spline_object
Call:
smooth.spline(x = internodes, y = concentrations)

Smoothing Parameter  spar= -1.217033  lambda= 1.193794e-14 (17 iterations)
Equivalent Degrees of Freedom (Df): 5.000001
Penalized Criterion: 1.075448e-19
GCV: 1.912538e-06
> new_internodes <- seq(3,10)
> new_internodes
[1]  3  4  5  6  7  8  9 10
> new_concentrations <- predict(spline_object,new_internodes)
> new_concentrations
$x
[1]  3  4  5  6  7  8  9 10

$y
[1]  28.70000  68.55824 105.92476 138.30000 163.55541 181.04654 190.50000
[8] 192.96088
```

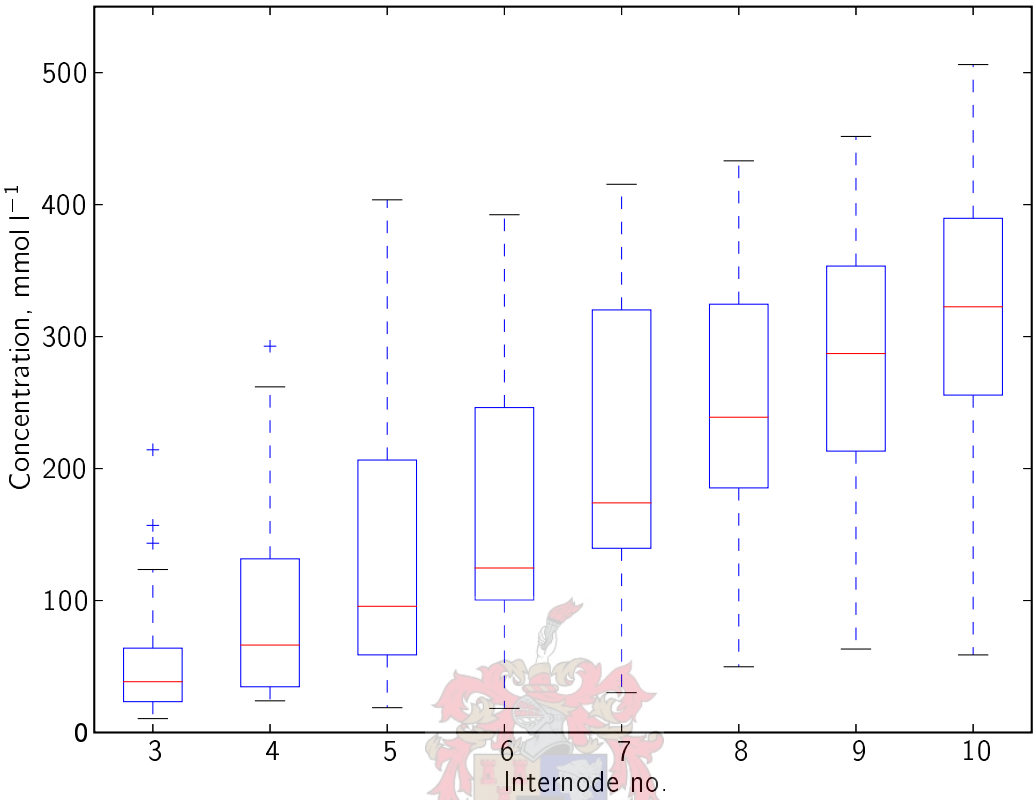

Figure 2.1: Boxplot showing the variation in sucrose concentration for internodes 3 to 10. Red lines are the median values, the box spans the inner quartile range (25% to 75%). Whiskers extend to the most extreme (minimum or maximum) value in the range, 1.5 times the range of the box. + indicates an outlier point.

2.2 Concentrations

Sucrose The converted and calculated sucrose concentrations are shown in Table 2.5 and the variation for each internode in Figure 2.1. The median values for each internode increases steadily from internode 3 to 10. The variance in concentration also increases with internode maturity. This is not unexpected, since the data set is composed of values taken from multiple varieties of sugarcane.

Fructose and glucose Less information on these sugars is available than for sucrose; 4 values each were found. The converted forms are shown in Table 2.6 together with the references of where they were found.

Table 2.5: Sucrose concentrations in mmol l^{-1} as calculated for internodes 3 to 10 from data found in the literature. See Table 2.1 for the origins of each set.

Data Set		3	4	5	6	7	8	9	10
1		25	50	90	125	117	240	319	333
2		123	172	223	278	337	395	452	506
3		33	76	162	278	362	360	353	434
4		23	109	223	305	343	343	356	430
5		38	77	147	246	322	325	317	373
6		14	28	56	100	148	186	226	285
7		11	24	50	84	126	179	257	366
8		15	33	63	106	140	148	172	256
9		11	26	50	78	107	140	188	257
10		11	35	49	36	72	219	365	390
11		29	29	19	18	30	50	63	59
12	Concentration (mmol l^{-1})	35	51	59	96	147	239	254	321
13		40	66	84	125	155	293	351	436
14		26	36	60	110	174	253	287	295
15		37	56	82	122	174	229	276	312
16		14	26	43	67	100	142	193	254
17		52	67	96	142	199	250	283	293
18		64	132	117	139	156	185	213	248
19		41	129	130	159	174	195	206	215
20		47	50	79	121	209	238	318	323
21		48	87	123	151	171	184	196	211
22		143	177	210	242	273	299	321	339
23		123	164	208	250	285	311	327	337
24		45	39	100	111	178	199	239	233
25		108	135	206	195	320	368	374	414
26		157	262	404	326	415	433	436	479
27		214	293	290	392	392	408	395	377
Median		38	66	96	125	174	239	287	323
Mean		57	90	126	163	208	252	286	325
s.d.		53	72	89	94	104	93	89	96

Table 2.6: Glucose and fructose concentrations in mmol l^{-1} as calculated for internodes 3 to 10 from data found in the literature. (abbreviations: conc. - concentration)

Internode	3	4	5	6	7	8	9	10	Reference
					Glucose				
Conc.	71.6	61.7	52.5	44.9	39.2	34.9	31.7	29.5	[8]
	89.6	68.0	48.0	31.1	18.9	10.7	5.9	3.7	[8]
	8.1	14.4	11.1	10.4	7.9	5.2	2.6	1.1	[9]
	26.4	24.0	21.7	19.6	17.7	16.0	14.5	13.1	[7]
Median	49.0	42.8	34.8	25.4	18.3	13.4	10.2	8.4	
Average	48.9	42.0	33.3	26.5	20.9	16.7	13.7	11.9	
s.d.	38.1	26.8	20.1	14.9	13.1	12.9	13.0	12.9	
					Fructose				
Conc.	78.0	63.4	49.8	38.2	29.4	22.8	18.2	15.1	[8]
	82.3	63.4	45.9	31.1	20.2	12.8	8.2	5.8	[8]
	7.3	12.6	9.7	9.5	8.0	6.6	4.9	3.7	[9]
	32.8	33.5	34.0	33.9	33.2	32.0	30.6	29.3	[7]
Median	55.4	48.4	39.9	32.5	24.8	17.8	13.2	10.4	
Average	50.1	43.2	34.8	28.2	22.7	18.5	15.5	13.4	
s.d.	36.3	24.8	18.0	12.8	11.2	11.2	11.6	11.7	

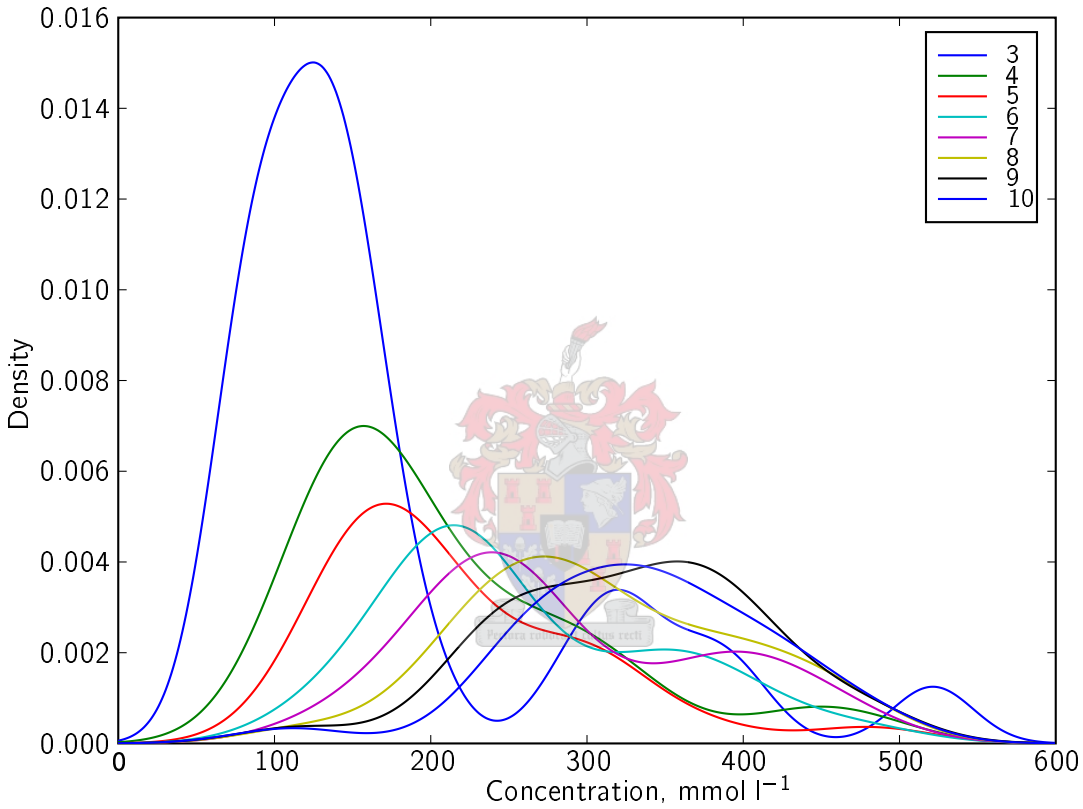

Figure 2.2: Density estimation plots of sucrose concentrations per internode. With increasing internode number, both the mean value and standard deviation are clearly increasing. Three peaks can be seen for internode three, see text for detail. These slowly disappear as the internodes mature.

Variation in the concentration values The amount of sucrose accumulated by sugarcane is subject to many factors. It should be kept in mind that the values captured here should be treated as a snapshot of what the possible sugar concentrations can be and not a definitive assertion of what the model predictions should be. The major factors that influence these experimental values are briefly summarised here.

1. **Varieties** Sugarcane is an allopolyploid, in other words huge genomic variability is the norm rather than the exception in hybrids. Given the long history of sugarcane cultivation to yield successively higher sugar yields, it is no surprise then that assaying different varieties will yield wildly different results [3, 56]. This is in great part due to significant differences in carbon partitioning between varieties [6, 7, 113]. An indication of this can be seen in Figure 2.2, internode 3. The three separate peaks are the result of differences in sucrose concentration. These peaks "blend" with internode maturity to produce the increasing standard deviation.

2. **Environment** Sucrose accumulation has been positively correlated with season, diurnal temperatures and light levels and water availability amongst other factors [25, 50, 52]. Relative abundance of nitrogen and phosphorous, and other minerals, as well as disease affect possible sucrose concentrations [2, 104].

3. **Experimental procedures** Invariably techniques for quantifying sugar amounts differ between researchers and are themselves subject to error. This further introduces differences in reported sucrose concentration values. The extent of methodological variability is pure conjecture since it is impossible to compare researchers' implementations of experimental protocols. A theoretical treatment of this phenomenon is given in [38].

2.3 The expected sugar profile of a kinetic model compared to experimental values

A chimeric model needs to be compared to representative experimental data There is no consistent sugar concentration profile in sugarcane as it matures. The only invariant that one may safely assume is that sucrose concentration increases as internodes mature, with concomitant increase in the variability of this concentration. The possibility exists for building variety-specific models. This requires all data, model parameters and comparative test data (metabolite concentrations) to be measured from one plant. This has yet to be done comprehensively.

The kinetic parameters used in building $\mathbf{M}_{\beta}$ and $\mathbf{M}_{\delta}^{(i)}$ (Table 1.1) are not representative of a single variety of sugarcane. As a consequence, the chimeric nature of the model requires the model outputs to be interpreted as a "general" solution. Alternatively stated, a model is expected to approximate or converge on the mean sugar concentrations when solved with a number of different

sets of initial conditions. This also presupposes that external metabolites are not clamped, such that realistic time course data may be obtained. Using the sugar concentrations as reported in Table 2.1 is therefore justified. The spread in the sugar test set provides the necessary variance in which such a solution should fit and still retain the important property, i.e. an increase in sucrose accumulation.

This chapter discussed an empirical sugar test set as a standard with which to compare theoretical model predictions. The next chapter describes building and analyzing such a model.

Chapter 3

Model extensions

Large models are difficult to construct. Exactly what constitutes a large model is subjective, but with each reaction that is added to a model the scope for making mistakes increases. The original sucrose accumulation model was reviewed in Chapter 1 and will be expanded in this chapter. The scope in which internodal sucrose concentrations may fall was discussed in Chapter 2. This chapter will now describe how the original model was elaborated upon to encompass more features of the sucrose accumulation process in sugarcane. Reactions will be added or modified sequentially and after each change an analysis is performed to determine the effect of the change on the model.

Recall that $\mathbf{M}_\alpha$ is the original sucrose accumulation model of Rohwer and Botha, $\mathbf{M}_\beta$ is the current standard model of Schäfer et al and $\mathbf{M}_\delta^{(i)}$ is the model as proposed in this work (Table 1.1 summarises this notation). Section 3.1 will describe the transition from $\mathbf{M}_\beta$ to $\mathbf{M}_\delta^{(i)}$. Model parameters are only changed if they affect the reaction being modified. At the end of this process we have a model with certain reactions that have not been adjusted at all. The maximal velocities for the modified reactions come from a cohesive set of velocities that span a number of internodes [12]. This set is not commensurate with those used by Rohwer and Botha [76], and it is preferable to use values that were measured under similar conditions or as close to similar as possible. Chapter 5 discusses in more detail the choice of kinetic parameters. Maximal velocities for the unmodified reactions, where available, are changed after all the reaction modifications have been introduced. Section 5.1 in Chapter 5 further describes differences and properties of partially and completely parameter substituted models with each other and with $\mathbf{M}_\beta$. In the remainder of the current chapter, Section 3.2 then delivers an in depth analysis of the fully substituted model solutions to internodes 3 to 10.

3.1 Building $\mathbf{M}_{\delta}^{(i)}$

$\mathbf{M}_{\delta}^{(i)}$takes account of two reactions for which isozymes have been characterised, three enzymes that drain metabolites into glycolysis and a reaction that channels hexoses into polysaccharide synthesis other than sucrose.

This model excludes the vacuole as an explicit compartment. Many studies of sugarcane vacuoles and tonoplast vesicles have been performed [23, 47, 68, 69, 70, 89, 91, 92], including kinetic studies of sucrose- and glucose uptake. Despite intensive investigation, the mechanism of sucrose uptake is still badly understood. Especially illustrative is the disparity between uptake rates in tonoplast vesicles from sugarcane parenchymal tissue and vacuoles from suspension cultures [23, 69]. Attempts at explicitly modelling vacuolar storage of sucrose have thus far been unsuccessful (data not shown). It is believed that an acid stable invertase isozyme is almost exclusively localised in the vacuole. It is also proposed that regulation of sucrose accumulation is largely due to acid invertase activity [117]. Vacuolar sucrose accumulation cannot be ignored. The mathematical description of this phenomenon will however have to wait for better experimental data to become available.

Sucrose, glucose and fructose transport across the cell envelope (by implication apoplastic sugar uptake) have also been investigated in tissue disks and suspension cultures [46, 98]. The claim has been made that phloem unloading is primarily symplastic [45]. A clear understanding of the route of uptake as well as mechanisms of assisted transport is lacking. The available data was not incorporated into $\mathbf{M}_{\delta}^{(i)}$ and the original sugar uptake rate equations and parameters of $\mathbf{M}_{\alpha}$ were retained.

Partitioning of carbon to starch is not included in the model either. Experimental data indicate that the flux into starch synthesis is negligible when compared to flux into fibre formation, respiration and storage [7] (Section 3.2.1 and Table 3.5).

One of three global paths can be taken by carbohydrates in storage parenchyma, viz. respiration, storage or structural. With the addition of the *UDPGDH* reaction, a representative reaction of each possible route is now included.

3.1.1 Methods

$\mathbf{M}_{\delta}^{(i)}$will be described in terms of the mass transfer between metabolites (the stoichiometry), the rates of conversion from one metabolite to another (the rate equations and ordinary differential equations) and the "fixed" terms in the rate equation (the input parameters). The nullcline intersection point of all the differential equations is the steady-state concentrations and fluxes of the system.

Our approach is to build $\mathbf{M}_{\delta}^{(i)}$ from $\mathbf{M}_{\beta}$ one reaction set at a time, comparing its influence on the model to $\mathbf{M}_{\beta}$ in a cursory analysis. Reaction parameters are changed from the $\mathbf{M}_{\beta}$ parameters

only when the reaction is new or an existing reaction is modified. Steady-state solutions (SSS) and a metabolic control analysis (MCA) are computed after each addition.

Steady-state solutions of a model In this study a set of Ordinary Differential Equations (ODEs) and a model are synonymous terms. Similarly, we also speak of the solution to a model or set of ODEs as being one and the same thing. In a steady-state analysis we are interested in the solution to a model where concentrations and fluxes do not change over time. The definition of a steady-state is given in Section 1.1. An important assumption is made when talking about SSS, that is that the physiological interpretation of such a solution holds true, i.e. that rates and concentrations in a cell are in fact time-invariant. This assumption is valid when looking at small time scales, where drastic changes in state variables are unlikely to happen. Another important feature of a steady-state is that it is only valid for a specific set of conditions. Cells are subjected to ever changing environments and if environmental conditions change, the conditions inside the cell change. This change in environment is reflected as a change in the parameters that govern a kinetic model, which in turn will lead to a different SSS, leading to the concept of a quasi-steady-state. At small time scales fluxes and concentrations in a cell are in steady-state, but this steady-state is itself also changing with time and over larger time scales we can no longer talk about a steady-state, but only a partial- or quasi-steady-state. Solutions to a model thus provide a snapshot of conditions in a cell. In other words, real living systems are *governed* by second or higher order differential equations, whereas kinetic modelling most frequently uses ordinary differential equations as a first order approximation to *describe* living systems. Describing living systems in terms of higher order differential equations requires, amongst other things, more experimental parameter data, larger computations and novel theoretical frameworks in which to work. Combined, these factors make first order approximations much simpler to solve, but with a concomitant trade-off in model accuracy. The difference between the steady-state as predicted by a model with static parameters and a quasi-steady-state that in all likelihood exists in a living cell should always be kept in mind when inferences are made about the one from the other.

Metabolic control analysis One of the central tenets of MCA is that control over a metabolic pathway can be shared between participating enzymes, rather than being located in a so-called "rate-limiting enzyme". Enzyme rates are dependent on substrate-, product- and modifier concentrations (collectively called species). An enzyme can be said to be under the control of every other enzyme that may affect these species concentrations. Since the same reasoning applies to a "controlling" enzyme one may conclude that every enzyme exerts some degree of control over every other enzyme. This is an intuitive, though slightly simplified, description of MCA. The degree of control can be quantified. Control coefficients can be associated with every enzyme indicating the fraction of the total control that it has on every other enzyme rate and species concentration.

When a system of reactions is at steady-state, control coefficients can be calculated by altering an enzyme rate by an infinitessimally small amount and tracking the changes in all enzyme rates and species concentrations as the system settles into a new steady-state. The change is usually called a perturbation or modulation and the change in an enzyme rate or species concentration is a response.

A control coefficient is defined as,

$$C_i^y = \frac{(\partial \ln |y| / \partial p_i)_{p_k}}{(\partial \ln |\nu_i| / \partial p_i)_{s_j, p_k}} \tag{3.1}$$

where y is the state variable (concentration or flux) responding to a modulation and i is an independent reaction step. p_i is the modulated parameter that directly affects i, p_k is every other unmodulated parameter and ν_i is the rate of reaction i. Response of ν_i to a perturbation is measured at constant substrate and product s_j. This definition is a modification of the original control coefficient definition due to Kacser & Burns and Heinrich & Rapoport [29, 39]. In this definition, control coefficients are a function of enzyme rate rather than the number of enzymes. The adaptation was neccesary to take account of systems with moiety-conserved cycles, branches and futile cycles [41].

Software Software is an integral part of modern mathematical modelling. A number of tools exist that specifically address problems in computational systems biology [75]. These include Jarnac (http://www.sys-bio.org/software/jarnac.htm,[79]), JWS Online [87] and SBW (http://sbw.kgi.edu, [36, 37]). Chapter 4 will deal with software and programming in more detail.

All calculations were performed on an IBM G40 Thinkpad personal computer with the PySCeS suite of cellular simulation software (www.pysces.sourceforge.net,[63]). The interpreted programming language, Python (www.python.org), was used to manipulate data and script routines not available in PySCeS [62]. Calculations were verified by comparing SSS of $\mathbf{M}_\delta^{(5)}$using Jarnac and PySCeS. Greater detail on how the models were programmed and verified can be found in Chapter 4.

3.1.2 Model delineation and stoichiometry

The reactions and stoichiometry of $\mathbf{M}_\delta^{(i)}$ are outlined in Diagram 3.1. SuSy and FRK are modelled in terms of their respective isozymes as opposed to single reactions with averaged kinetic parameters. Partitioning to glycolysis includes *PFK*, *PFP* and the draining reaction is Aldolase. The only new reaction is *UDPGDH*, which drains hexose phosphates into *UDP*-Glucuronic acid (*UDPGA*). *UDPGlc*, *Fru-6-P*, *Glc-6-P* and *Glc-1-P* are assumed to be in equilibrium and are modelled as a single equilibrium block. Values for these metabolite concentrations are calculated as fractions of the total hexose phosphate pool, by using the equilibrium constants for the reactions, and substituted into

Diagram 3.1 The working model of sucrose accumulation in sugarcane storage parenchyma. This is the core model of Rohwer and Botha with *PFP*, *PFK*, *SuSy A, B & C*, *FRK A & B* and *UDPGDH* added. Diagonal dotted lines indicate transport steps across a membrane and solid lines indicate reaction steps. Rectangular frames indicate clamped metabolites. Ratios in brackets indicate reactant stoichiometry, if absent, stoichiometry is (1:1).

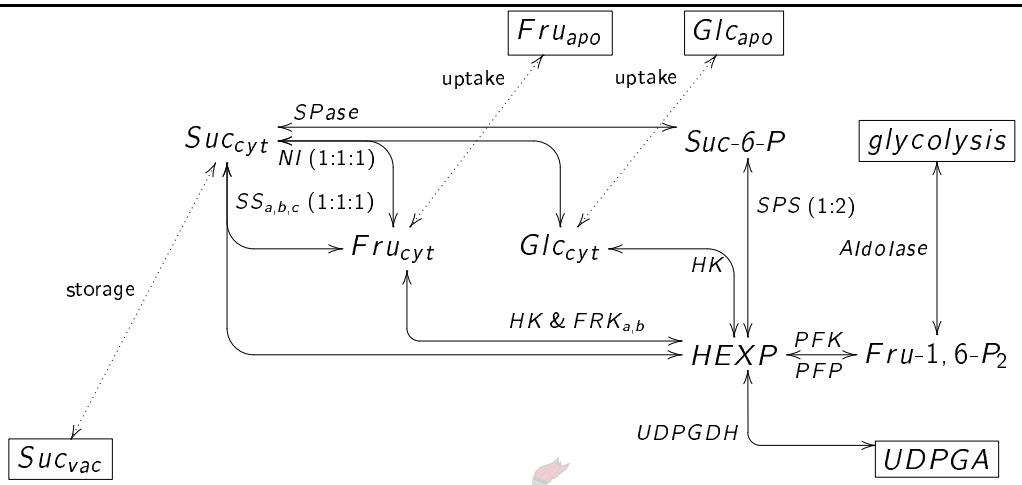

the rate equations upon numerical evaluation. This is the identical approach followed by Rohwer and Botha [76].

3.1.3 Glycolytic enzymes

Whereas $\mathbf{M}_\beta$ had metabolites drawn off to glycolysis directly from the hexose phosphate pool, $\mathbf{M}_\delta^{(i)}$ introduces a branched two-reaction path inbetween the hexose phosphate pool and the rest of glycolysis. The first step is catalyzed by two enzymes, *PFP* and *PFK*, and the second by Aldolase. This would be a trivial addition, had it not been for a) the reversibility of PFP and b) the allostery of both enzymes. This property introduces yet another futile cycle into the model, since it is now possible for hexoses to circulate between the *Fru*-1, 6-P_2 and hexose phosphate pools. ATP can act as a modifier of PFK behaviour, but since ATP concentration is clamped in this model, allosteric inhibition cannot be modelled. *Fru*-2, 6-P_2 is an activator of *PFP* [88], and can theoretically become another control point in the model. The allostery of these two enzymes is therefore not explicitly included, but the scope for doing so exists. In the final model *PFP*, *PFK* and Aldolase replace the original glycolytic reaction, R10, draining *Fru-6-P* into glycolysis. The maximal velocities for the glycolytic enzymes are shown in Table 3.2 and the kinetic parameters in Table 3.3.

The rate equations of the glycolytic enzymes

PFP *PFP* was modeled as a reversible two substrate two product Michaelis-Menten type rate equation assuming equilibrium binding of substrates and products.

$$\nu_{PFP} = \frac{\frac{V_{PFP}}{{}^{PFP}K_m^{Fru6P} \times {}^{PFP}K_m^{PP_i}} \left(\left[Fru6P\right]\left[PP_i\right] - \frac{\left[Fru\text{-}1,6\text{-}P_2\right]\left[P_i\right]}{{}^{PFP}K_{eq}} \right)}{\left(1 + \frac{\left[Fru\text{-}6\text{-}P\right]}{{}^{PFP}K_m^{Fru\text{-}6\text{-}P}} + \frac{\left[Fru\text{-}1,6\text{-}P_2\right]}{{}^{PFP}K_m^{Fru\text{-}1,6\text{-}P_2}}\right) \times \left(1 + \frac{\left[PP_i\right]}{{}^{PFP}K_m^{PP_i}} + \frac{\left[P_i\right]}{{}^{PFP}K_m^{P_i}}\right)} \tag{3.2}$$

PFK Phosphofructokinase was modelled as a two-substrate Hill type equation (Hofmeyr, Rohwer & Hanekom, in preparation)

$$\begin{aligned} \nu_{PFK} &= \frac{V_{PFK}\alpha\beta}{\frac{1+\mu}{1+\sigma^{4h}\mu} + \frac{(\alpha+\beta)\left(1+\sigma^{2h}\mu\right)}{1+\sigma^{4h}\mu} + \alpha\beta} \\ \text{where} \quad \alpha &= \left(\frac{\left[Fru6P\right]}{Fru6P_{0.5}}\right)^h \\ \beta &= \left(\frac{\left[ATP\right]}{ATP_{0.5}}\right)^h \\ \mu &= \left(\frac{\left[ATP\right]}{ATP_{0.5}^{modifier}}\right)^h \\ \sigma &= \text{coefficient of modification} \end{aligned}$$

Aldolase The Aldolase reaction (Diagram 3.1) is described by an irreversible Michaelis-Menten mechanism.

$$\nu_{ALD} = \frac{V_{ALD}\left[Fru\text{-}1,6\text{-}P_2\right]}{{}^{ALD}K_m^{Fru\text{-}1,6\text{-}P_2} + \left[Fru\text{-}1,6\text{-}P_2\right]} \tag{3.3}$$

The effect on $\mathbf{M}_\beta$ of adding the glycolytic enzymes

Steady state The new steady-state metabolite concentrations and fluxes after including *PFK*, *PFP* and *ALD* are shown in Figure 3.1 and Table A.1. If $Fru\text{-}1,6\text{-}P_2$ is clamped at too high a value (in this case 1 mmol l^{-1}), then the addition of either *PFP* or *PFP* and *PFK* leads to a negative flux through *PFP* (data not shown). Unclamping $Fru\text{-}1,6\text{-}P_2$ and adding *ALD* removes this negative flux. Flux through glycolysis for the $\mathbf{M}_\beta$+pfp+pfk+ald model is approximately four times less than

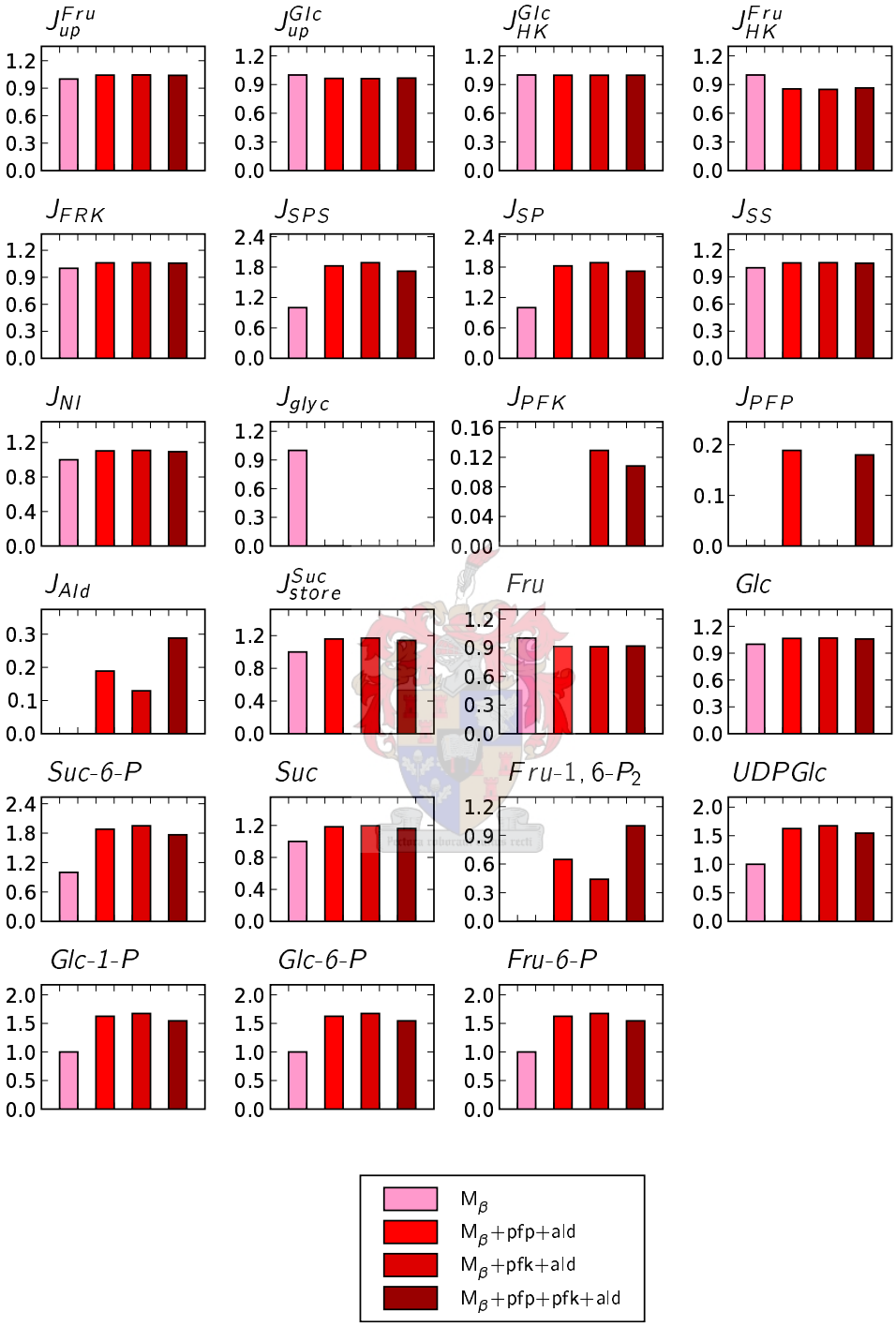

Figure 3.1: The relative changes in steady-state concentrations and fluxes of $\mathbf{M}_\beta$+pfp+ald, $\mathbf{M}_\beta$+pfk+ald and $\mathbf{M}_\beta$+pfp+pfk+ald compared to $\mathbf{M}_\beta$. Values are normalised against the reference value in $\mathbf{M}_\beta$, except *PFP*, *PFK* and *ALD* which are normalised against the original flux to glycolysis, J_{glyc}, and $Fru\text{-}1,6\text{-}P_2$ which is normalised against the $Fru\text{-}1,6\text{-}P_2$ concentration from $\mathbf{M}_\beta$+pfp+pfk+ald. The legend shows which additions were made.

that of the original model. This is despite the higher maximal velocities of the glycolytic enzymes compared to the glycolysis step in $\mathbf{M}_\beta$. The steady-state concentration for $Fru\text{-}1,6\text{-}P_2$ is very low. Compared to experimental values of approximately 0.63 mmol l^{-1} for internode 3 and 0.52 mmol l^{-1} for internode 6 this is a clear underestimation [8]. We did not specifically look for the concentration of $Fru\text{-}1,6\text{-}P_2$ at which flux through *PFP* becomes negative. It is possible that *PFP* may act as a "safety valve", pushing $Fru\text{-}1,6\text{-}P_2$ back into the general hexose phosphate pool if the glycolytic path is saturated or demand for $Fru\text{-}1,6\text{-}P_2$ decreases.

Metabolic control analysis The control exercised by the glycolytic enzymes in $\mathbf{M}_\delta^{(i)}$ and the glycolysis step in $\mathbf{M}_\beta$ is shown in Figure 3.2. Only the control exercised by these enzymes are shown. In the original model, glycolysis had a greater control over the other variables in the system. The addition of *PFP*, *PFK* and *ALD* eliminated most of this control. The maximal velocities for these three enzymes are all larger than the original glycolytic V_{max} and the rate equations for *PFP* and *PFK* include cofactor terms. These two properties of the model could account for the disappearance of the control. This would also explain why *PFP* and *PFK* had the most control over their own flux. *ALD* only exercised substantial control over $Fru\text{-}1,6\text{-}P_2$. This is because *ALD* is the only enzyme using $Fru\text{-}1,6\text{-}P_2$ as substrate. From the steady-state analysis it was seen that the model predicts a low $Fru\text{-}1,6\text{-}P_2$ concentration. It is possible that the discrepancy between the experimental and calculated concentrations are largely due to *ALD* not being modelled correctly. *ALD* could possibly have had a maximal actvity that is too high or *PFK* should have a higher rate. Studies that have focused only on *PFP* and *PFK* have reported maximal activities of up to double the values we used. These values were not used in our model because of reasons discussed in Chapter 5.

3.1.4 The isoform additions

The degree of control that a particular reaction step has on a metabolite concentration is not as easily discernable where multiple isozymes exist for catalysing a specific reaction. The reason is that isozymes each have their own distinct kinetic parameters that govern their behaviour. From previous studies it is known that isoform profiles are strongly correlated to phenotype [90]. As an example, peroxidase and esterase isozyme profiles indicate the degree of de-differentiation of subcultured calli initiated from sugarcane leaves [15]. If the ability to accumulate sucrose is considered a phenotype, then it possible that different isozyme profiles can effect different internodal sucrose concentrations. This is again because of the different kinetics of each isozyme, but also because the expression profiles for isozymes may change in different tissues. This prompted the inclusion of as much isozyme data as was possible. *HK*, *FRK*, *TPP* and *SuSy* have known isozymes [8, 31, 82]. *TPP* and *HK* are not modelled since the former forms part of the trehalose pathway and the latter

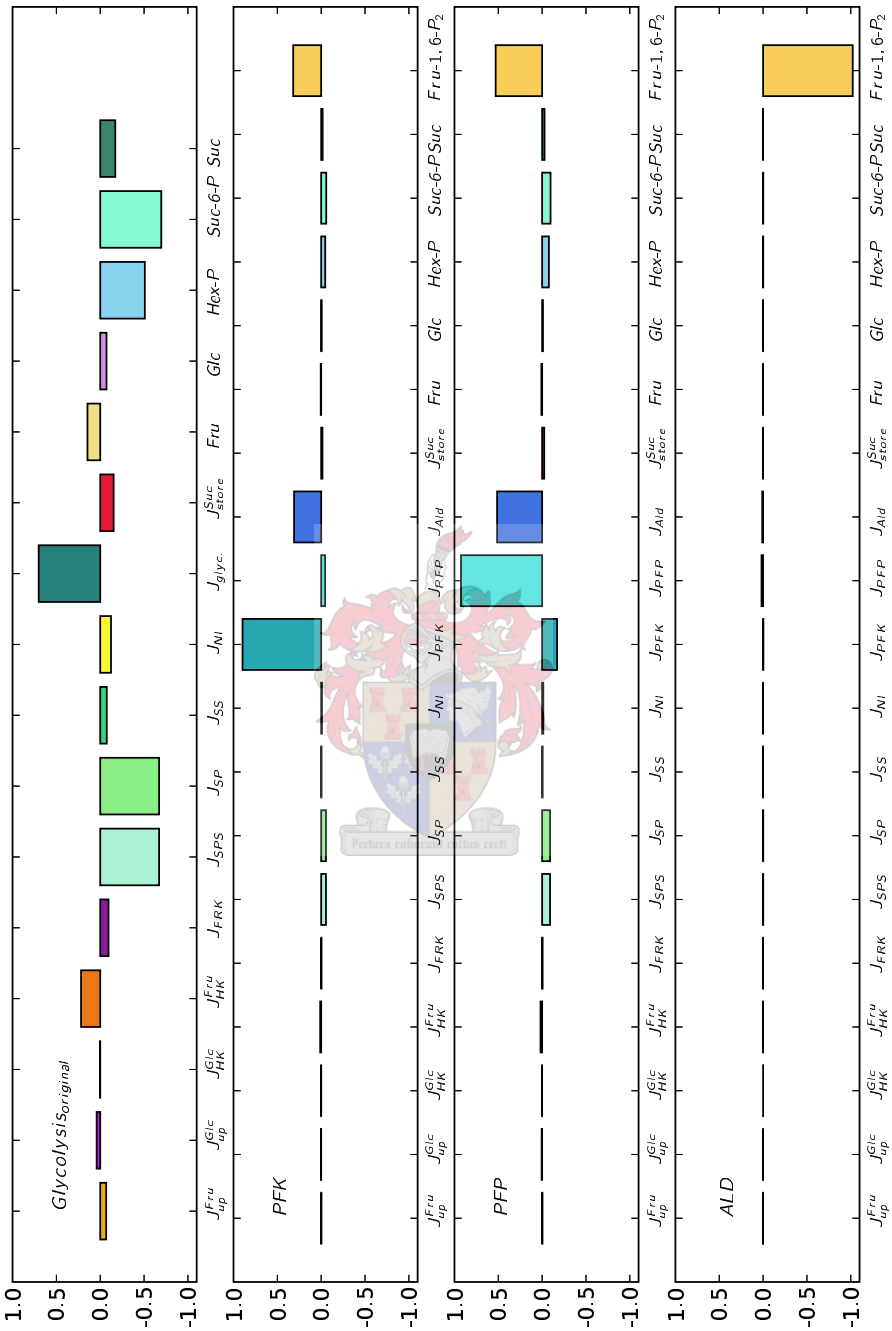

Figure 3.2: Flux and concentration control coefficients for $\mathbf{M}_\beta$ with the glycolytic enzymes added. Parameters are those for internode 5. The label in the upper left hand corners indicate the modulated reaction and the x-axis shows the response variables.

has a paucity of kinetic data. Only *FRK* and *SuSy* are included.

The plethora of isozymes in plants comes as no surprise when the number of homologues for a particular alelle is considered. Unfortunately a biochemical analysis of the accompanying enzymes is not as simple as finding the responsible nucleic acid transcripts. Characterising isozymes allows a finer resolution from a kinetic analysis of a reaction network.

SuSy rate equations and calculation of individual isozyme maximal activities

Three forms of *SuSy* have been studied and are simply denoted *SuSy A, B & C* [82]. These differ significantly in terms of their kinetic properties, K_m values, and specifically V_f/V_r ratios (see below). The original reversible ordered bireactant mechanism was used for *SuSy C* since inhibitor data exists for this form [76, 80]. *SuSy A & B* were modelled using a reversible two substrate two product Michaelis-Menten type rate equation assuming equilibrium binding of substrates and products.

$$\nu_{SS\,a,b} = \frac{\dfrac{-V_{SS\,a,b}}{{}^{SS\,a,b}K_m^{Suc} \times {}^{SS\,a,b}K_m^{UDP}}\left([UDP][Suc] - \dfrac{[Fru][UDPGlc]}{{}^{SS}K_{eq}}\right)}{\left(1 + \dfrac{[UDPGlc]}{{}^{SS\,a,b}K_m^{UDPGlc}} + \dfrac{[UDP]}{{}^{SS\,a,b}K_m^{UDP}}\right) \times \left(1 + \dfrac{[Fru]}{{}^{SS\,a,b}K_m^{Fru}} + \dfrac{[Suc]}{{}^{SS\,a,b}K_m^{Suc}}\right)} \tag{3.4}$$

where $\nu_{SS\,a,b}$ is the rate of *SuSy A & B* in the breakdown direction, $V_{SS\,a,b}$ is the maximal velocity of *SuSy A & B*, K_m^S are Michaelis constants with respect to metabolite S, and ${}^{SS}K_{eq}$ is the equilibrium constant for the reaction. $\nu_{SS\,a,b}$ and ${}^{SS}K_{eq}$ are defined in terms of the *sucrose breakdown* reaction. The model reaction is defined in the direction of *sucrose synthesis*. In keeping with the approach of Rohwer and Botha to obtain positive steady-state fluxes, the negative sign was appended [76].

Individual SuSy isozyme activities Maximal activities are not always available for individual isozymes. For the three *SuSy* isozymes the individual V_f/V_r ratios, total combined V_f/V_r and total combined V_f have been measured [81, 82]. It should be noted that inconsistencies exist in the experimental data. The smallest breakdown/synthesis ratio measured was 0.0791 for *SuSy A*, the largest was 0.426 for *SuSy C* [82]. The highest combined breakdown/synthesis ratio for total sucrose synthase is reported as approximately 1.5 in [81]. These sets of measurements are clearly incompatible with each other since no combination of isozymes could give such a large total breakdown/synthesis ratio. Hence, the following assumptions were made to calculate forward maximal velocities for each isozyme:

Table 3.1: Factors used in calculating individual isoform forward maximal activities. Values for *SuSy* represent fractions of the total *SuSy* forward maximal velocity, those for *FRK* represent the ratio of *FRK B* to *FRK A* forward maximal velocities. See text for details.

	Internode (i)							
Enzyme	3	4	5	6	7	8	9	10
SuSy A	0.427	0.298	0.210	0.145	0.096	0.057	0.026	0.000
SuSy B & C	0.287	0.351	0.395	0.427	0.452	0.471	0.487	0.500
$\frac{FRKB}{FRKA}$	1.100	0.866	0.719	0.618	0.543	0.486	0.441	0.404

1. *SuSy A* maximal activity decreases, whereas *SuSy B* maximal activity increases with internode maturity. This assumption is based on a comparison of the elution profiles from affinity chromatography studies where *SuSy* isozymes were extracted from non sucrose-accumulating leaf roll tissue and mature sucrose-accumulating internode 9. The ratio of the *SuSy A* activity peak to that of *SuSy B* decreased from 14.5 to 0.88 [82].

2. *SuSy C* was only extracted from sugarcane tissue collected during winter and *SuSy A* and *SuSy B* from autumn collected tissue. *SuSy B* and *SuSy C* always eluted at the same salt concentration producing similar chromatogram peaks. It was impossible to further separate this peak into individual *SuSy B* and *SuSy C* peaks. Since it is beyond the scope of this project to model seasonal changes in sugarcane, but rather to produce a more general sucrose accumulation model, it was decided to include all three isozymes and treat *SuSy B* and *SuSy C* maximal activity as equal.

3. A linear gradient of the total synthesis/breakdown ratio was calculated by assuming that immature, non sucrose-accumulating internode 1 had only *SuSy A* present (i.e. equivalent to leaf roll tissue) and internode 10 had only *SuSy B* and *SuSy C* present. It was also assumed that *SuSy B* and *SuSy C* had equal forward maximal activities (see the point above).

4. We treated the breakdown direction of sucrose as the forward reaction, since this is the direction that *SuSy* is assayed in most often. The V_f/V_r ratios are less than one in all three cases, implying that the maximal rate of synthesis is higher than that of sucrose breakdown. *SuSy A* has the lowest V_f/V_r ratio and was expected to contribute the most to sucrose synthesis, whereas *SuSy C* has the highest ratio and was expected to contribute the most to sucrose breakdown.

It was assumed that $V_f^{SS\,b} = V_f^{SS\,c}$ (the maximal forward activities for *SuSy B* and *SuSy C* are equal) which gives $V_f^{SS\,a} + 2V_f^{SS\,b} = Y$ where $Y = V_f^{total}$ (the total, combined forward maximal

activity). If we let $\frac{V_f^{SS\ a,b,c}}{V_r^{SS\ a,b,c}} = A, B, C$ and $X = \frac{Y}{V_r^{total}}$ then,

$$\begin{aligned}
\frac{Y}{X} &= V_r^{total} \\
&= \frac{V_f^{SS\ a}}{A} + \frac{V_f^{SS\ b}}{B} + \frac{V_f^{SS\ c}}{C} \\
&= \frac{Y - 2V_f^{SS\ b}}{A} + \frac{V_f^{SS\ b}}{B} + \frac{V_f^{SS\ b}}{C} \qquad (3.5) \\
\frac{Y}{X} - \frac{Y}{A} &= V_f^{SS\ b}\left(-2A^{-1} + B^{-1} + C^{-1}\right) \\
V_f^{SS\ b} &= Y\left(\frac{X^{-1} - A^{-1}}{-2A^{-1} + B^{-1} + C^{-1}}\right)
\end{aligned}$$

and substitution yields,

$$V_f^{SS\ a} = Y\left(1 - 2\left(\frac{X^{-1} - A^{-1}}{-2A^{-1} + B^{-1} + C^{-1}}\right)\right) \qquad (3.6)$$

where A, B, C, X and Y are constants. We have experimental data for all of these, though experimentally determined X contradicts values measured for A, B, C [81, 82] (see above). A linear gradient of increasing X was calculated by setting X to 0.0791 (V_f/V_r for *SuSy A*) for internode 1 and 0.372 for internode 10. The value of 0.372 was calculated by setting the forward maximal velocity for *SuSy A* to 0 and solving for a total breakdown/synthesis ratio using eqs. 3.5 and 3.6. This value lies between the breakdown/synthesis ratio of 0.33 for *SuSy B* and 0.426 for *SuSy C* as one would expect. The calculated *SuSy* distribution factors are summarised in Table 3.1. From this we can calculate a forward velocity for *SuSy A, B & C* (Table 3.2). Kinetic parameters are shown in Table 3.3.

The effect on $\mathbf{M}_\beta$ of modelling SuSy in terms of isozymes

Steady state Steady-state properties differ depending on how the total *SuSy* activity is distributed between the three forms (Figure 3.3 and Table A.2 in the Appendix). Differences in the steady-state properties depend on how maximal activities were allocated to each isozyme. As a first approximation the total forward maximal velocity was distributed equally between the isozymes. Figure 3.3 shows that the difference between this model and $\mathbf{M}_\beta$ is quite substantial in some cases. For example, J_{HK}^{Fru} is approximately 3 times lower, J_{FRK} is about 50% higher and the fructose concentration is about 2.5 times lower than previously. Total sucrose synthesis by *SuSy* was identical regardless of whether or not each enzyme had an equal share of the total maximal activity or adjusted *SuSy* activities (see Table A.2). Assigning the individual isozyme activities as outlined in

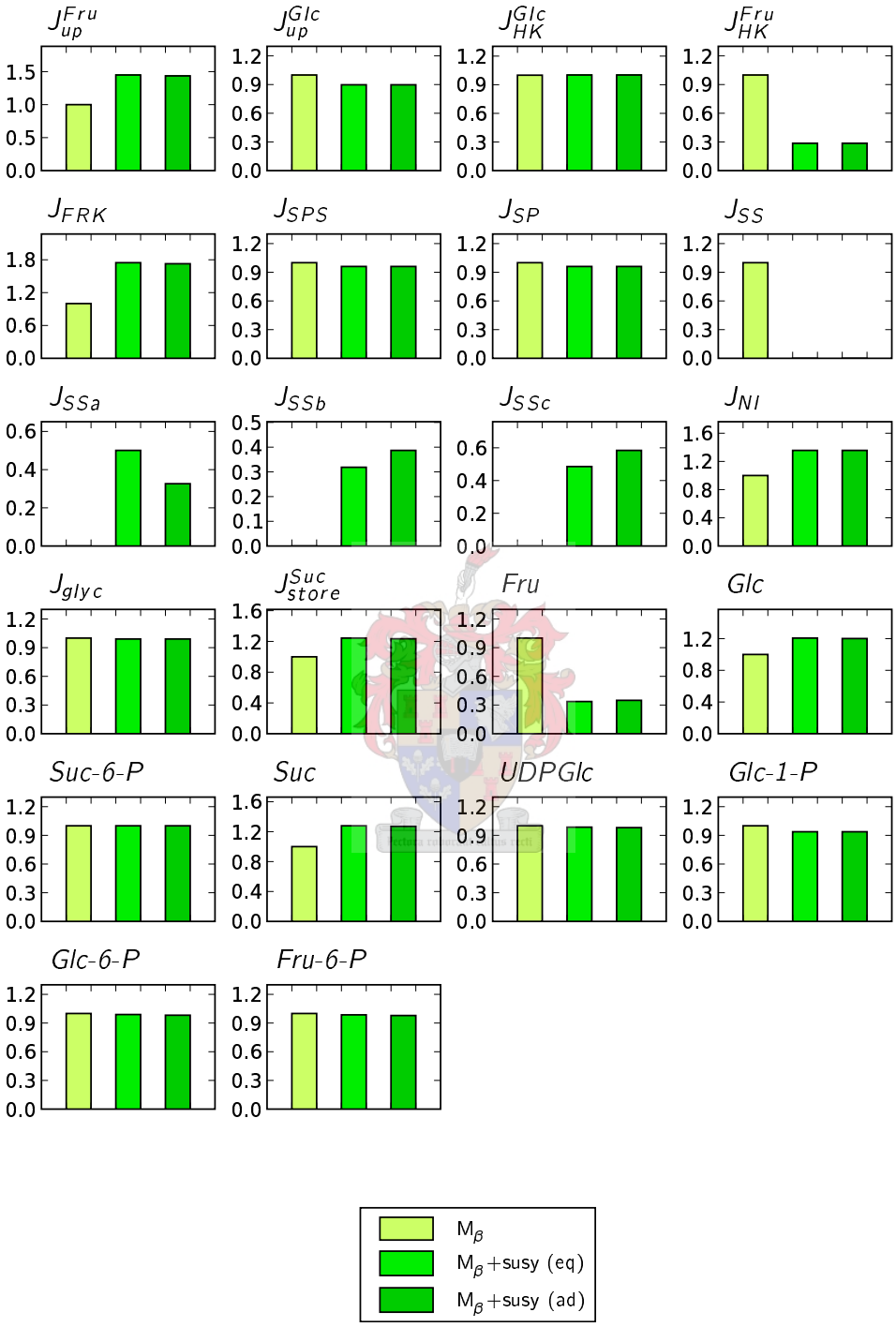

Figure 3.3: The relative changes in steady-state concentrations and fluxes of $\mathbf{M}_\beta$+susy (eq) and $\mathbf{M}_\beta$+susy (ad) compared to $\mathbf{M}_\beta$ where "eq" and "ad" respectively refer to equal and adjusted (according to Table 3.1) distribution of maximal forward activity between isozymes. Values are normalised against the reference value in $\mathbf{M}_\beta$, except for the fluxes through the *SuSy* isozymes which are normalised against the original flux through *SuSy*, J_{SS}. The legend shows which additions were made.

Equations 3.5 and 3.6 resulted in a steady-state total *SuSy* flux that was approximately 30% higher than the original steady-state solution of $\mathbf{M}_\beta$. It can be speculated that this change is due to the two different types of equations being used to model the *SuSy* isozymes. If the steady-state rate through *SuSy C* is calculated first using the generic equation (as used for *SuSy A & B* in this work) without Haldane adjusted parameters, second with adjusted parameters, and third with the ordered bi-reactant mechanism (as used by [76]), we find that for steady-state values of $\mathbf{M}_\beta$ +susy we get 0.170, 0.044 and 0.076 mM/s respectively. For steady-state values of $\mathbf{M}_\delta^{(5)}$we obtain 0.112, 0.030 and 0.060 mM/s. In the first case the generic equation gives rates much higher than the ordered equation, in the second case much lower values are obtained. Clearly, correcting parameters to fit the Haldane relationship does have an effect on the steady-state rate through an enzyme. In the thermodynamically correct case, where the K_m are adjusted before substitution into the generic equation, the ordered mechanism equation gives a higher rate than the generic equation. $\mathbf{M}_\beta$+susy, however, shows 30% higher total flux through *SuSy*. It cannot be unambiguously concluded that the presence of any product inhibition terms in the ordered reaction gives rise to this increase.

When going from equal to adjusted distribution os *SuSy* isozyme activities, the steady-state flux through each isozyme changed with a change in its respective forward maximal activities, but left the total flux through *SuSy* unaffected. The *Suc* concentration is higher than the original model for both models shown in the figures and table (equal and adjusted distribution of forward maximal velocities). Sucrose flux into the vacuole was also higher when the *SuSy* isozymes were added.

Metabolic control analysis The MCA for the model was done for the adjusted distribution of the maximal activities. The three isozymes had the most control over themselves and negative control over each other. This is not really surprising since they all compete for the same substrate. This would also explain why all three enzymes had negative control over flux through fructose phosphorylating hexokinase. In all cases the relationship

$$C_{SS_a}^{J_x} : C_{SS_b}^{J_x} : C_{SS_c}^{J_x} = J_{SS_a} : J_{SS_b} : J_{SS_c} \tag{3.7}$$

was true where J_x is any steady-state flux other than through the *SuSy* isozymes. Any enzyme has a certain amount of control over the fluxes and concentrations in a system. This control is shared by the isoforms of that enzyme. The size of the fraction of that control vested with an isoform is proportional to the size of the flux carried by that isoform.

FRK rate equations and calculation of individual isozyme maximal activities

Fructokinase only phosphorylates fructose as opposed to hexokinase, which takes both *Glc* and *Fru* as substrates. This enzyme occurs as two known isozymes, labeled *FRK A & B*. The rate equations used in the original characterisation were used to model the respective catalysis [31, 32].

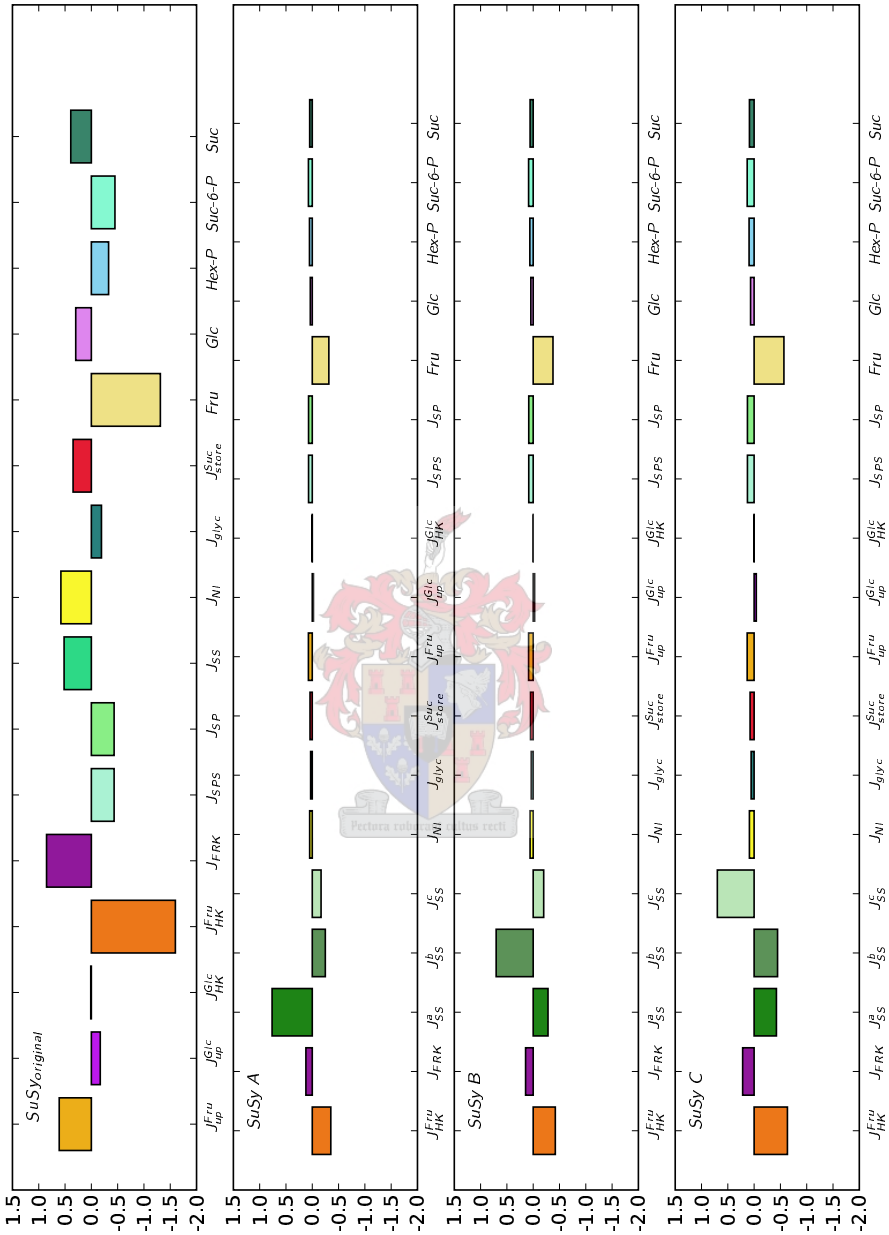

Figure 3.4: Flux and concentration-control coefficients for $\mathbf{M}_\beta$ with the sucrose synthase isozymes added. *SuSy* maximal activity was distributed between the isozymes according to Table 3.1.

$$\nu_{FRK\,a} = \frac{V_{FRK\,a}[Fru][ATP]}{^{FRK\,a}K_m^{ATP}[Fru] + ^{FRK\,a}K_m^{Fru}[ATP] + [Fru][ATP]} \tag{3.8}$$

$$\nu_{FRK\,b} = \frac{V_{FRK\,b}[Fru][ATP]}{^{FRK\,b}K_m^{ATP}[Fru] \times \left(1 + \frac{[Fru]}{^{FRK\,b}K_i^{Fru}}\right) + ^{FRK\,b}K_m^{Fru}[ATP] + [Fru][ATP]} \tag{3.9}$$

Individual isozyme activities The total forward maximal activity for *FRK* was allocated to the two isoforms based on the ratio of maximal forward velocities for *FRK A* and *FRK B*, obtained from [31]. From this data set the reported ratio $V_f^{FRK\,B}/V_f^{FRK\,A}$ of 0.72 was used to allocate a forward velocity to each isozyme for the internode 5 model analysed here. In [31], only three internodes (3, 5 & 9) were sampled for activity ratios. Ratios for the other internodes were extrapolated from a hyperbolic curve ($f(x) = m/x^n, m = 2.747, n = 0.833$) that was fitted to the three data points. A non-linear least squares routine from the R statistical package was used to perform the fit. It should be added that the parameters m and n have no physical interpretation and that a hyberbolic durve was selected purely on the basis of providing the best fit. The fitted values are shown in Table 3.1, the maximal activities in Table 3.2 and the kinetic parameters in Table 3.3.

The effect on $\mathbf{M}_\beta$ of modeling FRK in terms of individual isozymes

Steady state The steady-state concentrations and fluxes can be seen in Figure 3.5 and Table A.3 in the Appendix. Despite the lower total maximal velocity for FRK, the total flux through both isozymes is approximately 22% more than for *FRK* in $\mathbf{M}_\beta$. Despite the lower *Fru* concentration in the modified model, the $[Fru]/^{FRK\,a}K_m^{ATP}$ ratio for *FRK A* (the *FRK* isozyme carrying the majority of the flux) is higher, translating into a higher $\nu_{FRK\,a}/V_{FRK\,a}$ ratio. Invertase, glycolytic and sucrose storage flux increase. *Suc* does not increase much compared to $\mathbf{M}_\beta$.

Metabolic control analysis The total contribution of *FRK* to the control of flux through all reactions decreases with the addition of the isozymes. Regardless of this, the control profile of *FRK* remains the same. Control of the *FRK* specific fructose phosphorylation is not shared between the two isozymes. *FRK B* only has control over itself. This is probably because of the low flux through *FRK B*. It could be speculated that the decreased control over *Fru* accounts for the decreased control over *Suc*. If *FRK A* is less capable of mobilising its own substrate, competitive enzymes may increase the use thereof.

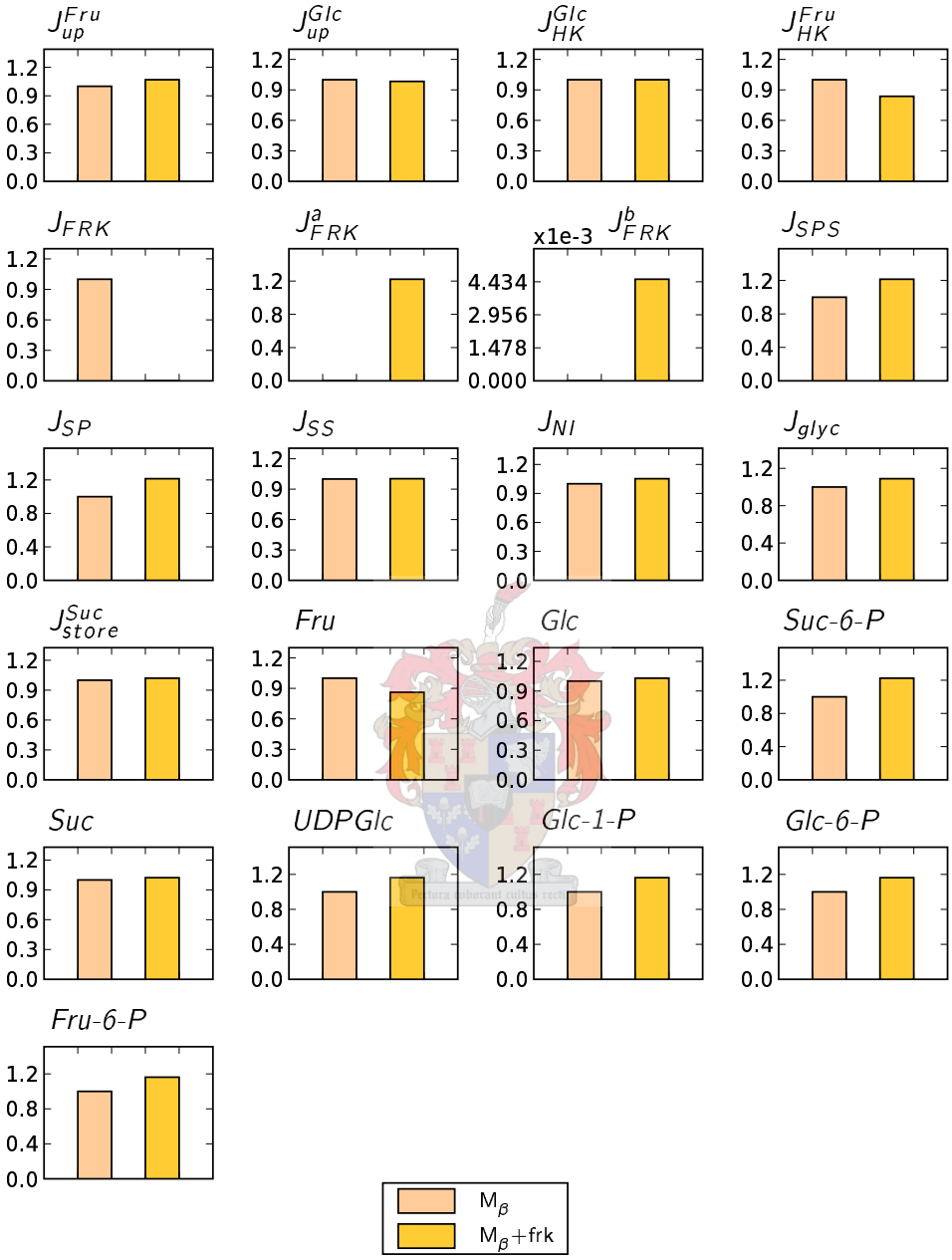

Figure 3.5: The relative changes in steady-state concentrations and fluxes of $\mathbf{M}_\beta$+frk compared to $\mathbf{M}_\beta$. Values are normalised against the reference value in $\mathbf{M}_\beta$. The legend shows which additions were made. *FRK* maximal activities were distributed between the two isoforms according to Table 3.1.

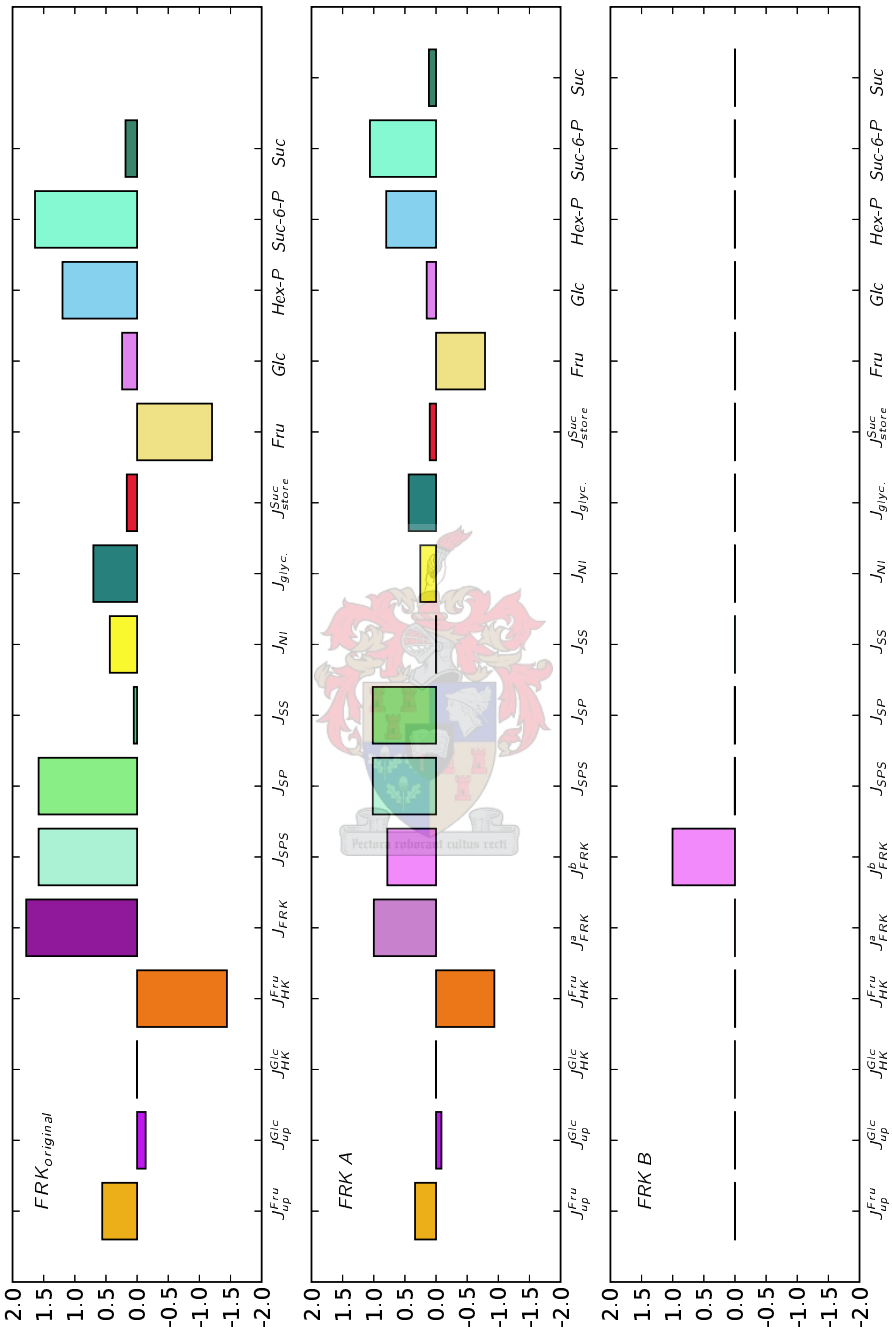

Figure 3.6: Flux and concentration-control coefficients for $\mathbf{M}_\beta$ with the fructokinase isozymes added. The x-axis shows the response variables, perturbations are in *FRK*.

3.1.5 Fibre

The rate equation of UDP-Glucose dehydrogenase

The inclusion of *UDPGDH* in the model introduces the third possible route that carbohydrates can follow in the sugarcane culm. This is a four electron transfer reaction and the net stoichiomety for this step is,

$$UDP\text{-Glucose} + 2NAD^{+} \rightarrow UDP\text{-Glucoronic acid} + 2NADH$$

UDP-Glucoronic acid is the precursor to pectin and hemicellulose, which in turn are the building blocks of extracellular matrix polysaccharides [100]. Storage and respiration are accounted for in the model and this reaction ensures that the hexose phosphate pool can be used for fibre formation. UDPGDH was modelled as an irreversible bi-uni-uni-bi reaction, using a three substrate Michaelis-Menten equation [100].

$$\nu_{UDPGDH} = \frac{V_{UDPGDH}\left[UDPGlc\right]\left[NAD^{+}\right]^{2}}{{}^{UDPGDH}K_{m}^{UDPGlc} \times {}^{UDPGDH}K_{m}^{NAD^{+}}\left[NAD^{+}\right] + 2\left({}^{UDPGDH}K_{m}^{NAD^{+}}\left[UDPGlc\right]\left[NAD^{+}\right]\right) + {}^{UDPGDH}K_{m}^{UDPGlc}\left[NAD^{+}\right]^{2} + \left[UDPGlc\right]\left[NAD^{+}\right]^{2}} \quad (3.10)$$

The effect of adding the fibre channel to M_{β}

Steady state The estimation of the *UDPGDH* maximal velocity is discussed in more detail in Section 3.1.6. The initial steady-state concentrations showed J_{UDPGDH} to be substantially higher than the flux to glycolysis (J_{10}) in the original model. This was inconsistent with experimental data [7], where the carbon allocation to fibre, as a percentage of glucose uptake and glycolytic flux, was approximately 16% and 30% respectively. The UDPGDH maximal velocity was lowered to adjust for this. The differences can be seen in Table A.4 in the Appendix.

Metabolic control analysis Only UDPGDH itself had any significant control over J_{UDPGDH} ($C_{UDPGDH}^{J_{UDPGDH}} \approx 1$). *UDPGDH* was able to exert negative control over a number of different fluxes, the largest being J_{SPS} and J_{SP} (Figure 3.8). *UDPGDH* and *SPS* both compete for *UDPGlc*. Since *UDPGDH* is modelled with an irreversible mechanism, *UDPGlc* is removed from the system which negatively impacts on flux through *SPS*. This is also reflected by the negative control *UDPGDH* has over *Suc-6-P* and the hexose phosphate pool. Flux to glycolysis and the vacuole is negatively impacted as well. This is also due to the removal of the respective precursor molecules from the system.

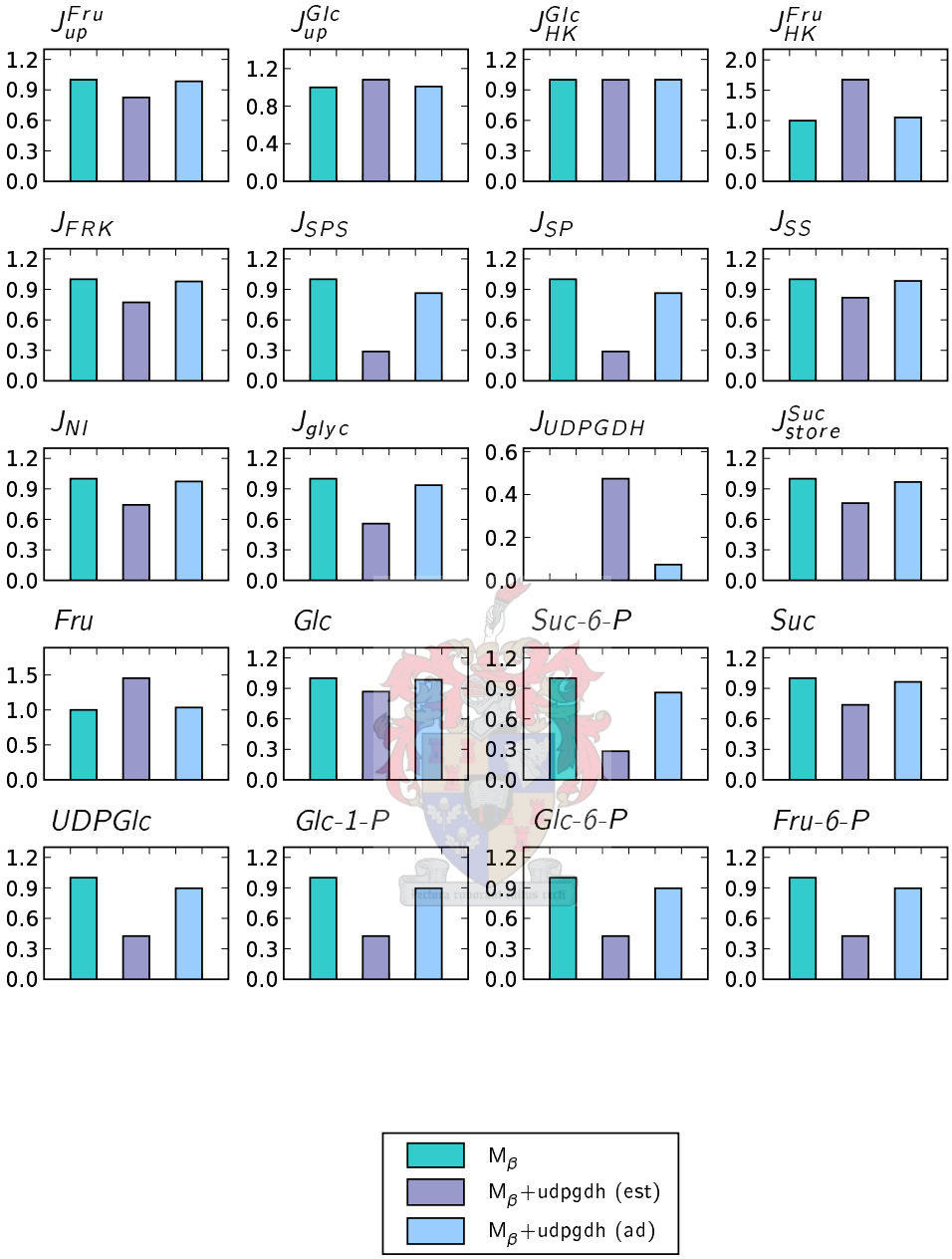

Figure 3.7: The relative changes in steady-state concentrations and fluxes of $\mathbf{M}_\beta$+udpgdh (est) and $\mathbf{M}_\beta$+udpgdh (ad) compared to $\mathbf{M}_\beta$ where "est" and "ad" are the two models where the *UDPGDH* maximal velocity was respectively estimated and adjusted (see discussion on p.45). Values are normalised against the reference value in $\mathbf{M}_\beta$, except for J_{UDPGDH} which is normalised against J_{up}^{Glc} from the original model. The legend shows which additions were made.

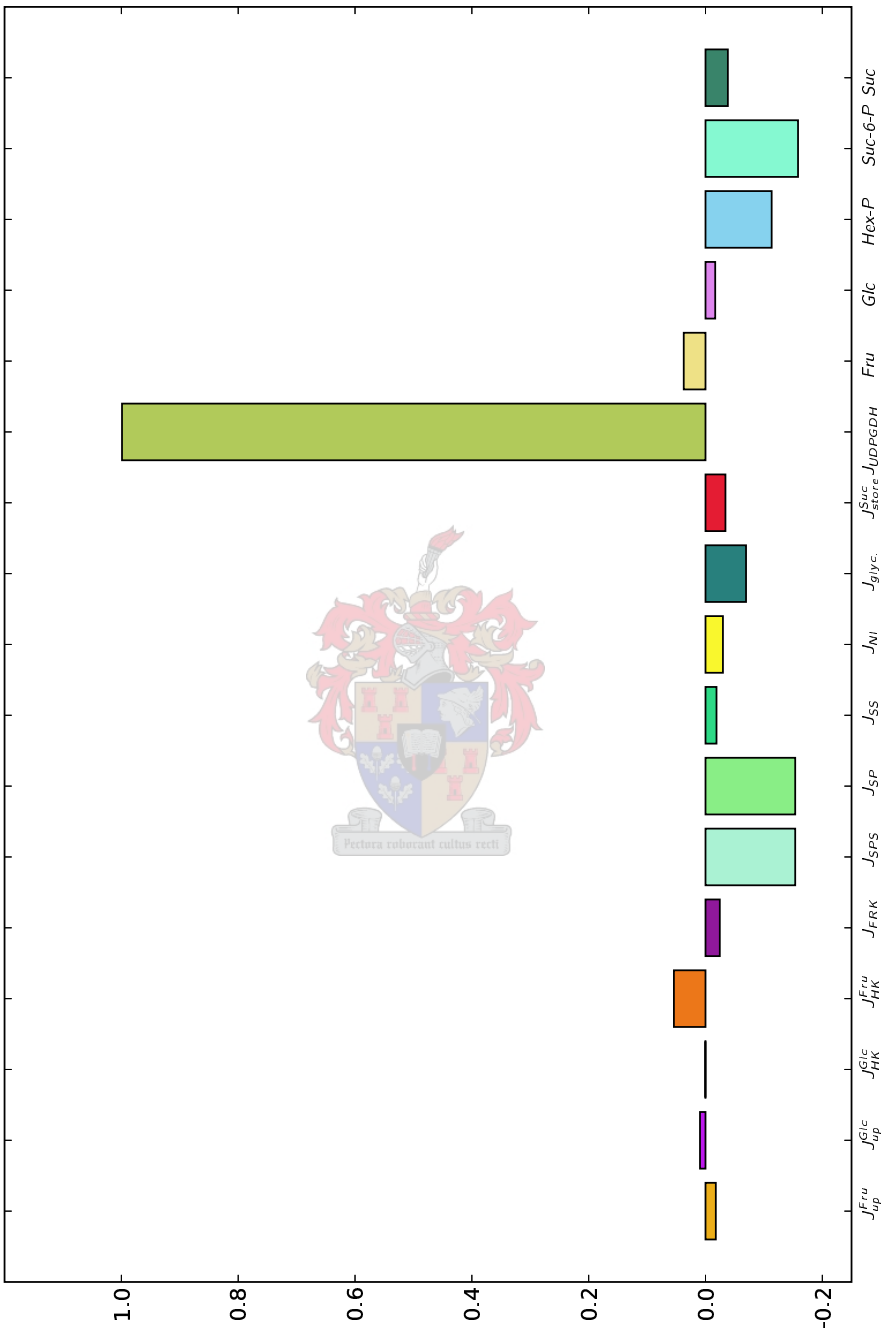

Figure 3.8: Flux and concentration control coefficients of *UDPGDH* for $\mathbf{M}_\beta$+udpgdh added.

3.1.6 Input parameters

The previous sections have outlined individual additions to he sucrose accumulation model, i.e. inclusion of the glycolytic reactions *PFP*, *PFK* and *ALD*, incorporation of isozyme details for *SuSy* and *FRK*, as well as addition of a branch to fibre synthesis. The present section will discuss in more detail the parameter changes that were introduced in making the model extensions.

Kinetic parameters were collected from a number of different literature sources. Reported enzyme maximal activities have large variation in their value. Ideally all activities should be measured under identical circumstances and preferably from the same source tissue and if possible by the same person. We assumed that all reported activities are maximal activities, these are summarised in Table 3.2. All parameters are *in vitro* measurements.

Activities that change with internode maturity

These activities restrict the model to the chosen internodes, i.e. 3 to 10, since enzymes from these are assayed most frequently. The experimental values used were usually reported as moles substrate converted per mass of total protein. A change in this quantity reflects a change in enzyme number. Changes in internode volume are accounted for in the conversion to our unit of choice, mmol $l^{-1}min^{-1}$. Conversion factors are the same as in Section 2.1. These two factors allow the extension of the model to various internodes since they transform the specific activities into a profile of catalytic activity changes during internode maturation.

UDPGDH A specific activity value (2.17 µmol min^{-1} mg $protein^{-1}$) was obtained for UDPGDH from [100]. Using this parameter after a unit conversion to mmol $l^{-1}min^{-1}$ led to serious numerical instability of the differential equation solvers employed. A reduced estimate was made by lowering the maximal velocity by one order of magnitude. This gave high steady-state flux values, which were absurd compared to *in vitro* flux measurements of [7]. V_{UDPGDH} was subsequently adjusted so that the steady-state flux to fibre as a fraction of glucose uptake matched experimental determinations.

Vacuolar sucrose uptake The vacuole uptake step acts as a sink, hence it is irreversible. This is not implausible, since uptake can occur against against a concentration gradient. No indication of saturation at physiological concentrations seem to exist [69]. Keeping the maximal uptake rate of 1 mmol $l^{-1}min^{-1}$ as used in $\mathbf{M}_\alpha$ ensured that the enzyme will not saturate and steady-state flux through the transporter could vary through a large range with model changes.

Activities that stay constant with internode maturity

SPS and SPase No activity values for *SPase* specific to each internode, were found. In this case the original value used by Rohwer & Botha [76] for *SPase* was assumed constant with internode

Table 3.2: Maximal activities for all enzymes and transport steps in $\mathbf{M}_{\delta}^{(i)}$ for each internode. The origin of this data is discussed in Section 3.1.6. p.c. - private communication

	Internode (i)								
Enzyme	3	4	5	6	7	8	9	10	References
V_{uptake}^{Fru}	0.286	0.286	0.286	0.286	0.286	0.286	0.286	0.286	[76]
V_{uptake}^{Glc}	0.286	0.286	0.286	0.286	0.286	0.286	0.286	0.286	
V_{store}^{Suc}	1.000	1.000	1.000	1.000	1.000	1.000	1.000	1.000	
$V_{f\ SPase}$	0.500	0.500	0.500	0.500	0.500	0.500	0.500	0.500	
$V_{f\ SPS}$	0.205	0.252	0.263	0.269	0.317	0.253	0.266	0.325	Botha,F.C. p.c.
$V_{r\ SPS}$	0.108	0.133	0.139	0.142	0.167	0.134	0.140	0.171	
V_{HK}^{Glc}	0.204	0.173	0.125	0.115	0.106	0.128	0.178	0.166	[12]
V_{HK}^{Fru}	0.204	0.173	0.125	0.115	0.106	0.128	0.178	0.166	
V_{NI}	0.320	0.399	0.238	0.213	0.147	0.197	0.174	0.235	
V_{PFP}	0.375	0.410	0.322	0.316	0.277	0.355	0.363	0.499	
V_{PFK}	0.189	0.272	0.132	0.143	0.168	0.265	0.278	0.365	
$V_{Aldolase}$	0.862	0.442	0.379	0.310	0.288	0.357	0.366	0.498	
V_{FRK}^{a}	0.155	0.137	0.059	0.078	0.055	0.072	0.055	0.080	[12], allocation to isoforms discussed in text
V_{FRK}^{b}	0.171	0.118	0.042	0.048	0.030	0.035	0.024	0.032	
V_{SS}^{a}	0.163	0.156	0.077	0.047	0.028	0.016	0.007	0.000	
V_{SS}^{b}	0.109	0.184	0.145	0.137	0.130	0.130	0.130	0.095	
$V_{f\ SS}^{c}$	0.109	0.184	0.145	0.137	0.130	0.130	0.130	0.095	
$V_{r\ SS}^{c}$	0.256	0.431	0.340	0.323	0.305	0.306	0.306	0.224	
V_{UDPGDH}	0.022	0.011	0.007	0.004	0.004	0.003	0.001	0.001	Estimate

maturity. *SPS* and *SPase* sit on the same branch, hence the steady-state flux through both enzymes will always be the same. *SPase* activity is higher than that of *SPS* for every internode, therefore steady-state flux through the branch can never be higher than the maximal velocity of *SPS*. The control profile for both enzymes is also expected to look the same. Together with *SPase*'s irreversible rate equation, the assumption of a maximal velocity that does not change with internode maturity is not detrimental to model accuracy.

K values

Michaelis-, half-saturation-, inhibition- and equilibrium constants are summarised in Table 3.3. Parameters which reference [76] are unchanged from $\mathbf{M}_\alpha$. Parameters for *SuSy A & B* were modified to adhere to the Haldane relationship,

$$K_{eq} = \frac{V_f K_m^P K_m^Q}{V_r K_m^A K_m^B} \tag{3.11}$$

where P, Q are products and A, B are substrates. V_f and V_r is the forward and reverse maximal activities respectively. Substitution of the experimental values obtained from [82] resulted in an inconsistency; calculating the equilibrium constant did not give 0.5, the value that it should be. The parameters were adjusted by introducing an error term,

$$\epsilon = \left(\frac{K_{eq}^{app}}{V_f / V_r} \right)^{\frac{1}{n}} \tag{3.12}$$

where K_{eq}^{app} is the apparent K_{eq} obtained from using the experimental data. Terms in the numerator were multiplied by ϵ and terms in the denominator were divided by ϵ. This approach was an attempt to distribute the error evenly. A fitting routine in Gnumeric supplied a value for the fitting parameter, n; it does not have any physical meaning, but it can be loosely interpreted as a measure of how far the experimental values deviate from the Haldane relationship. $n = 0.34$ for *SuSy A* and $n = 1.05$ for *SuSy B*. The parameters for *SuSy C* were left unchanged from the values used in [80] since they have already been adjusted to fit the Haldane relationship.

Parameters for *PFP* and *PFK* were estimated from values extracted from BRENDA [83, 84]. Values reported for a particular parameter in plants were averaged. σ had to be estimated because no information on this parameter exists. σ is a measure of the strength of an allosteric modifier. For $0 < \sigma < 1$, the modifier has an inhibitory effect — 0.9 was considered to be a conservative estimate.

3.1.7 Comparison of $\mathbf{M}_\beta$, fully substituted $\mathbf{M}_\delta^{(5)}$ and partially substituted $\mathbf{M}_\delta^{(5)}$

Table 3.3: Michaelis (m), half-saturation (0.5), inhibition (i) and equilibrium (eq) constants. Pre-superscripts indicate the specific isozyme, a post-superscript refers to the specific metabolite. Entries marked as Brenda were taken from the BRaunschweig ENzyme DAtabase [83, 84].

Parameter	Value	Reference
Fru & Glc uptake		
K_m^{Fru} K_m^{Glc}	0.2	[76]
K_i^{Fru} K_i^{Glc}	1	
Hexokinase		
K_m^{Glc}	0.07	
K_m^{ATP}	0.25	
K_m^{Fru}	10	[76]
$K_i^{Glc\text{-}6\text{-}P}$	0.1	
$K_i^{Fru\text{-}6\text{-}P}$	10	
SPS		
K_{eq}	10	
$K_i^{Suc\text{-}6\text{-}P}$	0.07	
$K_i^{P_i}$	3	
K_i^{UDPGlc}	1.4	
$K_i^{Fru\text{-}1,6\text{-}P_2}$	0.4	[76]
K_m^{UDPGlc}	1.8	
K_m^{UDP}	0.3	
$K_m^{Suc\text{-}6\text{-}P}$	0.1	
$K_m^{Fru\text{-}6\text{-}P}$	0.6	
FRK		
${}^{FRK\,A}K_m^{Fru}$	0.028	
${}^{FRK\,B}K_m^{Fru}$	0.074	
${}^{FRK\,A}K_m^{ATP}$	0.14	[32]
${}^{FRK\,B}K_m^{ATP}$	0.18	
${}^{FRK\,B}K_i^{FRU}$	0.016	
Vacuolar Suc uptake		
K_m^{Suc}	100	[76]
NI		
K_i^{Glc}	15	
K_i^{Fru}	15	[76]
K_m^{Suc}	10	
UDPGDH		
K_m^{UDPGlc}	0.0187	[100]
$K_m^{NAD^+}$	0.0722	

Parameter	Value	Reference
SuSy		
K_{eq}	0.5	
${}^{SuSy\,A}K_m^{Suc}$	22.51	
${}^{SuSy\,A}K_m^{UDP}$	0.58	
${}^{SuSy\,A}K_m^{UDPGlc}$	6.67	
${}^{SuSy\,A}K_m^{Fru}$	12.29	
${}^{SuSy\,B}K_m^{Suc}$	70.55	Values for *SuSy A & B* were modified from [82] to fit the Haldane relationship. Parameters for *SuSy C* were obtaned from [80]
${}^{SuSy\,B}K_m^{UDP}$	0.14	
${}^{SuSy\,B}K_m^{UDPGlc}$	0.82	
${}^{SuSy\,B}K_m^{Fru}$	18.08	
${}^{SuSy\,C}K_i^{UDP}$	0.0871	
${}^{SuSy\,C}K_i^{Suc}$	139	
${}^{SuSy\,C}K_i^{Fru}$	3.1	
${}^{SuSy\,C}K_i^{UDPGlc}$	0.103	
${}^{SuSy\,C}K_m^{Suc}$	35.9	
${}^{SuSy\,C}K_m^{UDP}$	0.00191	
${}^{SuSy\,C}K_m^{UDPGlc}$	0.234	
${}^{SuSy\,C}K_m^{Fru}$	6.49	
PFK		
$Fru\text{-}6\text{-}P_{0.5}$	0.758	[42]
$ATP_{0.5}$	0.155	[16, 42, 101]
$ATP_{0.5}^{modifier}$	2	Estimate
h^{PFK}	2.3	[105]
σ	0.9	Estimate
Aldolase		
$K_m^{Fru\text{-}1,6\text{-}P_2}$	0.015	Brenda
PFP		
$K_m^{Fru\text{-}6\text{-}P}$	1	
$K_m^{Fru\text{-}1,6\text{-}P_2}$	0.382	[43, 48, 54, 99, 115]
$K_m^{PP_i}$	0.12	
$K_m^{P_i}$	0.51	
K_{eq}	3.3	[88]
SPase		
$K_m^{Suc\text{-}6\text{-}P}$	0.1	[76]

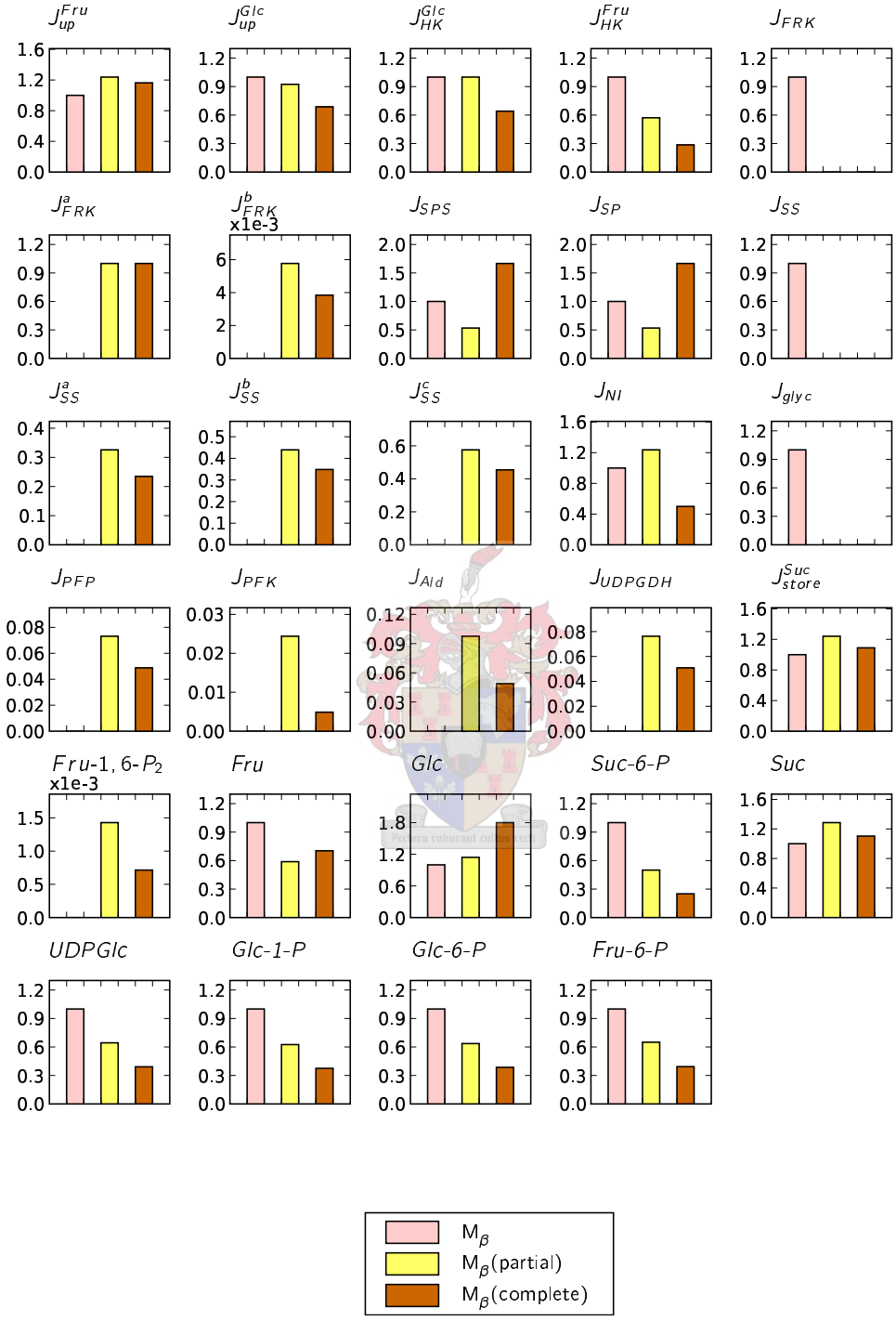

Figure 3.9: The relative changes in steady-state concentrations and fluxes of $\mathbf{M}_\delta^{(i)}$with partial and complete parameter substitution (see text on p.72) compared to $\mathbf{M}_\beta$. Values are normalised against the reference value in $\mathbf{M}_\beta$, except *PFP*, *PFK* and *ALD* which are normalised against the original flux to glycolysis (J_{glyc}) and Fru-1, 6-P_2 which is normalised against the Fru-1, 6-P_2 concentration from the completely substituted $\mathbf{M}_\beta$. The fluxes through the *SuSy* isozymes are normalised against the original flux through *SuSy* (J_{SS}) fluxes through *FRK A & B* against the original J_{FRK} and J_{UDPGDH} against J_{HK}^{Glc}. The legend shows which additions were made.

A steady-state comparison was performed on $\mathbf{M}_\beta$, the partially substituted, completely modified model and on the fully substituted $\mathbf{M}_\delta^{(5)}$ model (Figure 3.9). In this context substitution refers to parameters that were changed. The partially substituted model has maximal activity values for the glycolytic aditions, the isoform additions and *UDPGDH* taken from Table 3.2 while the remaining steps had maximal activity values that were used in $\mathbf{M}_\beta$. The fully substitued $\mathbf{M}_\delta^{(5)}$(and all the other $\mathbf{M}_\delta^{(i)}$'s) had every maximal activity in the model taken from Table 3.2. The activity set in Table 3.2 is incompatible with the values that were used in constructing $\mathbf{M}_\alpha$ or $\mathbf{M}_\beta$. There are two main reasons why this is the case.

1. The conversion factors in Chapter 2 that were used to change enzyme activity units into mmol min^{-1} l^{-1} are more accurate than those used in the original study of Rohwer & Botha, leading to more realistic maximal activity values.

2. $\mathbf{M}_\delta^{(i)}$ contains 14 enzyme catalysed reactions. We attempted to find maximal activity values for these enzymes that came from a single study, as opposed to values that were the result of studies that focused on only one or two of these enzymes. The discussion on p.71 elaborates on this issue.

Because of this it was neccesary to see if the fully substituted $\mathbf{M}_\delta^{(5)}$steady-state solution differed radically from $\mathbf{M}_\beta$ and the partially substituted $\mathbf{M}_\delta^{(5)}$.

In the final model all metabolite concentrations were lower than the original model except for *Glc* and *Suc*. Notably the hexose phosphate concentrations dropped to approximately a third of their original values. The *Suc* concentration was slightly higher and the glucose concentration almost 1.8 times higher. The reason for the higher glucose concentration is not clear. This was despite the lower steady-state flux of glucose uptake. The flux through glucose phosphorylating hexokinase was approximately two-thirds that of the other two models. This could perhaps account for the high cytoplasmic glucose concentration. HK^{Glc} is the only reaction that directly utilises *Glc*, which would imply that the hexose phosphate pool is in all likelihood replenished from *Fru* since there are three enzymes to phosphorylate *Fru*. An increased cytoplasmic *Glc* concentration would slow down the uptake of glucose and decrease the steady-state flux of *Glc* into the cell. The inhibition of glucose uptake by *Glc* is probably not big enough to prevent a build up of cytoplasmic *Glc*. There remains some doubt as to why the *Glc* concentration should be so high.

3.2 Analysis of fully substituted $\mathbf{M}_\delta^{(i)}$

All parameter substitutions dicussed above were made when the model was solved for internodes 3 to 10. Analysis, in this section, will refer to an combined analysis of all internodes, especially regarding the change in model properties from young to mature internodes. An increase in internode

maturity is modelled as a change in the amount of each enzyme present in an internode. This is reflected as a change in the apparent maximal velocity for an enzyme. Changes in enzyme activities are primarily due to an increase in volume of individual internodes as they mature and the amount of enzyme present. The shift in control from internode to internode will also be investigated.

3.2.1 Flux and concentration comparison

Measurements of carbon partitioning in sugarcane storage tissue were used to compare model predicted flux values (Table 3.5). Data were obtained from [7]. Flux values were only reported for internodes 3, 5 and 9; values for 4, 6, 7 and 8 were extrapolated from a spline interpolation. An artificial data point (0.1× the predictor for internode 9) was introduced for a fictitious internode twenty to anchor the spline. All predictor data were present in the spline values correct to an accuracy of approximately 1% or better. Data is presented as a ratio between glycolytic, storage and fibre fluxes and flux of glucose uptake. The version of the model used to calculate theoretical fluxes had the maximal activity of fructose uptake set to $1E-6$ (effectively zero). This was done to mimic the experimental protocol, in which only radiolabeled glucose was fed to tissue disks. The good correlation between experimental and model flux values for *UDPGDH* is due to the fact that the experimental data was used to estimate an activity value for *UDPGDH* (see also p.45). Flux ratios for $\frac{J^{Suc}_{store}}{J^{Glc}_{up}}$ do not show good correlation with experimental data. The reason for this is not immediately clear. It is possible that the model underestimates sucrose flux into the vacuole and overestimates flux into glycolysis.

The steady-state properties are shown in Table 3.4 and the pairwise Pearson linear correlation coefficients of the steady-state properties in Table 3.6. Correlation between data sets does not imply causation; however, correlation coefficients are valuable as a means of exploring large data sets to detect trends. In this particular case correlation coefficients were calculated to see how steady-state variable solutions changed with rescpect to other variables with internode maturity. Linear correlations are not necessarily expected. Where strong linear trends are seen, further investigation may be warranted. The following list describes some of the features of the correlation coefficients in Table 3.6.

1. *Fru* and *Glc* concentrations are negatively correlated to every other metabolite except with each other. This comes as no surprise, as the model only has *Fru* and *Glc* to act as carbon source. Care should be taken when interpreting concentration-concentration correlation coefficients. A negative correlation coefficient means that if one quantity decreases the other increases. This is only true for *Fru* and *Glc* if they are actually converted to some other molecule. If the flow of carbon into the cell decreases one expects the other metabolites in the cell to decrease to some degree, which would require the coefficient to be positive. This

Table 3.4: Steady-state concentrations and fluxes for fully substituted $\mathbf{M}_{\delta}^{(i)}$.

	Internode (i)							
	3	4	5	6	7	8	9	10
Metabolite	Steady-state metabolite concentrations (mM)							
Fru	2.7	3.1	15.9	11.4	12.2	12.4	13.4	13.5
Glc	39.9	55.9	62.3	70.0	59.3	59.2	35.3	42.6
Suc-6-P	0.008	0.005	0.001	0.001	0.001	0.002	0.002	0.005
Suc	17.0	17.5	13.9	14.8	15.1	15.0	16.9	15.3
Fru-1,6-P_2	0.0009	0.0009	0.0001	0.0002	0.0002	0.0003	0.0004	0.0006
UDPGlc	6.67	3.86	0.79	1.26	1.43	1.51	1.89	2.71
Glc-1-P	0.050	0.030	0.006	0.010	0.010	0.010	0.010	0.020
Glc-6-P	0.92	0.53	0.108	0.170	0.200	0.210	0.260	0.370
Fru-6-P	0.47	0.27	0.055	0.090	0.100	0.105	0.132	0.190
Reaction	Steady-state fluxes (mM/min)							
J_{up}^{Fru}	0.249	0.246	0.171	0.191	0.187	0.186	0.182	0.181
J_{up}^{Glc}	0.109	0.087	0.081	0.074	0.084	0.084	0.117	0.104
J_{HK}^{Glc}	0.160	0.137	0.100	0.092	0.102	0.102	0.141	0.131
J_{HK}^{Fru}	0.0001	0.0001	0.0002	0.0001	0.0001	0.0001	0.0004	0.0003
J_{FRK}^{a}	0.135	0.119	0.052	0.068	0.063	0.063	0.048	0.070
J_{FRK}^{b}	0.0054	0.0033	0.0002	0.0004	0.0003	0.0002	0.0002	0.0002
J_{SPS}	0.037	0.026	0.003	0.006	0.007	0.008	0.011	0.022
J_{SP}	0.037	0.026	0.003	0.006	0.007	0.008	0.011	0.022
J_{SS}^{a}	0.088	0.063	0.031	0.023	0.017	0.010	0.005	0.000
J_{SS}^{b}	0.024	0.038	0.046	0.049	0.053	0.056	0.066	0.060
J_{SS}^{c}	0.049	0.072	0.060	0.067	0.072	0.075	0.085	0.078
J_{NI}	0.052	0.050	0.019	0.017	0.018	0.018	0.024	0.027
J_{PFP}	0.015	0.011	0.002	0.003	0.004	0.004	0.005	0.010
J_{PFK}	0.032	0.015	0.0002	0.001	0.002	0.002	0.003	0.009
J_{Ald}	0.047	0.026	0.002	0.004	0.006	0.006	0.008	0.019
J_{UDPGDH}	0.019	0.009	0.006	0.004	0.003	0.003	0.001	0.001
J_{store}^{Suc}	0.146	0.149	0.122	0.129	0.131	0.131	0.144	0.133

Table 3.5: Comparison of $\mathbf{M}_{\delta}^{(i)}$- and experimentally determined fluxes. Fluxes are expressed as a fraction of carbon partitioning, either, incoming glucose or flux through *ALD*. exp. - Experimental values from [7]. mod. - model values. n.a. - not applicable

$100\times$	$\frac{J_{UDPGDH}}{J_{up}^{Glc}}$		$\frac{J_{Aldolase}}{J_{up}^{Glc}}$		$\frac{J_{store}^{Suc}}{J_{up}^{Glc}}$		$\frac{J_{Starch}}{J_{up}^{Glc}}$		$\frac{J_{UDPGDH}}{J_{Aldolase}}$	
Internode	exp	mod	exp	mod	exp	mod	exp		exp	mod
3	16	14	31	53	35	33	0.0045		52	27
4	10	8	27	55	50	37	0.0034		38	15
5	7	7	24	33	58	61	0.0013		29	21
6	5	5	23	32	62	64	0.0008	*n.a.*	23	15
7	4	3	21	43	65	53	0.0005		19	8
8	3	3	19	44	66	54	0.0005		15	6
9	1	1	17	49	66	50	0.0006		8	2

is supported by the positive correlation coefficients seen between J_{uptake}^{Fru} and J_{uptake}^{Glc} and all the metabolites except *Fru* and *Glc*. The one exception is the correlation coefficient between J_{uptake}^{Glc} and *Suc* which is negative. This value is sufficiently close to zero, compared to all the other values, to imply that no serious correlation exists.

2. Metabolites of the hexose phosphate pool, excluding Fru-1, 6-P_2, all have identical correlation profiles since the model assumes that these species are in equilibrium and were modelled as such. *Suc-6-P* is almost completely linearly correlated to the hexose phosphate pool for two reasons, a) *Suc-6-P* is only synthesised from hexose phosphates, and b) the *SPS* reaction sits on an independent branch in the model. It is immediately clear that if the hexose phosphate concentration increases then the *SPS* flux will increase and more *Suc-6-P* will be formed. *Suc-6-P* is negatively correlated to *Suc*, since dephosphorylation of *Suc-6-P* yields *Suc*.

3. $J_{storage}^{Suc}$ is completely, positively correlated to *Suc*. This is as expected, since the vacuolar sucrose uptake rate equation is a function of *Suc* only. After $J_{storage}^{Suc}$, *Suc* is most strongly, positively correlated to J_{SS}^{a} and J_{SS}^{c}. Comparison of these with the correlation between $J_{storage}^{Suc}$ and J_{SS}^{a} and J_{SS}^{c} shows that they have very similar values. The correlation with J_{SS}^{c} is as expected. Of the sucrose synthesising enzymes, J_{SS}^{c} has by far the largest steady-state flux. From this it can be inferred that the synthesis and storage of sucrose is mostly dependent on *SuSy C*.

Table 3.6: Pairwise Pearson correlation coefficients for steady-state fluxes and concentrations of all 8 internodes.

	Fru	Glc	$Suc\text{-}6\text{-}P$	Suc	$Fru\text{-}1,6\text{-}P_2$	UDPGLC	$Glc\text{-}1\text{-}P$	$Glc\text{-}6\text{-}P$	$Fru\text{-}6\text{-}P$
Fru	1.00								
Glc	0.21	1.00							
$Suc\text{-}6\text{-}P$	-0.83	-0.6	1.00						
Suc	-0.78	-0.62	0.75	1.00					
$Fru\text{-}1,6\text{-}P_2$	-0.87	-0.52	0.95	0.84	1.00				
$UDPGlc$	-0.87	-0.55	0.97	0.74	0.89	1.00			
$Glc\text{-}1\text{-}P$	-0.87	-0.55	0.97	0.74	0.89	1.00	1.00		
$Glc\text{-}6\text{-}P$	-0.87	-0.55	0.97	0.74	0.89	1.00	1.00	1.00	
$Fru\text{-}6\text{-}P$	-0.87	-0.55	0.97	0.74	0.89	1.00	1.00	1.00	1.00
J^{Fru}_{uptake}	-1.00	-0.22	0.84	0.78	0.87	0.88	0.88	0.88	0.88
J^{Glc}_{uptake}	-0.18	-0.99	0.56	0.61	0.47	0.52	0.52	0.52	0.52
J^{Glc}_{HK}	-0.64	-0.87	0.88	0.85	0.84	0.85	0.85	0.85	0.85
J^{Fru}_{HK}	0.65	-0.56	-0.27	-0.08	-0.3	-0.36	-0.36	-0.36	-0.36
J^{a}_{FRK}	-0.97	-0.22	0.9	0.68	0.89	0.92	0.92	0.92	0.92
J^{b}_{FRK}	-0.93	-0.33	0.88	0.69	0.82	0.95	0.95	0.95	0.95
J_{SPS}	-0.83	-0.6	1.00	0.76	0.95	0.97	0.97	0.97	0.97
J_{SP}	-0.83	-0.6	1.00	0.76	0.95	0.97	0.97	0.97	0.97
J^{a}_{SS}	-0.87	-0.09	0.71	0.53	0.67	0.81	0.81	0.81	0.81
J^{b}_{SS}	0.8	-0.07	-0.65	-0.34	-0.57	-0.74	-0.74	-0.74	-0.74
J^{c}_{SS}	0.45	-0.17	-0.39	0.06	-0.21	-0.53	-0.53	-0.53	-0.53
J_{NI}	-0.92	-0.46	0.93	0.83	0.96	0.92	0.92	0.92	0.92
J_{PFP}	-0.81	-0.61	1.00	0.75	0.95	0.96	0.96	0.96	0.96
J_{PFK}	-0.85	-0.53	0.96	0.68	0.86	1.00	1.00	1.00	1.00
J_{Ald}	-0.85	-0.56	0.98	0.71	0.9	1.00	1.00	1.00	1.00
J_{UDPGDH}	-0.82	-0.2	0.75	0.49	0.64	0.86	0.86	0.86	0.86
$J^{Suc}_{storage}$	-0.78	-0.63	0.75	1.00	0.84	0.74	0.74	0.74	0.74

	J^{Fru}_{uptake}	J^{Glc}_{uptake}	J^{Glc}_{HK}	J^{Fru}_{HK}	J^{a}_{FRK}	J^{b}_{FRK}	J_{SPS}	J_{SP}	J^{a}_{SS}	J^{b}_{SS}	J^{c}_{SS}	J_{NI}	J_{PFP}	J_{PFK}	J_{Ald}	J_{UDPGDH}	$J^{Suc}_{storage}$
J^{Fru}_{uptake}	1.00																
J^{Glc}_{uptake}	0.19	1.00															
J^{Glc}_{HK}	0.66	0.85	1.00														
J^{Fru}_{HK}	-0.65	0.59	0.12	1.00													
J^{a}_{FRK}	0.98	0.18	0.65	-0.66	1.00												
J^{b}_{FRK}	0.95	0.3	0.72	-0.58	0.96	1.00											
J_{SPS}	0.84	0.56	0.88	-0.27	0.89	0.87	1.00										
J_{SP}	0.84	0.56	0.88	-0.27	0.89	0.87	1.00	1.00									
J^{a}_{SS}	0.9	0.07	0.53	-0.71	0.9	0.95	0.7	0.7	1.00								
J^{b}_{SS}	-0.83	0.1	-0.36	0.81	-0.87	-0.89	-0.63	-0.63	-0.97	1.00							
J^{c}_{SS}	-0.49	0.18	-0.13	0.67	-0.58	-0.67	-0.37	-0.37	-0.78	0.88	1.00						
J_{NI}	0.94	0.42	0.84	-0.41	0.94	0.93	0.93	0.93	0.84	-0.74	-0.41	1.00					
J_{PFP}	0.82	0.57	0.88	-0.25	0.88	0.86	1.00	1.00	0.68	-0.61	-0.35	0.92	1.00				
J_{PFK}	0.87	0.49	0.83	-0.38	0.92	0.95	0.96	0.96	0.83	-0.78	-0.59	0.92	0.95	1.00			
J_{Ald}	0.86	0.52	0.85	-0.35	0.92	0.93	0.98	0.98	0.79	-0.74	-0.52	0.93	0.98	1.00	1.00		
J_{UDPGDH}	0.84	0.18	0.58	-0.63	0.87	0.96	0.74	0.74	0.97	-0.95	-0.84	0.8	0.72	0.89	0.85	1.00	
$J^{Suc}_{storage}$	0.78	0.62	0.85	-0.08	0.68	0.69	0.76	0.76	0.53	-0.33	0.06	0.82	0.75	0.68	0.71	0.48	1.00

Table 3.7: Futile cycling control coefficients for all eight internodes in order of increasing magnitude of the mean. The slope is the first derivative of a linear regression line and gives an indication by how much a coefficient changes with internode maturity.

	Internode (i)										
Perturbation	3	4	5	6	7	8	9	10	Mean	s.d.	Slope
ν_{up}^{Glc}	-0.802	-0.748	-0.904	-0.905	-0.926	-0.927	-0.972	-0.917	-0.888	0.074	-0.024
ν_{up}^{Fru}	-0.767	-0.69	-0.621	-0.583	-0.581	-0.58	-0.538	-0.548	-0.614	0.078	0.029
ν_{st}^{Suc}	-0.342	-0.328	-0.534	-0.495	-0.502	-0.504	-0.488	-0.489	-0.46	0.079	-0.021
ν_{SPS}	-0.069	-0.036	-0.01	-0.012	-0.015	-0.016	-0.021	-0.036	-0.027	0.02	0.003
$\nu_{SuSy\ A}$	-0.013	-0.009	0.004	0.003	0.003	0.002	0.001	0.	-0.001	0.006	0.002
ν_{SP}	-0.002	0.	0.	0.	0.	0.	0.	0.	0.	0.001	0.
ν_{ALD}	0.	0.001	0.	0.	0.	0.	0.	0.	0.	0.	0.
ν_{HK}^{Fru}	0.	0.	0.001	0.	0.	0.	0.001	0.001	0.	0.	0.
$\nu_{FRK\ B}$	0.01	0.004	0.001	0.001	0.001	0.001	0.	0.	0.002	0.003	-0.001
ν_{UDPGDH}	0.025	0.014	0.002	0.004	0.003	0.002	0.001	0.001	0.007	0.009	-0.003
$\nu_{SuSy\ B}$	-0.003	-0.006	0.006	0.007	0.009	0.011	0.017	0.017	0.007	0.008	0.003
ν_{PFP}	0.02	0.017	0.001	0.003	0.004	0.004	0.005	0.011	0.008	0.007	-0.001
$\nu_{SuSy\ C}$	-0.007	-0.011	0.008	0.01	0.013	0.015	0.022	0.022	0.009	0.012	0.005
ν_{PFK}	0.041	0.023	0.	0.001	0.001	0.002	0.003	0.01	0.01	0.015	-0.004
$\nu_{FRK\ A}$	0.24	0.15	0.171	0.139	0.141	0.141	0.102	0.134	0.152	0.04	-0.013
ν_{NI}	0.692	0.657	0.796	0.806	0.813	0.814	0.811	0.782	0.771	0.061	0.017
ν_{HK}^{Glc}	0.976	0.962	1.079	1.021	1.037	1.036	1.056	1.011	1.022	0.039	0.007

3.2.2 Futile cycling by neutral invertase

Futile cycling of sucrose is an energetically expensive process that decreases the amount of sucrose available for storage. An investigation into how this process is controlled may provide a means of reducing futile cycling by selection or engineering. The futile cycling control coefficients (FCCC) were calculated as $C_i^{J_{NI}/J_{Store}^{Suc}}$, according to [76]. This quantity may interpreted as the degree of control that each reaction has on the ratio of J_{NI} to J_{Store}^{Suc}. The smaller J_{NI}/J_{Store}^{Suc} is, the more sucrose is being stored as opposed to being broken down. It is therefore interesting to know which enzymes can negatively affect this value. The change in FCCC can be seen in Table 3.7. The results obtained for each internode do not differ from that obtained by [76]. Glc_{up}, Fru_{up} and Suc_{store} retain the largest negative impact on futile cycling, while HK^{Glc} and NI are still the main

Table 3.8: Fractional futile cycling of sucrose. The first row shows the fraction of sucrose that flows into the vacuole as opposed to being broken down by neutral inveratse. The second row shows γ, the fractional change in fractional futile cycling between succesive internodes. $\bar{\gamma}$ is the geometric mean of γ. The result shows that futile cycling decreases with internode maturity.

	Internode (i)							
Description	3	4	5	6	7	8	9	10
$J_{NI}/(J_{NI}+J_{Vac})$	0.26	0.25	0.13	0.12	0.12	0.12	0.14	0.17
$\gamma = \frac{J^i_{NI}/(J^i_{NI}+J^i_{Vac})}{J^{i-1}_{NI}/(J^{i-1}_{NI}+J^{i-1}_{Vac})}$	-	0.96	0.53	0.89	1.03	1.00	1.20	1.18
$\bar{\gamma} = (\gamma_1 \times \gamma 2 \times \cdots \times \gamma n)^{1/n}$					0.94			
percentage change in futile cycling					**-6 %** per internode			

cause of futile cycling. The analysis of FCCCs also show that the control over futile cycling does not shift radically with internode maturity. The conclusion is that the same enzymes are responsible for futile cycling regardless of changes in maximal rates for all enzymes for every internode.

The fraction of sucrose broken down as opposed to being transported into the vacuole is shown in Table 3.8. The decrease in futile cycling is commensurate with the decrease in neutral invertase maximal activity with internode maturity, while activity of vacuolar sucrose uptake remains constant. From Table 3.4 we can calculate the decrease in neutral invertase flux as -6% per internode. This decrease in futile cycling is due to a decrease in steady-state flux through neutral invertase, since sucrose flux into the vacuole remains relatively constant as internodes mature.

3.2.3 Parameter scans

ν^{Glc}_{HK} and ν_{NI} have the largest positive control over J_{NI}/J^{Suc}_{Store}, whereas ν^{Glc}_{up}, ν^{Fru}_{up} and ν^{Suc}_{store} have the largest negative control over J_{NI}/J^{Suc}_{Store}. These two groups of antagonistic enzymes are chosen for manipulation. It is predicted that enzymes with large negative control over futile cycling should increase their control even more if they have higher maximal activities assigned to them. The converse is true for enzymes with large positive control. Maximal activities for HK^{Glc} and NI were decreased and Glc_{up}, Fru_{up} and Suc_{store} activities were increased. Steady-state solutions were calculated for $\mathbf{M}^{(i)}_{\delta}$ as ν^{Glc}_{HK}, ν_{NI}, ν^{Glc}_{up}, ν^{Fru}_{up} and ν^{Suc}_{store} were incremented from their initial values (Figures 3.10 and 3.11). Activities were increased or decreased five fold from their reference values given in Table 3.2. Similar to $\mathbf{M}_{\alpha}$, futile cycling was found to decrease and conversion of

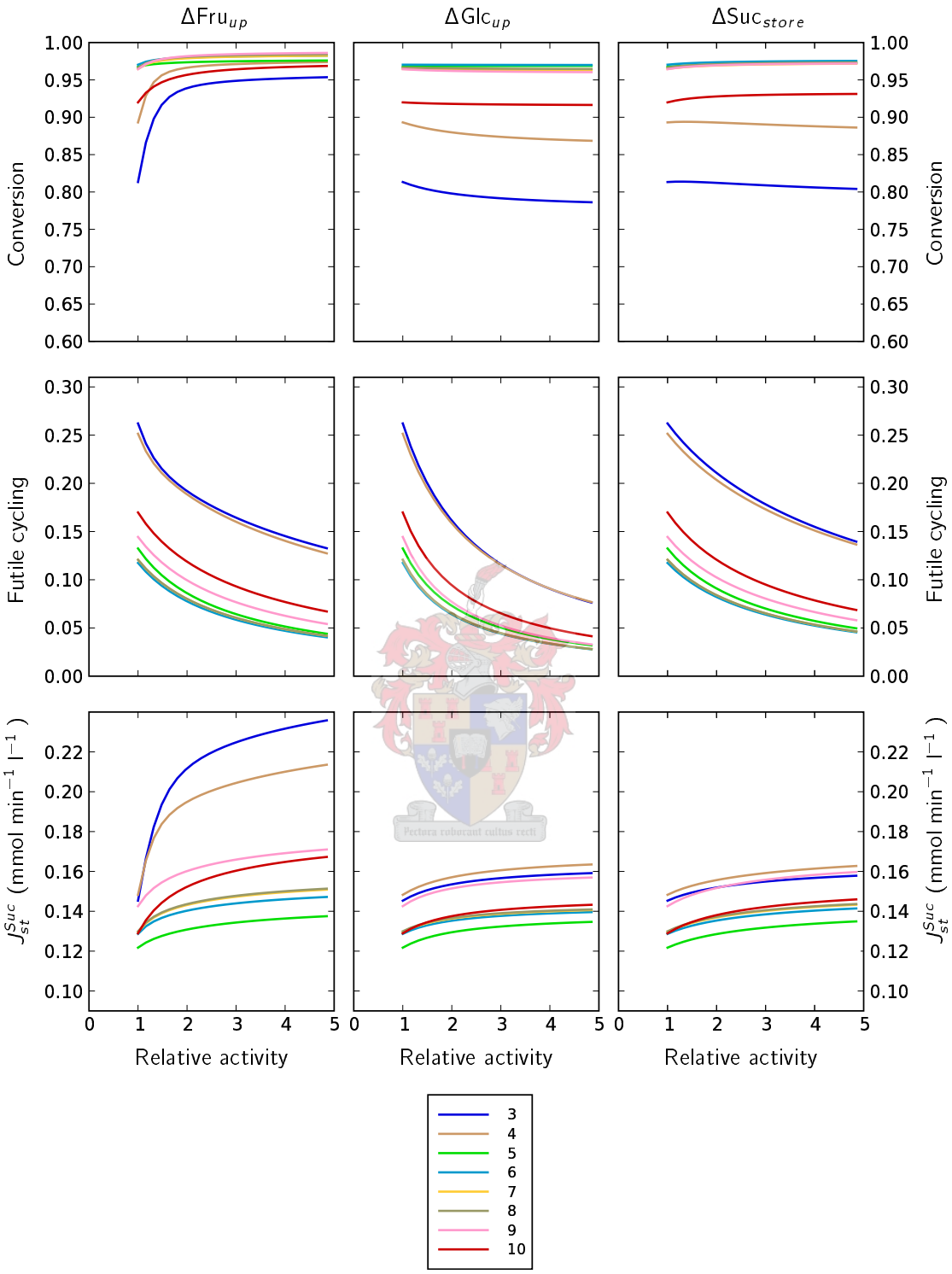

Figure 3.10: Changes in steady-state fractional carbohydrate to sucrose conversion and futile cycling of sucrose, and vacuolar sucrose uptake with a change in Glc_{up}, $Fru_{up}$and Suc_{store} activities. Actvities were increased by increments of 0.01 to a maximum of 5× their original value. Conversion is defined as $2J_{st}^{Suc}/(J_{up}^{Glc} + J_{up}^{Fru})$ and futile cycling as $J_{NI}/(J_{NI} + J_{st}^{Suc})$. The legend shows internode numbers.

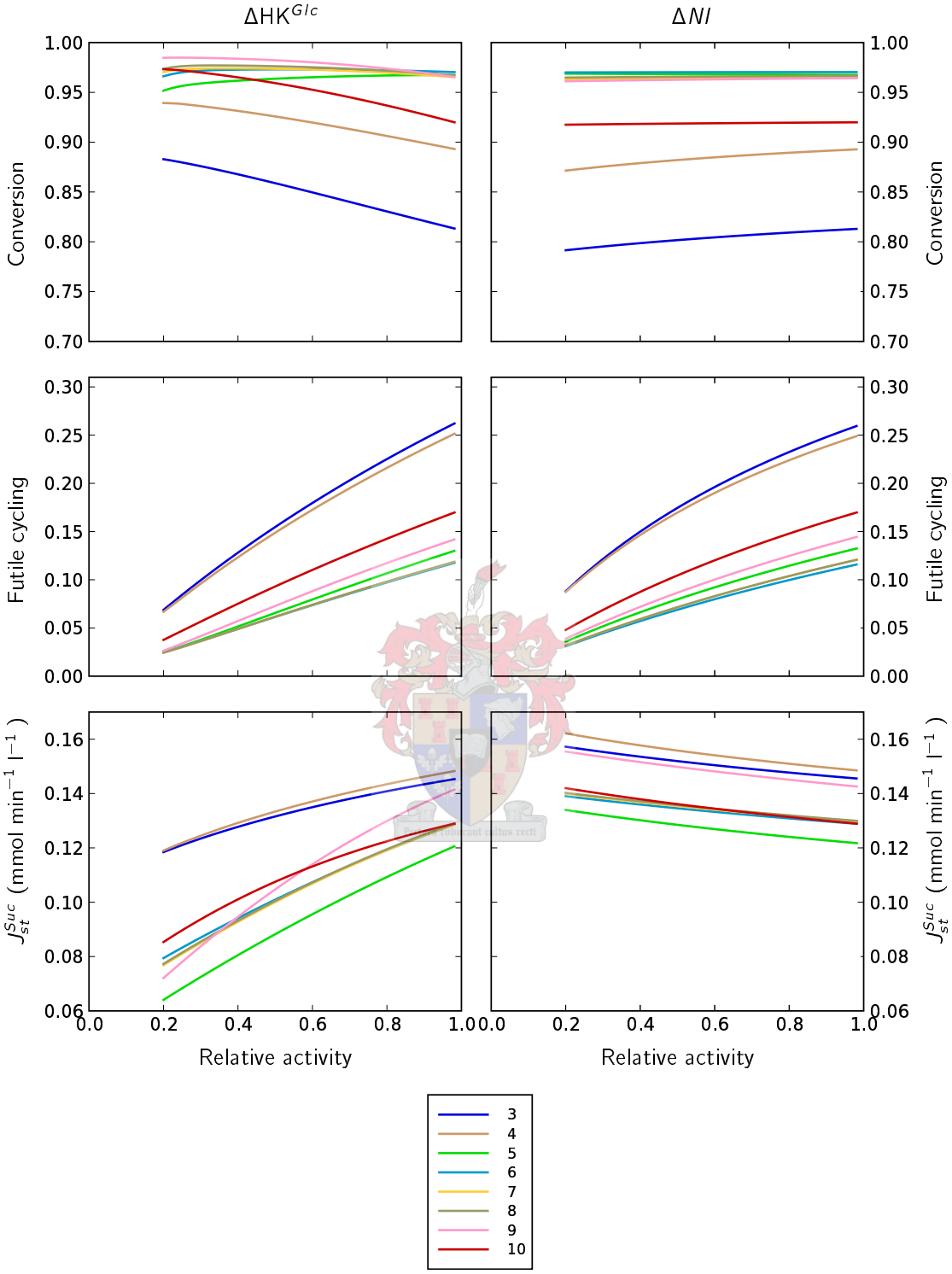

Figure 3.11: Changes in steady-state fractional carbohydrate to sucrose conversion and futile cycling of sucrose, and vacuolar sucrose uptake with a change in $NI$and HK^{Glc} activities. Actvities were decreased by increments of 0.01 to a minimum of 1/5 their original value. Conversion is defined as $2 \times J_{st}^{Suc}/(J_{up}^{Glc} + J_{up}^{Fru})$ and futile cycling as $J_{NI}/(J_{NI} + J_{st}^{Suc})$. The legend shows internode numbers.

sucrose remained constant with a change in all activities. Flux of sucrose into the vacuole increased with all the changes made except when ν_{HK}^{GIc} was decreased. These results are consistent with the findings of Rohwer & Botha in their original model [76].

Curves in the conversion plots of Figures 3.10 and 3.11 shift upwards as the internode number increases. The exception is the curves for internode 10 which drops to a position close to the curve of internode 4. In the futile cycling plots, curves shift down and internode 10 drifts around the internode 9 curve. Further investigation might discover why internode 10 behaves the way it does. It is possible that the parameter set is very close to that of a younger internode.

The plots do not show elaborate intersections, i.e. the trend seen with a parameter adjustment is preserved with internode maturity. The upwards progression of the parameter scan plots for the conversion and vacuolar flux, is consistent with increasing internodal sucrose accumulation and the shift seen in the futile cycling plots is consistent with a decrease in sucrose breakdown.

3.3 Remarks

This chapter described a greatly expanded model of sucrose accumulation in sugarcane compared to previous work by Rohwer & Botha and Schäfer et al [76, 80]. The original analysis of $\mathbf{M}_\alpha$ was expanded to include changes in physiological behaviour during internodal tissue maturation. Moreover, additional glycolytic reactions and branch to fibre were added to the model, and details on the variation in expression profiles of the *SuSy* and *FRK* isozymes were included. The behaviour of the various models did not differ much from each other. Trends in conversion, futile cycling and flux into the vacuole remained consistent as internodes matured. A 6% per internode decrease was seen in the breakdown of sucrose by *NI*. Control of futile cycling also remained fairly constant across internodes.

Chapter 4 will describe in greater detail how the model was programmed, how the large amounts of data were handled and how the model was checked for accuracy by validating it with another program.

Chapter 5 will provide a more general discussion of the results obtained here.

Chapter 4

Programming the model

The purpose of this chapter is to describe in brief the software and computer programming that was involved in this project. The chapter starts with a description of the central programming language Python, and then discusses various software applications that are accessible from or can access Python.

4.1 Software

Python

Python is a statically typed, interpreted, imperative programming language with *ad hoc* object oriented- (OO) and functional programming constructs added (www.python.org). Python has many advantages, some of them being

- Clear syntax wich enables quick development.
- Python scripts can make calls to C/C++ and Fortran routines and libraries through interface wrappers such as Swig and f2py.
- The Python interpreter can be embedded in other applications.

These three features make Python an ideal language as a modelling platform, as the following discussions will show. Python is able to act as "glue", bringing a number of useful software tools into a single environment.

Unless otherwise mentioned, all software being discussed in this chapter adheres to an open source philosophy (www.opensource.org) and is freely available on the world wide web. All software runs on the Linux operating system, although in some cases not exclusively.

Diagram 4.1 The relationship of data manipulation, storage and management and various software tools (discussed in the text) with the Python programming language.

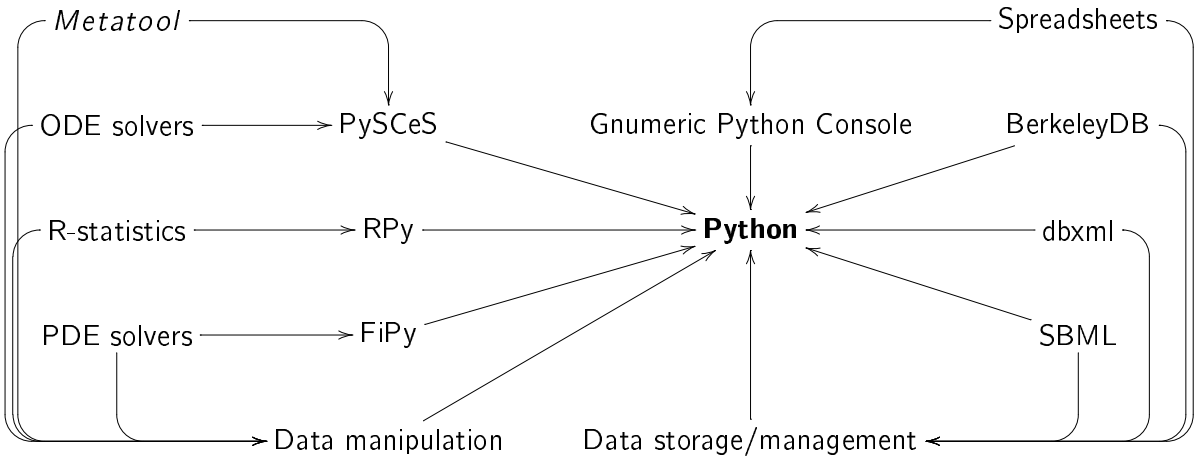

Data storage

Computational Systems Biology has the capacity for generating large volumes of data. In some instances, the input data alone accounts for sizable amounts of the information being processed in a project. For this reason, the following tools have proven useful in keeping data organised.

Gnumeric is a spreadsheet program created by the GNU foundation (www.gnumeric.org). Spreadsheets are valuable tools to visualize and graphically manipulate data. Often errors and anomalies in data are more easily detected when displayed in a human digestible format. Spreadsheets can be used to do quick calculations and aid in exploratory data analysis. They are often intuitive to operate and do not require complex scripting to be performed. The main advantage to Gnumeric is an embedded Python console, which allows easy input/ouput of data from other applications. The capacity for more complex data analysis is available because any of the powerful numerical packages available from inside Python can be called from the Gnumeric console. Gnumeric also allows plugins to be writen in Python which can, in turn, act on data in a spreadsheet. A useful tool in Gnumeric is the ability to export spreadsheets in LaTeX 2_ε.

Berkeley DB is a low-level database that stores data in key/value pairs [64]. An example of using Berkeley DB from Python is given in Example 4.4. All the features of a modern database are present, amongst others concurrent access and transactional control, such as multiple commits and rollback. The main advantage to Berkeley DB is the absence of a seperate query language. Berkeley DB can be embedded in any system written in one of the languages for which an interface exists, such as C/C++, Java, Perl and Python. This means that data can be inserted and extracted from the database in ways specific to the problem at hand, in the language of choice. This makes

Berkeley DB highly adaptable and easily customizable.

SBML SBML is an acronym for the Systems Biology Markup Language [22, 35]. As with any markup language it aims to provide metadata related to a document, in other words, describe data. SBML is an XML (eXtensible Markup Language, www.w3.org/XML) implementation. Example 4.1 shows an SBML fragment describing a reaction in a model. The SBML specification aims to give a complete description of biological models in terms of the components of a model, e.g. the rate equation, parameters and stoichiometry of a kinetic model. Any XML document is highly verbose, despite this it is widely used as a means of transporting data. Any application that can implement the SBML specification is able to extract the information stored in the document and use it as required. SBML aims to ease the dissemination and exchange of biological models, especially in a field where modelling software often specify their own input file format.

Berkeley DB XML Berkley DB XML is a database to store XML data in its native format (www.sleepycat.com). As mentioned, XML can be very verbose. Because the size of an XML document can be quite large it is necessary to organise data properly and ensure its integrity. A human operator would in many cases be unable to do this by inspection. For this reason specialised XML databases are required. Berkeley DB XML is an example of using Berkeley DB to create a new database. Berkeley DB XML stores XML documents either in their entirety or preferably in XML fragments for optimality. This optimisation is hidden from the programmer and is executed by the database itself. Since this is a Berkeley DB implementation, documents or fragments are retrieved from the database using keywords. Berkeley DB XML can also be queried via XQuery (the W3C specification for querying XML, www.w3.org/XML/Query). Storing XML in fragments also provides a natural way of storing various components of an SBML document. These XML fragments can be easily recombined in various ways to create new models, e.g. creating kinetic models with reactions added or subtracted. Two code examples of working with dbxml are shown in Examples 4.2 and 4.3.

Data manipulation

Data is a scientist's stock in trade. Experiments produce data, the manipulation and analyisis of which provide new insights and knowledge. The following software tools provide some of the mechanisms by which this can be achieved in the field of systems biology.

PySCeS is a suite of software that satisfies many of the requirements researchers have from systems biology software [63]. PySCeS has the ability to solve Ordinary Differential Equations (ODEs), determine Elementary Flux Modes (EFMs) and perform Metabolic Control Analysis (MCA). PySCeS is written in Python and takes advantage of interface wrappers to call routines

Example 4.1 An SBML fragment showing the description of the Aldolase reaction. The terms in angle brackets are tags. An opening tag, < ... >, and a closing tag, < /... >, enclose a model component.

```
<?xml version="1.0" encoding="UTF-8"?>
<sbml xmlns="http://www.sbml.org/sbml/level2" level="2" version="1">

...

      <reaction id="Aldolase" reversible="false">
        <listOfReactants>
          <speciesReference species="FRU16BP"/>
        </listOfReactants>
        <listOfProducts>
          <speciesReference species="glycolysis"/>
        </listOfProducts>
        <kineticLaw>
          <math xmlns="http://www.w3.org/1998/Math/MathML">
            <apply>
              <divide/>
              <apply>
                <times/>
                <ci> VmAldolase </ci>
                <ci> FRU16BP </ci>
              </apply>
              <apply>
                <plus/>
                <ci> KmFRU16BPaldolase </ci>
                <ci> FRU16BP </ci>
              </apply>
            </apply>
          </math>
          <listOfParameters>
            <parameter id="VmAldolase" value="0.379"/>
            <parameter id="KmFRU16BPaldolase" value="0.015"/>
          </listOfParameters>
        </kineticLaw>
      </reaction>
...
```

Example 4.2 Example of an interactive session in which an XML container is created in a Berkeley DB XML database and a SBML file stored.

```
>>> from dbxml import *
>>> manager   = XmlManager()
>>> container = manager.openContainer('my_xml_container.bdbxml',DB_CREATE)
>>> context   = manager.createUpdateContext()
>>> stream    = manager.createLocalFileInputStream('sugar.xml')
>>> container.putDocument('sugar',stream,context)
>>> container.sync()
>>> print container
<dbxml.XmlContainerPtr; proxy of C++ XmlContainer ...
...instance at _c85b0f08_p_XmlContainer>
```

from FORTRAN and C/C++. Modelling can be done either interactively in a Python shell or models can be scripted and reused. PySCeS differs from many modelling tools in that a number of different ODE solvers are available. This enables a program to fall back on other solvers should one of them not be able to find a solution.

R and RPy R is an open source implementation of the S engine [71]. It provides powerful statistical analysis in the form of a programming language. Many of Gnumeric 's functions are indirectly performed by R. The R-statistical package can be accessed from Python using the Python module RPy. RPy is not a true interface, it acts as a translation layer between a Python process and an R process running in the background. RPy shuttles data structures between Python and R allowing the strengths of each to be exploited.

SBW and Jarnac The Systems Biology Workbench (SBW) is an attempt at creating a unified platform for tools and data in computational systems biology (www.sbw.kgi.edu) [36, 37]. SBW clients are able to access resources and applications regardless of file input specifics, since data is transferred as SBML. Tools that are not available in a specific application can submit tasks to a broker service. The task is then farmed out to an appropriate service provider and the results sent back to the client. Jarnac is such a client [79]. Jarnac was used to submit the internode 5 sucrose accumulation model for a steady state analysis to compare it with the PySCeS solution, in order to cross-check and validate the analysis.

FiPy is a Partial Differential Equation (PDE) solver [112]. It is written in Python and takes full advantage of Python's OO abilities. FiPy solves PDEs using a standard Finite Volume (FV) method. FiPy differs from most other PDE solvers in that all terms in a coupled set of equations

Example 4.3 Example of an interactive Python session in which an XML container is opened and an SBML document retrieved.

```
>>> from dbxml import *
>>> manager   = XmlManager()
>>> container = manager.openContainer('my_xml_container.bdbxml')
>>> doc = container.getDocument('sugar')
>>> print doc.getContent()
<?xml version="1.0" encoding="UTF-8"?>
<!-- Created with PySCeS (0.1.6) on Thu, 08 Dec 2005 10:37:33 by lafras -->
<sbml xmlns="http://www.sbml.org/sbml/level2" level="2" version="1">
  <model name="sugar">
    <listOfCompartments>
      <compartment id="sugar" size="1"/>
    </listOfCompartments>
    <listOfSpecies>
      <species id="FRUcyt" name="FRUcyt" compartment="sugar" initialConcentration="1"/>
      <species id="G...

...etc.
```

are represented by term objects. An equation is a linear combination of one or more of the terms in a general conservation equation,

$$\underbrace{\frac{\partial(\rho\phi)}{\partial t}}_{\text{transient}} = \underbrace{\nabla\cdot(\vec{u}\phi)}_{\text{convection}} + \underbrace{[\nabla\cdot(\Gamma_i\nabla)]^n\,\phi}_{\text{diffusion}} + \underbrace{S_\phi}_{\text{source}} \tag{4.1}$$

where ϕ is the state-variable and ρ, $\vec{u}$ and Γ_i are coefficients (this equation was taken from the FiPy manual). Any equation to be solved by FiPy has to be written in the form of 4.1. FiPy is useful in that it brings the ability to solve PDEs to Python. None of the tools discussed so far are able to solve PDEs, however the need to do so is becoming greater as model descriptions increase in complexity. As proof of concept, $\mathbf{M}_\alpha$ was solved using FiPy and identical steady-state results were obtained as for the original. $\mathbf{M}_\alpha$ is defined solely in terms of ODEs, which is nothing but a set of PDEs in one dimension. As yet $\mathbf{M}_\delta^{(i)}$ has not been solved using FiPy. Numerical solvers are sensitive to many aspects of a problem, such as parameter values, initial values and floating point precision. Further optimisation is required to have $\mathbf{M}_\delta^{(i)}$ solved by FiPy.

The argument is far from new, but it can be seen from the above discussion that most of the tools that a computational systems biologist could need can be accessed from Python.

4.2 Some examples

Many models, one input file The sucrose accumulation model discussed in Chapter 3 can be considered to be eight independent models. From a programming perspective, this would require eight different model descriptions and therefore eight different input files. Python and PySCeS make it possible to get away with one input file. Maximal activities are entered and stored in a spreadsheet (Figure 4.1). Values are exported to a Berkeley DB database (Example 4.4) and a Python script calls changes from the database when reassigning new values to live model objects (Example 4.5). Notice that the values in Figure 4.1 are the same as those in Example 4.4. The list of values printed after the "activities" statement in the example is the *SPS* maximal activities in the fifth row of the spreadsheet. The possibility also exists of running an interactive PySCeS session inside the Gnumeric Python Console.

This chapter has summarised some of the software and programming strategies used in this project. The next chapter will discuss the work done, place it in a broader context, suggest some prospects for future work and deliver some concluding remarks.

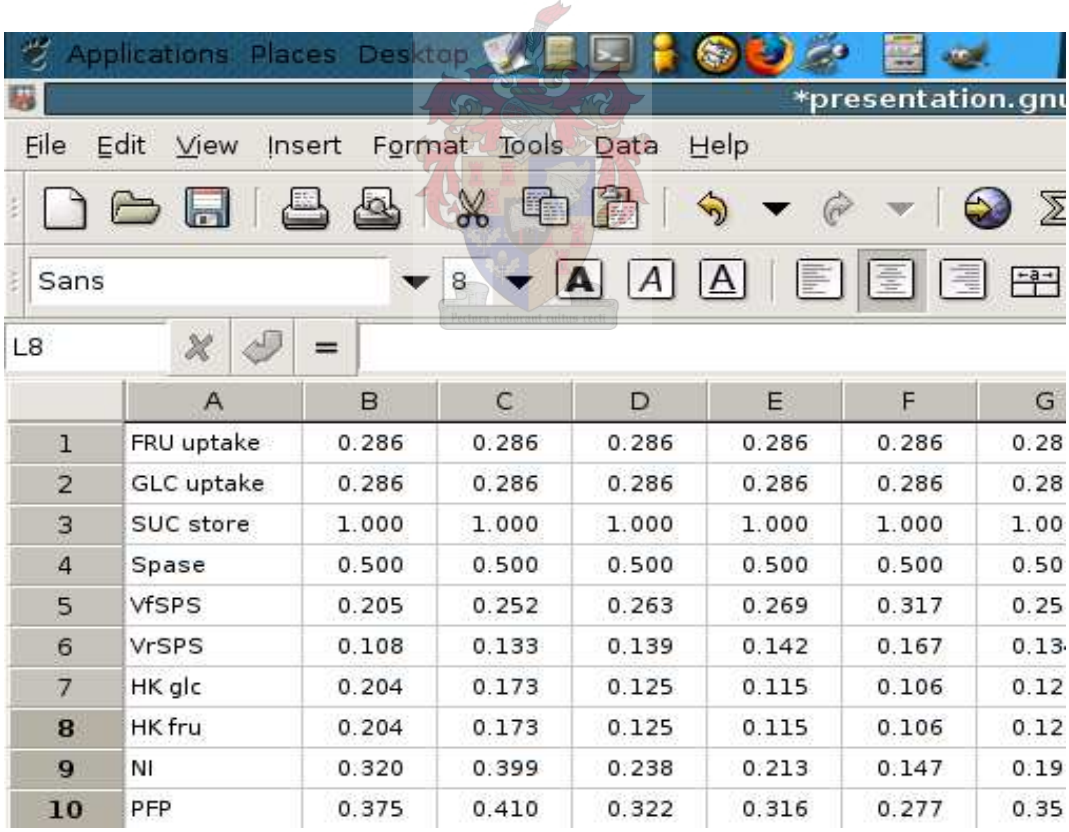

	A	B	C	D	E	F	G
1	FRU uptake	0.286	0.286	0.286	0.286	0.286	0.28
2	GLC uptake	0.286	0.286	0.286	0.286	0.286	0.28
3	SUC store	1.000	1.000	1.000	1.000	1.000	1.00
4	Spase	0.500	0.500	0.500	0.500	0.500	0.50
5	VfSPS	0.205	0.252	0.263	0.269	0.317	0.25
6	VrSPS	0.108	0.133	0.139	0.142	0.167	0.13
7	HK glc	0.204	0.173	0.125	0.115	0.106	0.12
8	HK fru	0.204	0.173	0.125	0.115	0.106	0.12
9	NI	0.320	0.399	0.238	0.213	0.147	0.19
10	PFP	0.375	0.410	0.322	0.316	0.277	0.35

Figure 4.1: Screenshot of activities stored in a Gnumeric spreadsheet

Example 4.4 Example of an interactive session in the Gnumeric Python console. Activity values are exported from a Gnumeric spreadsheet into a Berkeley DB database.

```
>>> import Gnumeric
>>> workbook = Gnumeric.workbooks()[0]
>>> workbook
<Workbook object at 0x8483290>
>>> sheet = workbook.sheets()[10]
>>> sheet
<Sheet object at 0x8483310>
>>> from bsddb import btopen
>>> berkeleydb = btopen('activities.bdb')
>>> from shelve import BsdDbShelf
>>> activities = BsdDbShelf(berkeleydb)
>>> activities
{}
>>> [sheet[i,4].get_value() for i in range(1,8)]
[0.20458740984827201, 0.25248149134543202, 0.26283728686883001,...
>>> activities['Vm9'] = [sheet[i,8].get_value() for i in range(1,8)]
>>> activities['VmPFP'] = [sheet[i,9].get_value() for i in range(1,8)]
>>> activities['VmPFK'] = [sheet[i,10].get_value() for i in range(1,8)]

...etc.

>>> activities.keys()
['Vf6', 'VfSSc', 'Vm3', 'Vm4', 'Vm9', 'VmAldolase', 'VmFRKa',...
>>> activities.sync()
>>> activities.close()
```

Example 4.5 Example Python code of using only one input file to describe a model and dynamically reassigning parameter values from a Berkeley DB database.

```
from bsddb import btopen
from shelve import BsdDbShelf
from os import listdir
import pysces

berkleydb = btopen('activities.bdb')          # open the database
activities = BsdDbShelf(berkleydb)            # extract the values
model = pysces.model('model.psc')             # create model object
model.doLoad()                                # parse the input file

internodes = 7
counter = 0

for internode in range(internodes):
    for vmax,values in activities.items():
        setattr(model,vmax,values[counter])   # set model parameters
    model.doState()                           # calculate a steady state
    model.showState()                         # print steady-state results
    counter+=1                                # increment counter
```

Chapter 5

Discussion and conclusions

This discussion will start with a summary of the key results from Chapters 2 and 3. A critical evaluation of the model described in Chapter 3 will follow and the effect of the core assumptions made in the construction of the model will be evaluated. This is followed by an argument for vacuolar sucrose accumulation. A synopsis of possible future work will then be given, followed by some concluding remarks.

5.1 Results of this work

5.1.1 Review of experimental sucrose concentrations

In Chapter 2 the work of various authors that have measured sucrose concentrations in immature sugarcane internodal tissue was reviewed. Reported sucrose concentrations were not always sampled from sequentially numbered internodes. In order to compare experimental values to values predicted by a model, "missing" data was exrapolated from spline fits to available data points. The data captured was resticted to sucrose concentrations for internodes 3 to 10 of maturing sugarcane.

The mean sucrose concentration per internode from the consolidated data sets increased linearly with internode maturity. The standard deviation for the data sets increased from internode 3 to 5, and then remained relatively constant for internodes 6 to 10. The data is summarised in Table 2.5. Values ranged from a mean sucrose concentration of 57 to 325 mmol l^{-1} for internodes 3 to 10 respectively.

5.1.2 Elaborating on an existing model

Chapter 3 showed how the sucrose accumulation model of Rohwer and Botha ($\mathbf{M}_\alpha$)[76], modified by Schäfer et al ($\mathbf{M}_\beta$) [80], was extended further. These extensions entailed the explicit modelling of the isoforms of sucrose synthase and fructokinase and glycolysis in terms of phosphofructokinase, phosphofructophosphatase and aldolase. The reaction that takes *UDP*-Glucose to *UDP*-Glucoronic

acid, the precursor to insoluble carbohydrates, was added to account for the fraction of the hexose phosphate pool that is diverted into fibre formation. All the major pathways that sequester carbon in the storage parenchyma are now present in the model. Other pathways, such as starch formation, also place a demand on hexose phosphates. It was considered reasonable to assume that flux to these pathways was neglible compared to flux into fibre, glycolysis and storage. This assumption is in line with experimental observations [7] (see p.51 and Table 3.5 for further details).

The modifications were first made individually and the effect on the model was analysed. The modifications were then combined to produce a model that was able to resolve in finer detail some of the properties of the sucrose accumulation process, such as the size and distribution of control amongst the isoforms of an enzyme. It was found that the new model, the one we called $\mathbf{M}_{\delta}^{(i)}$, did not differ radically from $\mathbf{M}_{\beta}$. The predicted steady-state values remained in the same order of magnitude with the exception of the glycolytic reactions, which have been discussed in detail on p. 29.

Data for maturing internodal tissue also made it possible to solve the model for 8 different internodes to provide a description of how sucrose accumulation changes with sugarcane stalk growth. There was no clear trend detected in how metabolite concentrations changed with internode maturity, i.e. no apparent linear correlation was discernable. The possible exception to this may be the sucrose concentration that remained fairly constant across internodes. Steady-state fluxes decreased slightly with internode maturity. Some large percentage decreases were seen in the smallest steady-state fluxes (e.g. *FRK B*), which in terms of absolute value were in fact negligible. Changes from internode to internode in steady-state flux values were in most cases to erratic to draw any conclusions. The exceptions were *ALD*, *PFK* and *PFP* steady-state fluxes which decreased with internode maturity. This trend agrees with the experimental observation that growth gives way to sucrose accumulation as internodes mature. Flux through *SuSy A* and into fibre also decreased. This is a consequence of maximal velocities for these enzymes being chosen to decrease with internode maturity. Similarly flux through *SuSy B* and *SuSy C* increased with internode maturity. Details of these manipulations can be found on pp. 33 and 45.

An investigation into the influence of various enzymes on the degree of futile cycling of sucrose showed that the control over this process did not change much with internode maturity. The same three transport steps as found by Rohwer and Botha (uptake of glucose and fructose, and vacuolar sucrose uptake) still had the largest negative control on the fraction of sucrose broken down again after synthesis. Similarly, glucose phosphorylating hexokinase and neutral invertase still retained the largest positive control over futile cycling. From the steady-state solution for each internode it was calculated that the percentage futile cycling per internode decreased by 6% per internode on average.

5.2 Evaluation of the model

If we assume that the sucrose concentration should be equal between apoplast, symplast and vacuole, then approximately 1 to 2 -fold higher sucrose concentrations are expected in the more mature internodes (internodes 6 and up) than predicted by the model (Figure 5.1). The following list discusses some problems that could have given rise to erroneous results.

1. The maximal velocities might not be an accurate reflection of reality. In kinetic studies that focused on a few enzymes, notably larger specific maximal velocities were reported when compared to attempts to assay many enzymes. We calculated a maximal activity of 0.925 mmol $min^{-1}l^{-1}$ for *FRK A* and 0.677 mmol $min^{-1}l^{-1}$ for *FRK B* for internode 5, based on the conversion factors in Section 2.1. These values are the result of research that focused only on fructokinase [31]. In contrast, the dataset used in the model (Table 3.2) has values of 0.059 and 0.042 mmol $min^{-1}l^{-1}$ for *FRK A* and *FRK B* respectively. These values are from a study that assayed 11 enzymes [12]. The forward maximal velocity these authors reported for fructokinase was the weighted average value for the different isozymes. We divided this between *FRK A* and *FRK B* using the forward maximal velocity ratios in Section 3.1. Clearly there is a difference of more than one order of magnitude between the focused and broader investigations. This is but one example of the disparity found between various reported enzyme maximal activities. The activities we used were from the broader study of Botha et al [12], in order to reduce or eliminate many of the possible causes that give rise to variations in enzyme assays. Specifically, this study used data

   (a) for plant samples from the same sugarcane variety and possibly even from the same plant,

   (b) where assay conditions were kept relatively similar for all the enzyme assays and,

   (c) where assays were performed in the same laboratory by one group of investigators.

   Furthermore the values reported in [12] included maximal velocities for almost all immature to mature internodes. These factors outweighed the choice to select values from more focused studies. Focused studies may perhaps be more accurate, but the assay conditions for these studies are in most cases incompatible with assay conditions for other enzymes. Kinetic models will be more realistic if experimentally introduced discrepancies in parameter values are minimised.

2. Inhibition of *PFK* by *ATP* and *PFP* by inorganic phosphate may play a role in the degree to which carbon is partitioned to glycolysis. Both *ATP* and inorganic phosphate concentrations were clamped in the model resulting in static inhibitory effects on these enzymes, and control

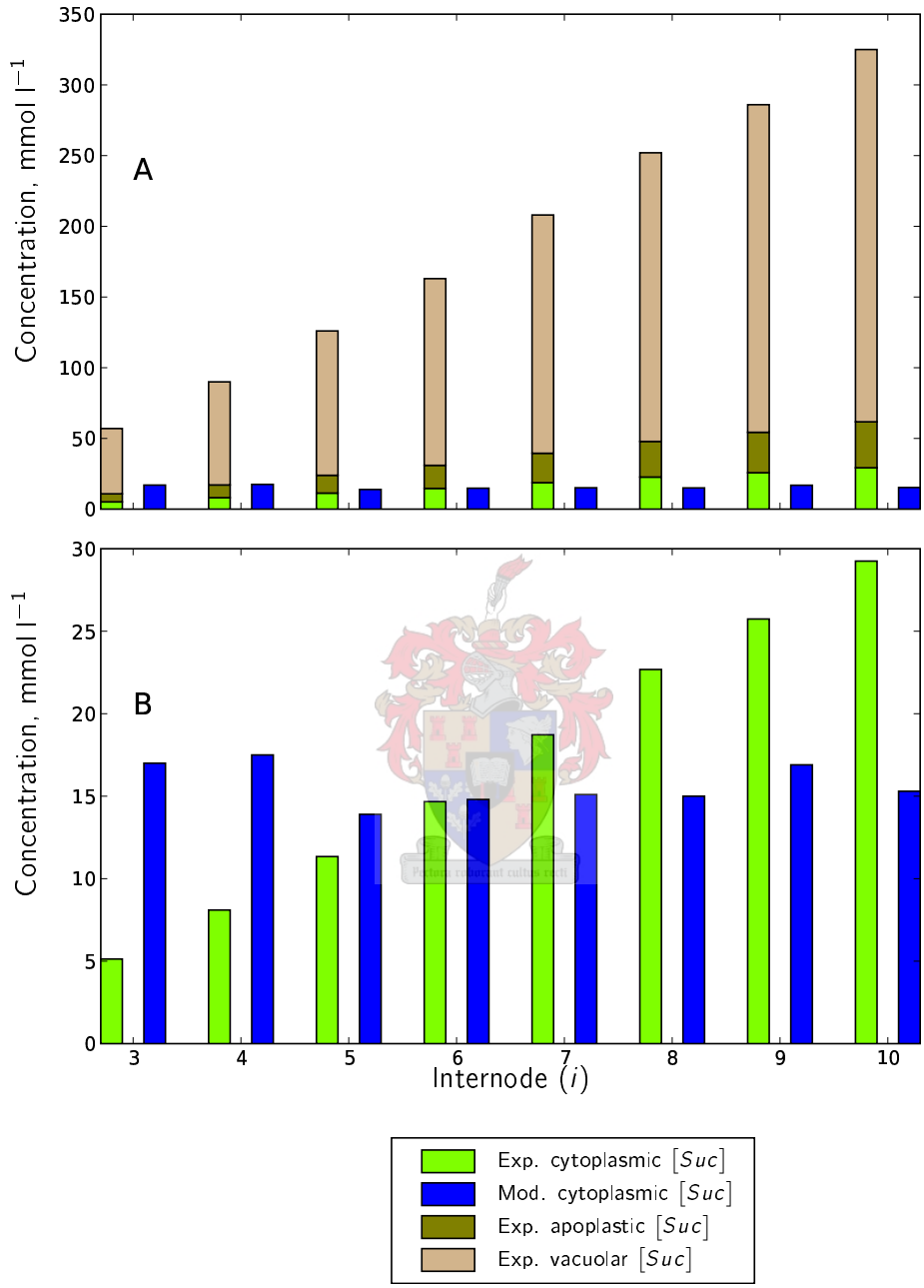

Figure 5.1: A comparison of experimental and model-predicted sucrose concentrations for internodes 3 to 10, assuming that sucrose concentrations are the same for the apoplast, cytoplasm and vacuole. A) The fraction of the total sucrose concentration accounted for by the model. Note that the model never included the vacuole or apoplast as explicit compartments. B) A direct comparison of the cytoplasmic sucrose concentrations for model and experiment. abbreviations: Exp. - Experimental, Mod. - Model.

of fluxes and concentrations by these enzymes on the rest of the model. These metabolites were kept at constant concentrations for the following reasons:

(a) no acceptable kinetic data was found for the regenaration of *ATP* and inorganic phosphate, therefore the reactions could not be modelled, and

(b) it was therefore assumed that the model was not limited by the regeneration of either of these species.

If *ATP* and inorganic phosphate concentrations were "floated" then the flux to glycolysis would run dry, because as substrates they would be used up if not replenished.

3. Some parameter estimates were made from measurements of related enzymes in other plant species. Steady-state solutions are often sensitive to small changes in parameters. Future refinements of the model would hopefully be able to correct this by including parameter values measured in sugarcane. As an example we calculate the response that a change in the half saturation constant for *PFK* with respect to *Fru-6-P* ($Fru\text{-}6\text{-}P_{0.5}$) will have on the flux through *PFK* (J_{PFK}). A response coefficient is defined as,

$$R^y_p = C^y_r \times \epsilon^r_p \tag{5.1}$$

where C^y_r is a control coefficient as defined in Section 3.1 and ϵ^r_p is an elasticity coefficient defined as,

$$\epsilon^r_p = \frac{\mathrm{d}\ln \nu_r}{\mathrm{d}\ln p} \tag{5.2}$$

where ν_r is the rate of a reaction and p is any parameter in the model. For the calculated values of $\epsilon^{PFK}_{Fru\text{-}6\text{-}P_{0.5}} = -2.29$ and $C^{J_{PFK}}_{PFK} = 0.99$ in internode 5, $R^{J_{PFK}}_{Fru\text{-}6\text{-}P_{0.5}} = -2.26$. This means that a 10% change in the value of $Fru\text{-}6\text{-}P_{0.5}$ should lead to an almost 23% decrease in J_{PFK}. This sort of amplification of a small change in a parameter into a larger change in a state-variable solution means that care must be taken with the selection of parameter values.

4. Sugar uptake is restricted to fructose and glucose, though it has been shown that sugarcane tissue disks are able to accumulate sucrose [46, 98]. The mechanism by which this occurs is not yet clear. We made an attempt at including this data into the sucrose accumulation model, steady-state solutions were however unattainable or in violation of what is biologically possible (data not shown). Introducing an extra source of sucrose in the model could possibly change the cytoplasmic sucrose profile of the maturing internodes.

5. There are possibly three isoforms of hexokinase [32]. It is conceivable that kinetic parameters would differ depending on whether fructose or glucose is phosphorylated. The possibility of

isoforms also exist for other enzymes. Explicitly modelling *SuSy* and *FRK* has shown that respective isozymes can have some effect on steady-state model solutions (Figures 3.3 and 3.5, Tables A.2 and A.3). Most importantly, inclusion of the respective isozymes has shown that the control of an enzyme is not equally distributed between isoforms (Figures 3.4 and 3.6). It is expected that if hexokinase, and any other enzyme for that matter, is modelled in terms of its isoforms, a metabolic control analysis would pinpoint which isozymes have significant efects on sucrose accumulation.

Possibility of vacuolar sucrose uptake The experimental sucrose concentrations in Table 2.5 and Figure 5.1 indicate a linear increase of the mean sucrose concentration as internodes mature. The gradient of increasing sucrose concentration from internodes 3 to 10 is 39 mmol l^{-1} $internode^{-1}$ In other words, the rate of increase of the total sucrose concentration with internode maturity is in the order of 34% per internode. In contrast the model showed virtually constant sucrose concentrations across the internodes. Thus a comparable percentage increase in sucrose concentration was not observed in the model compared to the experimental values. So the question is, where is the sucrose? If the majority of the sucrose is not in the cytoplasm, it has to be either in the vacuole or the apoplast. The pairwise Pearson correlation coefficient of *Suc* with J_{vac}^{Suc} is 1.0 (Table 3.6). From this it can be inferred that any increase in *Suc* will mean an increase in J_{vac}^{Suc}, which in turn will lead to a increase in the rate that *Suc* concentration is increasing in the vacuole. This is further supported by the fact that the only negative concentration control coefficient for sucrose was $C_{J_{store}}^{Suc}$. An increase in J_{vac}^{Suc} with *Suc* should not be that surprising. Vacuolar sucrose uptake is modelled as irreversible Michaelis Menten kinetics, making the flux directly dependent on *Suc*. A clearer conception is needed of what exactly the mechanism is of sucrose uptake across the tonoplast.

The modelling results show that *Glc* and *Fru* concentrations remain higher than that of sucrose. Since a net synthesis of sucrose exists, removal from the cytoplasmic compartment has to exist, otherwise higher cytoplasmic *Suc* concentrations should be seen. High precursor and low product concentrations would favour sucrose synthesis, so higher *Glc* and *Fru* concentrations can be expected to support net sucrose synthesis. It has been shown that vacuoles can accumulate sugars other that sucrose [69]. The model does not specifically account for this. The only way that carbohydrates can be mobilised from the vacuole again is by breakdown of vacuolar sucrose into glucose and fructose. It is unlikely that a large concentration gradient would exist between vacuolar and cytoplasmic glucose and fructose. It can be hypothesised that this state of affairs sustains the cytoplasmic synthesis of sucrose and immediate accumulation thereof by the vacuole.

Sucrose can enter an internode in one of three ways, from leaves attached to a node or via vascular tissue from the less mature internodes above and more mature internodes below. The sucrose concentration from below can be assumed to contribute to total internodal sucrose concentration

if sucrose unloading further down the plant is saturated. Incident radiation from sunlight decreases with canopy depth and increases with leaf size. The rate of sucrose unloading by the leaves per internode might be assumed to remain relatively constant. An internode does not retain all the sucrose that passes by in the phloem; it follows that the amount of sucrose available for uptake increases with internode maturity. This increased supply of sucrose is not reflected in the cytoplasmic sucrose concentration, leaving only the vacuole and the apoplastic space to store sucrose. Only the former has the available space to accumulate large amounts of sucrose. A larger model of sucrose accumulation would be able to address this.

It has been proposed that phloem transport occurs mostly because of an osmotic pressure gradient along phloem tubes. This phenomenon is called the "Osmotically Generated Pessure Flow" (OGPF) model and was first described by Münch [59, 60, 61]. The pressure gradient results from solutes being loaded into the phloem at the source tissue and removed at the sink tissues. The hydrostatic pressure drives solutes from source to sink. Thompson & Holbrook have published a theoretical model of this phenomenon and also provide a more in depth discussion of the OGPF model [94]. The Thompson & Holbrook model has subsequently been analysed and compared to known data on phloem transport in a number of plant species [93, 95, 96]. If this proves to be correct and it is assumed that phloem unloading in sugarcane is primarily symplastic, then no significant sucrose concentrations would be expected in the parenchymal cytoplasm, because high cytoplasmic sucrose concentrations would destroy any osmotic pressure differences between sink and source tissue. Accumulation in the vacuole, or possibly even the apoplast, would be an absolute necessity if a constant flow of photosynthate and signalling molecules is to be achieved. Solute concentrations in the cytoplasm, it could be argued, should not increase. This would allow the maintenance, or possibly regulation of an osmotic pressure difference, in which case the model predicted concentrations would be consistent with physiological concentrations. Unfortunately no reliable data on solute compartmentation exists in parenchymal tissue.

5.3 Future work

1. **Include the transport of sucrose and other sugars into the vacuole** The dynamics of sucrose accumulation would certainly change from the model proposed here if the sucrose available for storage does not only come from cytoplasmic synthesis but is also available from the vascular tissue.

2. **Unclamp cofactor concentrations** Moieties such as *ATP*, *ADP*, pyrophosphate and inorganic phosphate are currently kept at artificially constant concentrations, even though they have important regulatory roles in metabolic control. However, unclamping them would require a thorough knowledge of the kinetics of every important reaction that regenerates *ATP*

and PP_i.

3. **Expand competing pathways for carbon partitioning** The full control that glycolysis and fibre formation might have on flux into the vacuole is not completely captured by the model. It is therefore necessary to expand the reactions that direct carbon away from sucrose synthesis and storage, such as

   (a) reactions that compete for *UDPGlc*, e.g. *UDP*-Glucose pyrophosphorylase.

   (b) reactions that synthesise insoluble structural compounds, e.g. lignin, pectin and hemicellulose synthesising enzymes.

   (c) invertase reactions. Currently only one isoform of the enzyme is accounted for by the model. All the available evidence points towards a decrease in sucrose accumulation with increased futile cycling activity.

   (d) glycolytic reactions further downstream in glycolysis. It is likely that the possible control exercised by glycolysis on carbon partitioning is not completely captured yet by the model.

4. **Include phloem transport** The amount of sucrose that reaches the storage parenchyma is in part due to what is happening in the sugarcane vasculature. The flow to and from the storage parenchyma of sugarcane has implications for the amount of sucrose that can possibly be stored. Models of phloem- loading, -transport and -unloading, as well as xylem transport of minerals and water from the roots may be able to further improve the understanding of how sucrose is accumulated. The behaviour of water in the xylem affects the overall water status of a plant. Sucrose synthesis and storage is sensitive to dessication and drought [78], and therefore understanding xylem transport is important.

5. **Perform a detailed control analysis of Suc synthesis** Sucrose can not be stored faster than it is made. A clear understanding of the systemic properties of sucrose synthesis will provide a means of describing the control that reactions in the leaves have on sucrose accumulation.

The points outlined in the above list are reasonable extensions that can be made to the sucrose accumulation model. In some cases, experimental data is already available to make further modifications to the model. Work is already underway to model pathways in leaf tissue and compartmentation effects in the storage parenchyma.

A more speculative, possible extension to the model would be to include environmental parameters, such as climate and soil conditions into the model. Kinetic models usually to not take these factors into account, yet process-based, phenomenological models exist to describe theoretical yields from sugarcane harvests [40, 51, 52, 85]. Amongst other approaches, enzyme rates will

have to be made dependent on temperture terms and photosynthetic rates dependent on environmental light conditions. A synthesis of the two modelling approaches would clearly lead to a better understanding of the ecological context of sucrose accumulation.

As the size and complexity of mathematical models increases, software tools and programming environments, in which large amounts of data can be accommodated and analysed, need to be developed. Furthermore, the need to assess the reliability of a model also becomes important. It should be possible to assign a number to individual model outputs that give a degree of confidence in such a theoretical predictions. One possible way of going about this is to perform Monte Carlo analysis. This approach has already been successfully applied to quantifying errors in metabolic control analysis and estimating the size and shape of the allowable steady-state flux space [1, 114].

5.4 Conclusion

The results presented here suggest that sucrose is not accumulated in the cytoplasm of the storage parenchyma, but is rather transported into another compartment. The control of sucrose accumulation also does not shift drastically with the maturation of internodes, in fact, the majority of control was vested in the same set of enzymes in all eight internodes investigated. Lastly, the futile cycling of sucrose seems to decrease as sugarcane internodes mature. There is still much to be learnt about the process by which carbon is captured, built up into sucrose and stored by sugarcane.

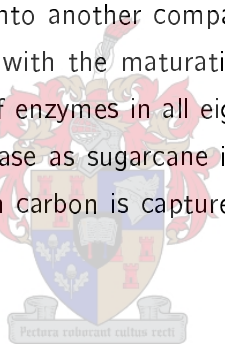

Appendix A

Supplementary Data

Table A.1: Steady-state fluxes and metabolite concentrations for $\mathbf{M}_\beta$ with permutations of *PFP*, *PFK* and *ALD* replacing R10.

	$\mathbf{M}_\beta$	$\mathbf{M}_\beta$+pfp+ald	$\mathbf{M}_\beta$+pfk+ald	$\mathbf{M}_\beta$+pfp+pfk+ald
Metabolite	Steady-state metabolite concentrations (mmol l^{-1})			
Fru	22.6	20.7	20.6	20.8
Glc	34.6	36.8	36.9	36.6
Suc-6-P	0.0037	0.0069	0.0072	0.0065
Suc	12.6	14.9	15.1	14.6
Fru-1,6-P_2	-	0.0003	0.0002	0.0005
UDPGlc	2.0	3.3	3.4	3.1
Glc-1-P	0.016	0.026	0.026	0.024
Glc-6-P	0.277	0.45	0.464	0.428
Fru-6-P	0.141	0.229	0.236	0.218
Reaction	Steady-state flux (mmol $l^{-1}min^{-1}$)			
J_{up}^{Fru}	0.147	0.153	0.153	0.153
J_{up}^{Glc}	0.118	0.114	0.114	0.114
J_{HK}^{Glc}	0.156	0.155	0.155	0.155
J_{HK}^{Fru}	0.001	0.001	0.001	0.001
J_{FRK}	0.052	0.055	0.055	0.055
J_{SPS}	0.018	0.032	0.033	0.03
J_{SP}	0.018	0.032	0.033	0.03
J_{SS}	0.132	0.139	0.139	0.138
J_{NI}	0.038	0.041	0.042	0.041
J_{glyc}	0.041	-	-	-
J_{PFK}	-	-	0.005	0.004
J_{PFP}	-	0.008	-	0.007
J_{Ald}	-	0.008	0.005	0.012
J_{vac}^{Suc}	0.112	0.130	0.131	0.128

Table A.2: Steady-state fluxes and concentrations of $\mathbf{M}_\beta$ with sucrose synthase isozyme reactions added. eq - total susy activity equally distributed amongst isozymes. ad - isozyme activities calculated using Equations 3.6 and 3.5

	$\mathbf{M}_\beta$	$\mathbf{M}_\beta$+ SuSy(eq)	$\mathbf{M}_\beta$+ SuSy(ad)
Metabolite	Steady-state metabolite concentrations (mM)		
Fru	22.6	7.6	7.9
Glc	34.6	41.7	41.5
Suc-6-P	0.004	0.004	0.004
Suc	12.6	16.1	16.0
UDPGlc	2.0	2.0	2.0
Glc-1-P	0.02	0.02	0.02
Glc-6-P	0.28	0.27	0.27
Fru-6-P	0.14	0.14	0.14
Reaction	Steady-state fluxes (mM/min)		
J_{up}^{Fru}	0.147	0.213	0.211
J_{up}^{Glc}	0.118	0.106	0.106
J_{HK}^{Glc}	0.156	0.156	0.156
J_{HK}^{Fru}	0.0007	0.0002	0.0002
J_{FRK}	0.052	0.091	0.090
J_{SPS}	0.018	0.017	0.017
J_{SP}	0.018	0.017	0.017
J_{SS}	0.132	-	-
J_{SS}^{a}	-	0.066	0.043
J_{SS}^{b}	-	0.042	0.051
J_{SS}^{c}	-	0.064	0.077
J_{NI}	0.038	0.051	0.051
$J_{glycolysis}$	0.041	0.041	0.041
J_{vac}^{Suc}	0.112	0.139	0.138

Table A.3: Steady-state concentrations and fluxes of $\mathbf{M}_\beta$ with *FRK A & B* added.

	$\mathbf{M}_\beta$	$\mathbf{M}_\beta$+ frk
Metabolite	Steady-state metabolite concentrations (mM)	
Fru	22.6	19.5
Glc	34.6	35.6
Suc-6-P	0.004	0.004
Suc	12.6	12.9
UDPGlc	2.0	2.3
Glc-6-P	0.016	0.018
Glc-1-P	0.28	0.32
Fru-6-P	0.14	0.16
Reaction	Steady-state fluxes (mM/min)	
J_{up}^{Fru}	0.147	0.157
J_{up}^{Glc}	0.118	0.116
J_{HK}^{Glc}	0.156	0.156
J_{HK}^{Fru}	0.0007	0.0006
J_{FRK}	0.05	-
J_{FRK}^{a}	-	0.064
J_{FRK}^{b}	-	0.0002
J_{SPS}	0.018	0.022
J_{SP}	0.018	0.022
J_{SS}	0.132	0.132
J_{NI}	0.038	0.040
J_{glyc}	0.041	0.045
J_{vac}^{Suc}	0.112	0.114

Table A.4: Steady-state concentrations and fluxes of $\mathbf{M}_\beta$ with the *UDPGDH* sink reaction added. Values are shown for the initial maximal velocity addition and the subsequent adjustment. See text for details.

	$\mathbf{M}_\beta$	$\mathbf{M}_\beta$+ udpgdh	$\mathbf{M}_\beta$+ adjusted udpgdh
Metabolite	Steady-state metabolite concentrations (mM)		
Fru	22.6	32.9	23.4
Glc	34.6	30.0	34.0
Suc-6-P	0.004	0.001	0.003
Suc	12.6	9.3	12.1
UDPGlc	2.02	0.86	1.81
Glc-1-P	0.016	0.007	0.014
Glc-6-P	0.277	0.118	0.248
Fru-6-P	0.141	0.06	0.126
Reaction	Steady-state fluxes (mM/min)		
J_{up}^{Fru}	0.147	0.121	0.145
J_{up}^{Glc}	0.118	0.128	0.119
J_{HK}^{Glc}	0.156	0.156	0.156
J_{HK}^{Fru}	0.001	0.001	0.001
J_{FRK}	0.052	0.040	0.051
J_{SPS}	0.018	0.005	0.015
J_{SP}	0.018	0.005	0.015
J_{SS}	0.132	0.108	0.130
J_{NI}	0.038	0.028	0.037
$J_{glycolysis}$	0.041	0.023	0.039
J_{UDPGDH}	-	0.056	0.009
J_{vac}^{Suc}	0.112	0.085	0.108

Table A.5: Comparison of steady-state properties between $\mathbf{M}_{\beta}$, partially substituted $\mathbf{M}_{\delta}^{(i)}$ and fully substituted $\mathbf{M}_{\delta}^{(i)}$ for internode 5.

	$\mathbf{M}_{\beta}$	partial $\mathbf{M}_{\delta}^{(i)}$	full $\mathbf{M}_{\delta}^{(i)}$
Metabolite	Steady-state metabolite concentrations (mM)		
Fru	22.6	13.3	15.9
Glc	34.6	39.5	62.3
Suc-6-P	0.004	0.002	0.001
Suc	12.6	16.2	13.9
Fru-1,6-P_2	-	0.0002	0.0001
UDPGlc	2.02	1.3	0.79
Glc-1-P	0.016	0.010	0.006
Glc-6-P	0.28	0.178	0.108
Fru-6-P	0.14	0.09	0.06
Reaction	Steady-state fluxes (mM/min)		
J_{up}^{Fru}	0.147	0.182	0.171
J_{up}^{Glc}	0.118	0.109	0.081
J_{HK}^{Glc}	0.156	0.156	0.100
J_{HK}^{Fru}	0.0007	0.0004	0.0002
J_{FRK}	0.052	-	-
J_{FRK}^{a}	-	0.052	0.052
J_{FRK}^{b}	-	0.0003	0.0002
J_{SPS}	0.018	0.010	0.030
J_{SP}	0.018	0.010	0.030
J_{SS}	0.132	-	-
J_{SS}^{a}	-	0.043	0.031
J_{SS}^{b}	-	0.058	0.046
J_{SS}^{c}	-	0.076	0.060
J_{NI}	0.038	0.047	0.019
J_{glyc}	0.041	-	-
J_{PFP}	-	0.003	0.002
J_{PFK}	-	0.001	0.0002
J_{ALD}	-	0.004	0.002
J_{UDPGDH}	-	0.009	0.006
J_{vac}^{Suc}	0.112	0.139	0.122

Bibliography

[1] Ainscow, E. K. and Brand, M. D. [1998]. Errors associated with metabolic control analysis: Application of Monte-Carlo simulation of experimental data, *J. Theor. Biol.* **194**: 223 – 233.

[2] Alexander, A. G. [1973]. *Sugarcane Physiology*, Elsevier scientific publishing Co. Amsterdam-London-New York.

[3] Arro, J. A. [2005]. *Genetic diversity among sugarcane clones using target region amplification polymorphism (trap) markers and pedigree relationships*, Master's thesis, Louisiana State University and Agricultural and Mechanical College.

[4] Berding, N. and Hurney, A. P. [2005]. Flowering and lodging, physiological-based traits affecting cane and sugar yield: What do we know of their control mechanisms and how do we manage them?, *Field Crops Research* **92**(2-3): 261–275.
URL: *http://www.sciencedirect.com/science/article/B6T6M-4FP1J7W-1/2/489b3ee90bf6319baefd84a573a9157a*

[5] Berding, N., Hurney, A., Salter, B. and Bonnett, G. [2005]. Agronomic impact of sucker development in sugarcane under different environmental conditions, *Field Crops Research* **92**(2-3): 203–217.
URL: *http://www.sciencedirect.com/science/article/B6T6M-4FJD9G9-2/2/c902909593a95f9ad87512ef0ce7f798*

[6] Bindon, K. A. [2000]. *Carbon partitioning in sugarcane internodal tissue with special reference to the insoluble fraction*, Master's thesis, University of Stellenbosch.

[7] Bindon, K. and Botha, F. [2002]. Carbon allocation to the insoluble fraction, respiration and triose-phosphate cycling in the sugarcane culm., *Physiologia Plantarum* **116**: 12–19.

[8] Bosch, S. [2005]. *Trehalose and carbon partitioning in sugarcane*, PhD thesis, University of Stellenbosch.

[9] Bosch, S., Grof, C. and Botha, F. [2004]. Expression of neutral invertase in sugarcane, *Plant science* **166**: 1125–1133.

[10] Bosch, S., Rohwer, J. M. and Botha, F. C. [2003]. The sugarcane metabolome, *Proc. S. Afr. Sug. Technol. Ass.* **7**: 129–132.

[11] Botha, F. C. and Black, K. G. [2000]. Sucrose phosphate synthase and sucrose synthase activity during maturation of internodal tissue in sugarcane, *Aust. J. Plant Physiol.* **27**: 81–85.

[12] Botha, F. C., Whittaker, A., Vorster, D. J. and Black, K. G. [1996]. Sucrose accumulation rate, carbon partitioning and expression of key enzyme activities in sugarcane stem tissue, *in* J. R. Wilson, D. M. Hogarth, J. A. Campbell and A. L. Garside (eds), *Sugarcane: Research Towards Efficient and Sustainable Production*, CSIRO division of Tropical Crops and Pastures, Brisbane, pp. 98–101.

[13] Bourne, E. J., Davies, D. R. and Pridham, J. B. [1970]. α-amylase activity in sugar cane (*Saccharum officinarum*) chloroplasts, *Phytochemistry* **9**(2): 345–348.
URL: *http://www.sciencedirect.com/science/article/B6TH7-42HX8YN-9Y/2/1aeb389a93a70c3e48255cba5389879c*

[14] Cannell, M. and Thornley, J. [2000]. Modelling the components of plant respiration: some guiding principles, *Annals of Botany* **85**: 45–54.

[15] Carrillo-Castañeda, G. and Mata, A. [2000]. Succession of esterase and peroxidase isozymes associated with the in vitro sugarcane tissue dedifferentiation and shoot induction, *Biotecnologia Aplicada* **17**: 225–230.

[16] Cawood, M., Botha, F. and Small, J. [1988]. Properties of the phosphofructokinase isoenzymes from germinating cucumber seeds, *J. Plant Physiol* **132**: 204–209.

[17] Chitnis, P. [2001]. Photosystem i: Function and physiology., *Annu. Rev. Plant Physiol. Plant. Mol. Biol.* **52**: 593–626.

[18] Doedel, E., Keller, H. and Kernevez, J. [1991a]. Numerical analysis and control of bifurcation problems, part i, *Int. J. Bifurcation and Chaos* **3**: 493–520.

[19] Doedel, E., Keller, H. and Kernevez, J. [1991b]. Numerical analysis and control of bifurcation problems, part ii, *Int. J. Bifurcation and Chaos* **4**: 745–772.

[20] Du, Y.-C., Nose, A., Wasano, K. and Uchida, Y. [1998]. Responses to water stress of enzyme activities and metabolite levels in relation to sucrose and starch synthesis, the Calvin cycle and the C4 pathway in sugarcane (*Saccharum* sp.) leaves., *Aust. J. Plant Physiol.* **25**: 253–260.

[21] Edwards, G., Franceshi, V., Ku, M., Voznesenskaya, E.V.and Pyankov, V. and Andreo, C. [2001]. Compartmentation of photosynthesis in cells and tissues of C4 plants., *J. Exp. Bot.* **52**: 577–590.

[22] Finney, A. and Hucka, M. [2003]. Systems biology markup language: Level 2 and beyond, *Biochem. Soc. Trans.* **31**: 1472?1473.

[23] Getz, H., Thom, M. and Maretzki, A. [1991]. Proton and sucrose transport in isolated tonoplast vesicles from sugarcane stalk tissue., *Physiologia Plantarum* **83**: 404–410.

[24] Glasziou, K. [1960]. Accumulation and transformation of sugars in sugar cane stalks, *Plant Physiol.* pp. 895–901.

[25] Glasziou, K., Bull, T., Hatch, M. and Whiteman, P. [1965]. Physiology of sugarcane VII: Effects of temperature, photoperiod duration, and diurnal and seasonal temperature changes on growth and ripening, *Aust. J. Biol. Sci.* **18**: 53–66.

[26] Glasziou, K., Waldron, J. and Bull, T. [1966]. Control of invertase synthesis in sugar cane: Loci of auxin and glucose effects., *Plant Physiol.* **41**: 282–288.

[27] Glaz, B., Morris, D. and Daroub, S. [2004]. Sugarcane photosynthesis, transpiration, and stomatal conductance due to flooding and water table., *Crop Sci.* **44**: 1633–1641.

[28] Hatch, M. D. and Glasziou, K. T. [1963]. Sugar accumulation cycle in sugar cane II: Relationship of invertase activity to sugar content and growth rate storage tissue of plants grown in controlled environments, *Plant Physiol.* **38**: 344–348.

[29] Heinrich, R. and Rapoport, T. A. [1974]. A linear steady-state treatment of enzymatic chains. general properties, control and effector strength, *Eur. J. Biochem.* **42**: 89–95.

[30] Heinrich, R. and Schuster, S. [1996]. *The Regulation of Cellular Systems*, Chapman & Hall, New York.

[31] Hoepfner, S. W. and Botha, F. C. [2003]. Expression of fructokinase isoforms in the sugarcane culm, *Plant Physiol. Biochem.* **41**: 741–747.

[32] Hoepfner, S. W. and Botha, F. C. [2004]. Purification and characterisation of fructokinase from the culm of sugarcane, *Plant Sci.* **167**: 645–654.

[33] Hofmeyr, J.-H. S. and Cornish-Bowden, A. [2000]. Regulating the cellular economy of supply and demand, *FEBS Lett.* **476**: 47–51.

[34] Hofmeyr, J. H. S. and Westerhoff, H. V. [2001]. Building the cellular puzzle - control in multi-level reaction networks, *J. Theor. Biol.* **208**: 261–285.

[35] Hucka, M. e. a. [2003]. The systems biology markup language (SBML): a medium for representation and exchange of biochemical network models, *Bioinformatics* **19**(4): 524–531.
URL: *http://bioinformatics.oxfordjournals.org/cgi/content/abstract/19/4/524*

[36] Hucka, M., Finney, A., Sauro, H. and Bolouri, H. [2001]. The ERATO systems biology workbench: Architectural evolution, *in* T.-M. Yi, M. Hucka, M. Morohashi and H. Kitano (eds), *The Proceedings of the 2nd International Conference on Systems Biology*.

[37] Hucka, M., Sauro, H., Finney, A. and Bolouri, H. [2003]. Introduction to the systems biology workbench.
URL: *http://sbw.kgi.edu/caltechSBW/sbwDocs/docs/intro/html/intro.html*

[38] Ioannidis, J. P. A. [2005]. Why most published research findings are false, *PLoS Medicine* **2**(8): –.
URL: *http://dx.doi.org/10.1371/journal.pmed.0020124*

[39] Kacser, H. and Burns, J. A. [1973]. The control of flux, *Symp. Soc. Exp. Biol.* **27**: 65–104.

[40] Keating, B. A., Robertson, M. J., Muchow, R. C. and Huth, N. I. [1999]. Modelling sugarcane production systems I: Development and performance of the sugarcane module, *Field Crops Research* **61**(3): 253–271.
URL: *http://www.sciencedirect.com/science/article/B6T6M-3W7X9KS-6/2/ad7f813f7e5b8e952af44934ba862716*

[41] Kholodenko, B. N., Molenaar, D., Schuster, S., Heinrich, R. and Westerhoff, H. V. [1995]. Defining control coefficients in non-ideal metabolic pathways, *Biophysical Chemistry* **56**(3): 215–226.
URL: *http://www.sciencedirect.com/science/article/B6TFB-3YYTFG3-2/2/59d0553bf8ac08ef2c1915756e1d8cf9*

[42] Knowles, V., Greyson, M. and Dennis, D. [1990]. Characterization of ATP-dependent fructose 6-phosphate 1-phosphotransferase isozymes from leaf and endosperm tissues of Ricinus communis, *Plant Physiol.* **92**: 155–159.

[43] Kombrink, E., Kruger, N. and Beevers, H. [1984]. Kinetic properties of pyrophosphate:d-fructose-6-phosphate phosphotransferase from germinating castor bean endosperm, *Plant Physiol.* **74**: 395–401.

[44] Komor, E. [1994]. Regulation by futile cycles: the transport of carbon and nitrogen in plants, *in* E. D. Schulze (ed.), *Flux Control in Biological Systems*, Academic Press, San Diego, pp. 153–201.

[45] Komor, E. [2000]. The physiology of sucrose storage in sugarcane, *in* A. K. Gupta and N. Kaur (eds), *Carbohydrate Reserves in Plants - Synthesis and Regulation*, Elsevier Science, Amsterdam, pp. 35–54.

[46] Komor, E., Thom, M. and Maretzki, A. [1981]. The mechanism of sugar uptake by sugarcane suspension cells, *Planta* **153**: 181–192.

[47] Komor, E., Thom, M. and Maretzki, A. [1982]. Vacuoles from sugarcane suspension cultures iii: protonmotive potential difference, *Plant Physiol.* **69**: 1326–1330.

[48] Kowalczyk, S., Januszewska, B., Cymerska, E. and Maslowski, P. [1984]. The occurence of inorganic pyrophosphate;d-d-fructose-6-phosphate 1-phosphotransferase in higher plants I: Initial characterization of partially purified enzyme from sanseviera trifasciata leaves, *Physiol. Plant.* **60**: 31–37.

[49] Lampinen, M. J. and Noponen, T. [2003]. Thermodynamic analysis of the interaction of the xylem water and phloem sugar solution and its significance for the cohesion theory, *Journal of Theoretical Biology* **224**(3): 285–298.
URL: *http://www.sciencedirect.com/science/article/B6WMD-4938KWR-1/2/c3ccc78e0e45f78add354a56f680241e*

[50] Lingle, S. [2004]. Effect of transient temperature change on sucrose metabolism in sugarcane internodes., *J. Am. Soc. Sug. Cane Tech.* **24**: 132–141.

[51] Lisson, S., Inman-Bamber, N., Robertson, M. and Keating, B. [2005]. The historical and future contribution of crop physiology and modelling research to sugarcane production systems, *Field Crops Research* **92**(2-3): 321–335.
URL: *http://www.sciencedirect.com/science/article/B6T6M-4FJD9G9-1/2/f467f5ea32d0f767883720d4921637b8*

[52] Liu, D. and Helyar, K. [2003]. Simulation of seasonal stalk water content and fresh weight yield of sugarcane, *Field Crops Research* **82**: 59–73.

[53] Ma, H., Albert, H., Paull, R. and Moore, P. [2000]. Metabolic engineering of invertase activities in different subcellular compartments affects sucrose accumulation in sugarcane cells., *Aust. J. Plant Physiol.* **27**: 1021–1030.

[54] Mahajan, R. and Singh, R. [1989]. Properties of pyrophosphate:d-fructose-6-phosphate phosphotransferase from endosperm of developing wheat (triticum aestivum l.) grains, *Plant Physiol.* **91**: 421–426.

[55] Mendes, P. [1993]. GEPASI: A software package for modelling the dynamics, steady states and control of biochemical and other systems., *Comput. Applic. Biosci.* **9**: 563–571.

[56] Ming, R., Liu, S. C., Moore, P. H., Irvine, J. E. and Paterson, A. H. [2001]. QTL analysis in a complex autopolyploid: genetic control of sugar content in sugarcane., *Genome Res* **11**(12): 2075–84.
URL: *http://dx.doi.org/10.1101/gr.198801*

[57] Morgan, J. A. and Rhodes, D. [2002]. Mathematical modeling of plant metabolic pathways, *Metabolic Engineering* **4**(1): 80–89.
URL: *http://www.sciencedirect.com/science/article/B6WN3-457MDX6-B/2/eaa8a39790cd93bda05cc4c137ab8331*

[58] Most, B. and Vlitos, A. [1966]. Gibberellins of sugarcane, *Plant Physiol.* **41**: 1090–1094.

[59] Münch, E. [1926]. Über dynamik der saftströmungen., *Ber. Deut. Bot. Ges.* **44**: 68–71.

[60] Münch, E. [1927]. Versuche über den saftkreislauf., *Ber. Deut. Bot. Ges.* **45**: 340–356.

[61] Münch, E. [1930]. *Die Stoffbewegungen in der Pflanze.*, Vol. 45, Jena: Gustav Fischer.

[62] Olivier, B. G., Rohwer, J. M. and Hofmeyr, J.-H. S. [2002]. Modelling cellular processes with python and scipy, *Mol. Biol. Rep.* **29**: 249–254.

[63] Olivier, B. G., Rohwer, J. M. and Hofmeyr, J.-H. S. [2005]. Modelling cellular systems with pysces, *Bioinformatics* **21**(4): 560–561.
URL: *http://bioinformatics.oxfordjournals.org/cgi/content/abstract/21/4/560*

[64] Olson, M., Bostic, K. and Seltzer, M. [1999]. Berkeley DB, *Proceedings of the 1999 Summer Usenix Technical Conference*.

[65] Patrick, J. [1997]. Phloem unloading: Sieve element unloading and post-sieve element transport, *Annu. Rev. Plant Physiol. Plant. Mol. Biol.* **48**: 191–222.

[66] Pfündel, E., Nagel, E. and Meister, A. [1996]. Analyzing the light energy distribution in the photosynthetic apparatus of C4 plants using highly purified mesophyll and bundle-sheath thylakoids, *Plant Physiol.* **112**: 1055–1070.

[67] Prado, F. E., Fleischmacher, O. L., Vattuone, M. A. and Sampietro, A. R. [1980]. Cell wall invertases of sugar cane, *Phytochemistry* **21**(12): 2825–2828.
URL: *http://www.sciencedirect.com/science/article/B6TH7-42M8344-S2/2/8081318422244240794 8a3d2188bf0b4*

[68] Preisser, J. and Komor, E. [1988]. Analysis of the reaction products from incubation of sugarcane vacuoles with uridine-diphosphate-glucose: No evidence for the group translocator, *Plant Physiol.* **88**: 259–265.

[69] Preisser, J. and Komor, E. [1991]. Sucrose uptake into vacuoles of sugarcane suspension cells, *Planta (Historical Archive)* **186**(1): 109–114.
URL: *http://www.springerlink.com/openurl.asp?genre=articleid=doi:10.1007/BF00201505*

[70] Preisser, J., Sprügel, H. and Komor, E. [1992]. Solute distribution between vacuole and cytosol of sugarcane suspension cells: Sucrose is not accumulated in the vacuole, *Planta (Historical Archive)* **186**(2): 203–211.
URL: *http://www.springerlink.com/openurl.asp?genre=articleid=doi:10.1007/BF00196249*

[71] R Development Core Team [2005]. *R: A language and environment for statistical computing*, R Foundation for Statistical Computing, Vienna, Austria. ISBN 3-900051-07-0.
URL: *http://www.R-project.org*

[72] Rae, A., Grof, C., Casu, R. and Bonnett, G. [2005]. Sucrose accumulation in the sugarcane stem: pathways and control points for transport and compartmentation., *Field Crops Research* **92**: 159–168.

[73] Rae, A. L., Perroux, J. M. and Grof, C. P. L. [2005]. Sucrose partitioning between vascular bundles and storage parenchyma in the sugarcane stem: a potential role for the ShSUT1 sucrose transporter., *Planta* **220**(6): 817–25.
URL: *http://dx.doi.org/10.1007/s00425-004-1399-y*

[74] Rheinboldt, W. and Burkardt, J. [1983]. A locally parameterized continuation process., *ACM Trans. Math. Softw.* **9**: 215–235.

[75] Rohwer, J. [2005]. Strategies and tools for computational systems biology, *Screening* **6**: 23–25.

[76] Rohwer, J. M. and Botha, F. C. [2001]. Analysis of sucrose accumulation in the sugar cane culm on the basis of *in vitro* kinetic data, *Biochem. J.* **358**: 437–445.

[77] Rose, S. and Botha, F. [2000]. Distribution patterns of neutral invertase and sugar content in sugarcane internodal tissues, *Plant Physiol. Biochem.* **38**: 819–824.

[78] Saliendra, N. and Meinzer, F. [1991]. Symplast volume, turgor, stomatal conductance and growth in relation to osmotic and elastic adjustment in droughted sugarcane., *J. Exp. Bot.* **42**: 1251–1259.

[79] Sauro, H. [2000]. Jarnac: a system for interactive metabolic analysis, *in* J.-H. Hofmeyr, J. Rohwer and J. Snoep (eds), *Animating the Cellular Map: Proceedings of the 9th International Meeting on BioThermoKinetics*, p. 221?228.

[80] Schäfer, W. E., Rohwer, J. M. and Botha, F. C. [2004a]. A kinetic study of sugarcane sucrose synthase, *Eur. J. Biochem.* **271**: 3971–3977.

[81] Schäfer, W. E., Rohwer, J. M. and Botha, F. C. [2004b]. Protein-level expression and localization of sucrose synthase in the sugarcane culm, *Physiol. Plantarum* **121**: 187–195.

[82] Schäfer, W. E., Rohwer, J. M. and Botha, F. C. [2005]. Partial purification and characterisation of sucrose synthase in sugarcane, *J. Plant Physiol.* **162**: 11–20.

[83] Schomburg, I., Chang, A., Ebeling, C., Gremse, M., Heldt, C., Huhn, G. and Schomburg, D. [2004]. BRENDA, the enzyme database: updates and major new developments., *Nucleic Acids Res* **32**(Database issue): D431–3.
URL: *http://dx.doi.org/10.1093/nar/gkh081*

[84] Schomburg, I., Chang, A., Hofmann, O., Ebeling, C., Ehrentreich, F. and Schomburg, D. [2002]. BRENDA: a resource for enzyme data and metabolic information., *Trends Biochem Sci* **27**(1): 54–6.

[85] Singels, A. and Bezuidenhout, C. N. [2002]. A new method of simulating dry matter partitioning in the canegro sugarcane model, *Field Crops Research* **78**(2-3): 151–164.
URL: *http://www.sciencedirect.com/science/article/B6T6M-46MBDY6-5/2/86c22e37b63ad4210aeef1b0d41618b6*

[86] Smith, D., Inman-Bamber, N. and Thorburn, P. [2005]. Growth and function of the sugarcane root system, *Field Crops Research* **92**(2-3): 169–183.
URL: *http://www.sciencedirect.com/science/article/B6T6M-4G33794-3/2/62da2ff588eb3445ff7307189c6a411f*

[87] Snoep, J. L. and Olivier, B. G. [2002]. Java Web Simulation (JWS); a web based database of kinetic models, *Mol. Biol. Rep.* **29**: 259–263.

[88] Stitt, M. [1990]. Fructose-2,6-bisphosphate as a regulatory molecule in plants, *Annu. Rev. Plant Physiol. Plant. Mol. Biol.* **41**: 153–185.

[89] Thom, M., Komor, E. and Maretzki, A. [1982]. Vacuoles from sugarcane suspension cultures II: characterization of sugar uptake., *Plant Physiol.* **69**: 1320–1325.

[90] Thom, M. and Maretzki, A. [1970]. Peroxidase and esterase isozymes in Hawaiian sugarcane, *Hawaiian Planters Record* .

[91] Thom, M. and Maretzki, A. [1985]. Group translocation as a mechanism for sucrose transfer into vacuoles from sugarcane cells., *Proc. Nat. Acad. Sci* **82**: 4697–4701.

[92] Thom, M., Maretzki, A. and Komor, E. [1982]. Vacuoles from sugarcane suspension cultures I: isolation and partial characterisation, *Plant Physiol.* **69**: 1315–1319.

[93] Thompson, M. [2005]. Scaling phloem transport: Elasticity and pressure-concentration waves, *J. Theor. Biol.* **236**: 229–241.

[94] Thompson, M. and Holbrook, N. [2003a]. Application of a single-solute non-steady-state phloem model to the study of long distance assimilate transport, *J. Theor. Biol.* **220**: 419–455.

[95] Thompson, M. and Holbrook, N. [2003b]. Scaling phloem transport: water potential equilibrium and osmoregulatory flow, *Plant, Cell and Environment* **26**: 1561–1577.

[96] Thompson, M. and Holbrook, N. [2004]. Scaling phloem transport: information transmission, *Plant, Cell and Environment* **27**: 509–519.

[97] Thornley, J. and Cannell, M. [2000]. Modelling the components of plant respiration: Representation and realism, *Annals of Botany* **85**: 55–67.

[98] Titus, C. [2005]. *Sucrose transporters and sucrose uptake mechanisms in sugarcane*, Master's thesis, University of Stellenbosch.

[99] Tripodi, K. and Podesta, F. [1997]. Purification and structural and kinetic characterization of the pyrophosphate:fructose-6-phosphate 1-phosphotransferase from the crassulacean acid metabolism plant, pineapple, *Plant Physiol.* **113**: 779–786.

[100] Turner, W. and Botha, F. C. [2002]. Purification and kinetic properties of UDP-glucose dehydrogenase from sugarcane., *Arch Biochem Biophys* **407**(2): 209–16.

[101] Turner, W. and Plaxton, W. [2003]. Purification and characterization of pyrophosphate- and atp-dependent phosphofructokinases from banana fruit, *Planta* **217**: 113–121.

[102] Van Bel, A. [1993]. Strategies of phloem loading, *Annual Review of Plant Physiology and Plant Molecular Biology* **44**(1): 253–281.
URL: *http://arjournals.annualreviews.org/doi/abs/10.1146/annurev.pp.44.060193.001345*

[103] Van Bel, A. [2003]. The phloem, a miracle of ingenuity., *Plant, Cell and Environment* **26**: 125–149.

[104] van Dillewijn, C. [1952]. *Botany of sugarcane*, Waltham Co. Mass. USA.

[105] Van Schaftingen, E., Lederer, B., Bartrons, R. and Hers, H.-G. [1982]. A kinetic study of pyrophosphate: fructose-6-phosphate phosphotransferase from potato tubers, *European Journal of Biochemistry* **129**: 191–195.

[106] Vattuone, M. A., Prado, F. E. and Sampietro, A. R. [1981]. Cell wall invertases from sugar cane, *Phytochemistry* **20**(2): 189–191.
URL: *http://www.sciencedirect.com/science/article/B6TH7-42K6FBJ-DV/2/1ac16cd7cb59cc86d54d4f9bfbdb8105*

[107] Venkataramana, S., Naidu, K. M. and Singh, S. [1991]. Invertases and growth factors dependent sucrose accumulation in sugarcane, *Plant Science* **74**(1): 65–72.
URL: *http://www.sciencedirect.com/science/article/B6TBH-47T8P0C-13M/2/989edaf6df029fb359fba188d00914c4*

[108] Vorster, D. J. and Botha, F. C. [1998]. Partial purification and characterisation of sugarcane neutral invertase, *Phytochem.* **49**: 651–655.

[109] Vorster, D. J. and Botha, F. C. [1999]. Sugarcane internodal invertases and tissue maturity, *J. Plant Physiol.* **155**: 470–476.

[110] Walsh, K., Sky, R. and Brown, S. [2005]. The anatomy of the pathway of sucrose unloading within the sugarcane stalk, *Func. Plant. Biol.* **32**: 367–374.

[111] Welbaum, G. and Meinzer, F. [1990]. Compartmentation of solutes and water in developing sugarcane stalk in tissue, *Plant Physiol.* **93**: 1147–1153.

[112] Wheeler, D., Guyer, J. and Warren, J. [2005]. *FiPy User's guide*, version 1.0 edn, NIST Metallurgy division and the center for computational materials science, Materials science and engineering building.

[113] Whittaker, A. and Botha, F. C. [1997]. Carbon partitioning during sucrose accumulation in sugarcane internodal tissue, *Plant Physiol.* **115**: 1651–1659.

[114] Wiback, S., Famili, I., Greenberg, H. and Palsson, B. [2004]. Monte Carlo sampling can be used to determine the size and shape of the steady-state flux space., *JTB* **228**: 437–447.

[115] Wong, J., Kang, T. and Buchanan, B. [1988]. A novel pyrophosphate d-fructose-6-phosphate 1-phosphotransferase from carrot roots: Relation to PFK from the same source, *FEBS Lett.* **238**: 405–410.

[116] Woo, K., Anderson, J., Boardman, N., Downton, W., Osmond, C. and Thorne, S. [1970]. Deficient photosystem II in agranal bundle sheath chloroplasts of C4 plants, *Proc. Nat. Acad. Sci* **67**: 18–25.

[117] Zhu, Y. J., Komor, E. and Moore, P. H. [1997]. Sucrose accumulation in the sugarcane stem is regulated by the difference between the activities of soluble acid invertase and sucrose phosphate synthase, *Plant Physiol.* **115**: 609–616.